Dissertation
submitted to the
Combined Faculty of Natural Sciences and Mathematics
of the Ruperto Carola University Heidelberg, Germany
for the degree of
Doctor of Natural Sciences

Presented by

M.Sc. Atalay Tok

born in: Istanbul

Oral examination: 25.10.2019

Divergent Mechanisms of Head-Trunk Separation in Dipteran Flies

Referees: Prof. Dr. Joachim Wittbrodt
Jun.-Prof. Dr. Steffen Lemke

Abstract

Evolution has led to an immense diversity in the form and shape of animals that we can observe today. As a result of an evolutionary trend called cephalization, most animals develop a head as a separate entity than the trunk. Foundations of head as an isolated body part become evident while the animal body plan is established during the early development. Mechanisms of head and trunk separation, however, are poorly understood. Studying how and which developmental programs contribute to the divergence of head-trunk separation mechanism is, therefore, essential. As our understanding of morphogenesis, the making of morphology, has drastically changed over the years, we can now tackle such phenomenon in greater detail.

In my thesis, I interrogated the head-trunk separation mechanisms during early gastrulation among dipteran flies as a model. Dipteran tree of flies present a valuable diversity in head-trunk separation strategies. While derived cyclorrhaphan fruit fly *Drosophila melanogaster* and basal cyclorrhaphan scuttle fly *Megaselia abdita* embryos employ a head fold called the cephalic furrow, which physically separates embryonic head from trunk; basal non-cyclorrhaphan midge fly *C. riparius* embryos, like most insects, do not form a head fold. In *D. melanogaster*, the cephalic furrow formation is a deep epithelial infolding event, that invariably appears in the same position, critically requires the overlapping expression of two transcription factors, *even-skipped* and *buttonhead.* My findings suggested that the absence of a head fold in *C. riparius* coincides with non-overlapping expression patterns these two genes, while *M. abdita* has a similar overlap with some differences. I further identified that in the absence of such a visible separator, differential arrangement of subcellular contractile actomyosin networks in the anteroposterior axis has a pivotal role in head-trunk separation in *C. riparius*. Furthermore, uncovering prominent out-of-plane divisions in the *C. riparius'* head development allowed me to speculate a putatively analogous function to the cephalic furrow in higher flies, as a number of cells sink below the embryo surface in both cases. Taken together, my thesis shed light onto the variation of head-trunk separation strategies, underlying genetics, and its implementation at the cellular, tissue and embryonic level in dipteran flies.

Zusammenfassung

Im Reich der Tiere hat sich im Laufe der Evolution eine immense Vielfalt an Formen und Gestalten entwickelt. Infolge eines evolutionären Trends, der als Cephalisierung bezeichnet wird, entwickeln die meisten Tiere einen Kopf, der getrennt vom Rumpf, als eine separate Einheit bildet. Schon früh in der Tierkörperentwicklung werden die Grundlagen für die Entwicklung des Kopfes festgelegt, jedoch sind die Mechanismen zur Kopfspezifischen Entwicklung und die Entwicklung des Kopfes getrennt vom restlichen Rumpf noch wenig verstanden. Daher ist es wichtig zu untersuchen, wie und welche Entwicklungsprogramme zur Divergenz des Mechanismus der Trennung von Kopf und Rumpf beitragen. Da sich unser Verständnis von der Morphogenese (die Entstehung der Morphologie) im Laufe der Jahre drastisch verbessert hat, können wir dieses Phänomen nun genauer untersuchen.

In meiner Dissertation habe ich den Mechanismus der Trennung von Kopf und Rumpf während der frühen Gastrulation in Dipteren-Fliegen als Modell untersucht. Der Dipteren-Stammbaum bietet dabei eine wertvolle Vielfalt an Strategien zur Trennung von Kopf und Rumpf. Während zum Beispiel die beiden Fliegen, die höher entwickelte Cyclorrhaphan-Frucht-Fliege Drosophila melanogaster und die basale Cyclorrhaphan-Buckel-Fliege Megaselia abdita, in der Embryonalentwicklung eine Kopffalte einstülpen, die als Cephale-Furche bezeichnet wird und die den embryonalen Kopf physikalisch vom Rumpf trennt, bildet die basale nicht-cyclorrhaphische Mücken-Fliege C. riparius in ihrer Embryonalentwicklung, wie die meisten Insekten, keine Kopffalte.

In D. melanogaster handelt es sich bei der Bildung der Cephalen-Furche um ein tief eingestülptes Epithel, das immer an derselben Position im Embryo auftritt und über die überlappende Expression von zwei Transkriptionsfaktoren, Even-Skipped und Buttonhead festgelegt wird. Meine Ergebnisse legen nahe, dass das Fehlen einer Kopffalte bei C. riparius mit nicht überlappenden Expressionsmustern dieser beiden Gene zusammenfällt, während M. abdita mit einigen Unterschieden eine ähnliche Überlappung aufweist. Ich identifizierte ferner, dass in Abwesenheit

eines solchen sichtbaren Separators die spezifische Anordnung subzellulärer kontraktiler Aktin-Myosin-Netzwerke in der Anterior-, Posterioren-Achse eine zentrale Rolle, bei der Trennung von Kopf und Rumpf in C. riparius, spielt. Darüber hinaus konnte ich, durch das Aufdecken von markanten Teilungen außerhalb der Ebene in der Kopfentwicklung von C. riparius, eine mutmaßlich analoge Funktion für die Cephale-Furche in höheren Fliegen feststellen, da in beiden Fällen eine Anzahl von Zellen unter die Embryooberfläche sinkt. Zusammenfassend befasst sich meine Dissertation mit der Variation von Strategien zur Trennung von Kopf und Rumpf, die zugrunde liegende Genetik und deren Implementierung auf zellulärer, Gewebe- und embryonaler Ebene bei Dipteren-Fliegen.

Contents

1 INTRODUCTION

The humans and flies shared their last common ancestor about 500 million years ago (Knoll and Carroll, 1999). All bilaterian animals that derived from this common ancestor, and likely including the common ancestor itself, display a subdivision of the body plan into head and trunk. Such a universal phenomenon among bilaterian animals is implemented via head-trunk separation mechanisms during early embryonic development. One powerful model system to study head-trunk separation mechanisms is the early fly development. The fruit fly *Drosophila melanogaster* has been vastly studied over the decades, thereby becoming the main reference model organism for animal morphogenesis studies. For tissue separation research, the *D. melanogaster* embryo has also represented a well-defined framework where both morphological and genetic aspects of boundary formation can be studied (Lawrence et al., 1987; Martinez-Arias and Lawrence, 1985). Since differences of *D. melanogaster* development to satellite fly species have also been well-described over the recent years, it allows us attempt to decipher the diversity of head-trunk separation during development. For instance, some derived lineages of dipteran flies separate developing head from trunk by an epithelial infolding event, called the cephalic furrow (CF) formation. Most insects however do not form the CF, nonetheless, accomplish bisecting the embryonic body plan. While the *D. melanogaster* and its distantly related dipteran relative *Megaselia abdita* employ the CF formation, basal non-cyclorrhaphan *Chironomus riparius* naturally lacks the CF (Figure 1). As a foundation to unravel the cell-biological and genetic basis of the divergence of head-trunk separation mechanisms, in my thesis I studied the early fly development with or without head fold formations.

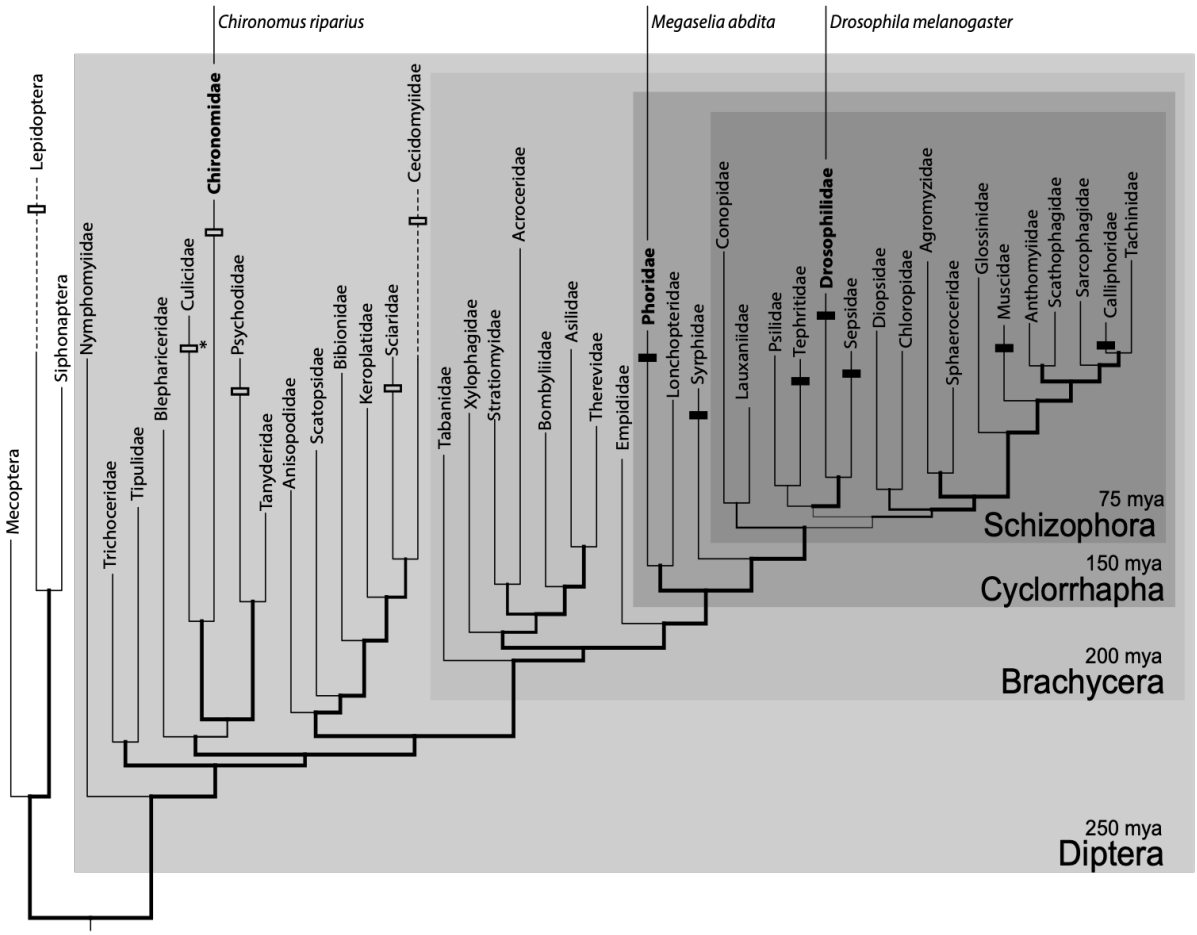

Figure 1. Phylogenetic tree of dipteran flies and outgroups. Three fly species that were subjected in this project are indicated in italics, and the corresponding families are written in bold (*Chironomus riparius* (Chironomidae); *Megaselia abdita* (Phoridae); *Drosophila melanogaster* (Drosophilidae). Black boxes denote the fly families that were identified for the presence cephalic furrow formation during embryonic development. (Steffen Lemke, unpublished data). The tree was adapted from Wiegmann, 2011. (Mya: million years ago)

1.1 Head-trunk separation in animals

Animal body plan is mainly established during early embryonic development. It has been largely acknowledged that similar anteroposterior (AP) and dorsoventral (DV) organizations, albeit inverted in DV, are found in insects and vertebrates (reviewed in (De Robertis and Sasai, 1996)). In addition to the similar overall animal plan, head and trunk development also exhibit striking resemblance between insects and vertebrates. Among all bilaterian organisms, the trunk specification is controlled by *Hox* activity, which is regulated by upstream gap and pair-rule gene network. Different combinations of *Hox* activity assigns different identities to different segments (Kmita, 2003). Interestingly, anterior head development is not *Hox*-dependent, but regulated by a paired-type homeodomain-containing transcription factor called Orthodenticle (Otd). *Otd* in arthropods and its vertebrate homologous gene *Otx* share remarkable sequence similarity, indicating high degree of conservation (Reichert and Simeone, 1999). In addition, the Drosophila Otd protein have been found to rescue *Otx* mutant mice and vice versa (Acampora et al., 2001; 2000; Leuzinger et al., 1998).

Whether such a commonality is also found at head-trunk separation boundaries in flies and vertebrates has been subjected to debate (L. Z. Holland and N. D. Holland, 1999). At the large morphological level, a homologous head-to-trunk transition zone can be suggested as a hinge domain in some flies and vertebrates, characterized by infolding of the tissue surface, i.e. the cephalic furrow in the *Drosophila* epidermis and the mid-hindbrain vesicles in the central nervous system (CNS) of vertebrates. Previous reports however indicated obvious differences in these regions between insects and vertebrates, that weakened this hypothesis. For instance, at the mid-hindbrain boundary, head and trunk patterning systems were reported to not overlap, as in *D. melanogaster* (Hartmann and Reichert, 1998; Hirth et al., 1998). Therefore, another junction in the caudal hindbrain instead was put forward as the reminiscent of the CF in *Drosophila,* due to similar overlap of patterning systems. At this domain gap-like genes (i.e. *krox-*

20) and *Hox* genes are co-expressed; and as a result, an analogous overlap of patterning systems was found (Schneider-Maunoury et al., 1993; Swiatek and Gridley, 1993). Recent studies in mice, zebrafish and flies, however, confirmed utilization of homologous genes to control mid- hindbrain boundary formation and the CF formation. For example, the vertebrate homolog of *Drosophila* gene *buttonhead (btd)* acts in a similar way, integrating the head and trunk segmentation at the head-trunk boundary in zebrafish (Tallafuss et al., 2001) and mice (Treichel et al., 2003). Evolutionary implications of these studies suggest a genetic convergence step, possibly responsible for the formation of analogous head-trunk separation strategies during the animal morphogenesis.

1.2 Mechanisms of tissue separation

A key step during early development is the subdivision of initially homogeneous fields of cells into domains, which then lead to distinct fates and functions of these tissues. Gene regulatory networks has been shown to be adequate to define and organize these distinct domains *in silico* (Oliveri et al., 2008). In addition to having a particular fate; however, cells divide, change their shapes and migrate *in vivo*. Thus, cells must change their physical features continuously to adapt to their environment in a dynamic manner during development. In addition, as result of mitotic divisions and large-scale migration events, cells are inclined to intermingle during development. Opposing this tendency to mix, there are crucial mechanisms that provide physical separation between cell populations which are called tissue separation boundaries. In developing epithelium, cells cannot undertake limitless shape changes, due to its tightly packed organization. In addition, epithelial cells must comply with the physical constraints, in harmony with neighboring cells and tissues. By delimiting cell shape changes in local subdomains which are controlled in a coordinated manner, tissue separation mechanisms therefore undertake a crucial role during morphogenesis. Such

separation of embryonic cell populations is fundamental to the metazoan development (Dahmann et al., 2011; Tepass, 2002).

During embryonic development, these boundaries can arise before the tissue differentiation takes place. For example, embryonic tissue separation boundaries can be formed while the cell morphology on two neighboring domains is not readily discernable. A number of embryonic boundaries have been identified so far: ectoderm-mesoderm boundary in frogs (Rohani et al., 2011) and in fish (Kimmel et al., 1995), rhombomere boundaries during the hindbrain segmentation in chicken (Guthrie and Lumsden, 1991); and, most notably, parasegment (Lawrence et al., 1987) and imaginal disc boundaries (García-Bellido et al., 1973) in the fruit fly *Drosophila melanogaster.*. Defects at embryonic boundaries can cause detrimental effects. For instance, in humans defects at compartment boundaries are thought to induce malignant invasion and congenital defects (Davy et al., 2006; Pomares and Foty, 2006; Twigg et al., 2004).

There have been several models proposed to explain tissue separation mechanisms. Earlier explanations stemmed from cell-sorting experiments in sponges (Wilson, 1907), chicken (A. Moscona and H. Moscona, 1952) and amphibians (Townes and Holtfreter, 1955) where cells taken from different embryonic tissues were mixed-up in aggregates, which then sorted itself into segregated cell populations. These studies suggested that cells were able to maintain their identity when surrounded by other types of cells via their basic property called as ‘cell affinity’ (Holtfreter, 1939). Later this basic idea of cell affinity was broadened with including physical principle of surface tension (Differential Adhesion Hypothesis; (Steinberg, 1970)). Subsequently, theoretical ideas structured around cortical tension emerged as being an important factor in boundary formation (Harris, 1976). *In vivo* evidence for this came from *Drosophila* studies. For example, during wing imaginal disc formation, increased accumulation of myosin and actin proteins was identified at the dorsoventral (Major and Irvine, 2005) and anteroposterior boundaries (Landsberg et al., 2009). Recently, such regulation of the cytoskeleton has also been found to establish compartment

boundaries in early *Drosophila* embryo, namely parasegment boundaries (Monier et al., 2010).

1.3 Head and trunk development in insects

The head is the sensory and feeding center of the fly body plan. The *Drosophila* embryo has a highly evolved head structure among other arthropod embryos. Arthropods (e.g. insects) and annelids (e.g. earthworms) share similarities during development, such as having segmental units, that are also known as

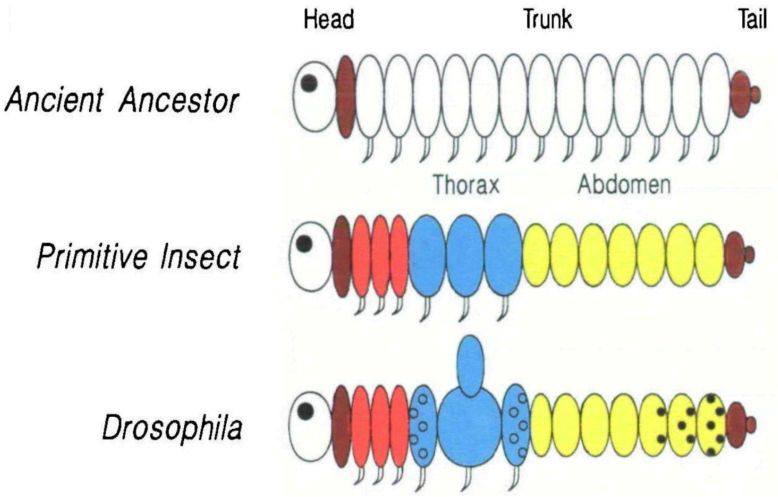

Figure 2. A schematic representation of evolution of Drosophila body plan. Ancestral body plan (Articulate 'common ancestor' of annelids and arthropods) was composed of structurally equivalent segments. Primitive insects incorporated anterior trunk segment in the head (cephalization; red segments). In derived lineage of Drosophila, further specification of the segments lead to the separation of head, thorax (blue) and abdomen (yellow) and tail (Adapted from 3Akam et al 1988, Filkelstein et al 1991).

metameric subunits, which were proposed to be simply body divisions of the embryo (Snodgrass, 1935). As a result of this early understanding of metameric

body organization, and as well as widely accepted 'Articulata hypothesis' at the time, that put annelids and arthropods as sister groups (Cuvier, 1817), following studies in *Drosophila* embryo mostly focused on the development of the central, explicitly segmented trunk. In contrast to annelids, however, these metameric characteristics are less apparent in the embryonic head regions. Thereby, embryonic head development among dipteran flies in general was rather understudied until recently, when identification of genes responsible for head development were achieved (Cohen and Jürgens, 1990a; Finklstein and Perrimon, 1990; Schmidt-Ott et al., 1994; Wimmer et al., 1995). Concomitantly, even less is now known for how the head is partitioned off the rest of the developing body in flies.

Evolution of head formation involves an important morphogenetic innovation called 'cephalization' which implies the addition of anterior trunk structures into head region (Snodgrass, 1935; Weber, 1966). During the course of fly evolution, segments added to head region undertook specialized roles contributing to head formation (Figure 2). Namely, procephalon which is found anterior to the mount parts assumed a more sensory role (antennal, intercalary segments, and the ocular region); gnathocephalon is built by three segments (mandibular, maxillary and labial) which are the appendages surrounding the mouth opening, therefore undertaking feeding roles. Except for the mandibular segment, other gnathocephalon segments were found to be patterned like trunk segments (Vincent et al., 1997). Likewise, trunk region has become subdivided into thoracic and abdominal segments during evolution, according to the well-documented hierarchical cascade involving maternally deposited coordinate genes; and zygotic gap, pair-rule and segment polarity genes (St Johnston and Nüsslein-Volhard, 1992). Further specialization of head and trunk regions constitutes the overall fly body plan.

Currently, most insights into insect genetic patterning derive from studies in *D. melanogaster.* A maternally deposited anterior morphogen bicoid (bcd) leads to the activation of head gap genes *empty spiracles (ems), orthodenticle (otd)* and *buttonhead (btd).* Interestingly, the *bcd* gene is only found in higher dipterans (Lynch and Desplan, 2003; McGregor, 2005; Sommer and Tautz, 1991; Stauber et

al., 1999). For instance, another gene named *panish* was reported to provide head-to-tail polarity in basal non-cyclorrhaphan midge *C. riparius* (Klomp et al., 2015). In addition, the outgroup insect flour beetle *Tribolium castaneum* was reported to have no *bcd* homologue isolated (Brown et al., 2001). Under this genetic patterning, the core cellular events shaping up the embryonic fly head are mitotic divisions (Guillot and Lecuit, 2013). There are several mitotic domains identified in the D. melanogaster, which become active soon after the gastrulation starts (Foe, 1989).

The trunk development in *D. melanogaster*, on the other hand, is mainly characterized by the germband elongation which is driven by cell intercalation events (Irvine and Wieschaus, 1994). Cells first converge in the dorsoventral axis, which is then followed by their resolution in the anteroposterior axis. This movement of the trunk cells constitutes the convergent extension. The genetic patterning of such dynamic cell neighbor exchange events in trunk have been found to be tightly regulated by the pair-rule genes (St Johnston and Nüsslein-Volhard, 1992).

1.4 General morphogenetic events in *D. melanogaster* early development

In *D. melanogaster* and other flies, prior to gastrulation, the nuclei divide multiple times constituting a syncytium (Campos-Ortega and Hartenstein, 1997). After the 8th nuclear division in *D. melanogaster* embryo, nuclei start to migrate to the periphery (Foe and Alberts, 1983). During the 14th division cycle, nuclei on the periphery elongate and simultaneously plasma membrane starts descending around the nuclei, thereby establishing the first epithelium cellular blastoderm (approx. 6000 cells) (Foe and Alberts 1983). Once blastoderm forms, gastrulation starts in the embryo. At the onset of gastrulation, two infolding events occur, namely the ventral furrow and the cephalic furrow formations (Turner and Mahowald, 1977). While the VF formation eventually give rise to the mesoderm (Leptin et al., 1992; Thisse et al., 1988), invaginated cells of the CF retracts back to the embryo surface

in later stages, contributing to the ectoderm (Campos-Ortega and Hartenstein, 1997; Turner and Mahowald, 1977). Shortly after the onset of gastrulation, germband extends posteriorly and folds dorsally, anterior and posterior midgut precursors invaginate, and the mesoderm internalizes along most of the ventral midline (Anderson, 1966). As a result of gastrulation that comprises the first large-scale morphogenetic processes in the forming of a fly that result in three cell layers: the endoderm, mesoderm and ectoderm.

1.5 Head-Trunk Separation in *D. melanogaster*: Cephalic Furrow Formation

The CF starts forming as a shallow groove each lateral side of the embryo, along the dorsoventral axis (Turner and Mahowald, 1977). Then, it extends ventrally and dorsally to eventually form a complete ring that demarcates the embryonic head region from the trunk region (Figure 3.). Unlike other infolding events in gastrulating embryo, the CF formation starts with shortening of a row of cells, known as the initiator cells (Spencer et al., 2015; Vincent et al., 1997).

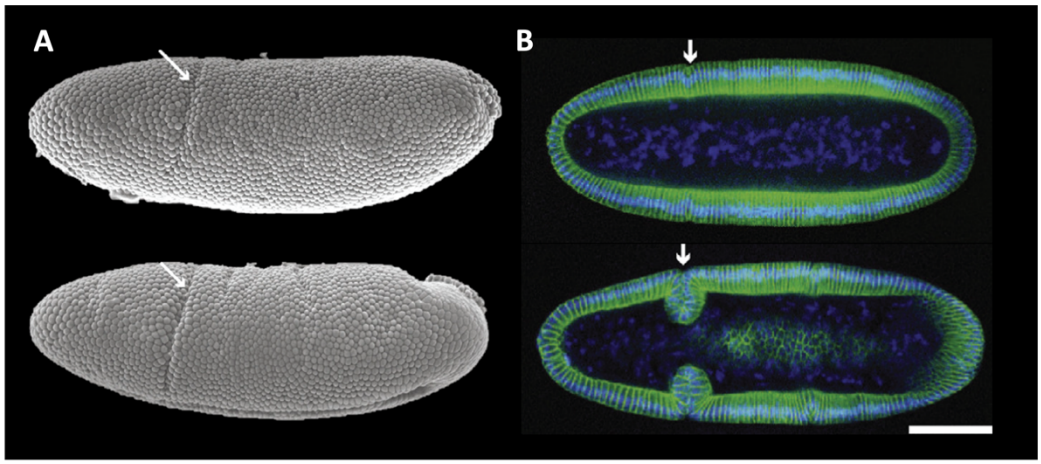

Figure 3. Initiation and progression of the CF formation. A) Electron micrographs of lateral *D. melanogaster* embryo showing the CF initiation as a shallow groove. **B)** Confocal images of dorsal embryo (green, cell membrane; blue; nuclei). Scale bar:20µm. Adapted from (Spencer et al., 2015).

By the end of stage 7, the furrow becomes deepened around the embryo and tilted by extending germband posterodorsally and anteroventrally. Meanwhile, the initiator cells change their columnar shapes to adopt a wedge-like shape via cell shortening coupled with basal expansion. Subsequently, cells adjacent to the initiator cells roll over into the deepening cleft, further deepening the furrow (Costa et al., 1993; Vincent et al., 1997). Starting in stage 8, cell divisions in the invaginated furrow further deepens the overall structure (Foe, 1989). After germband extension has completed by stage 11, the CF cells retract to the embryo surface (Turner and Mahowald, 1977).

1.5.1 Genetics of Head-Trunk Separation in *D. melanogaster*

In *D. melanogaster*, the cephalic furrow formation has been found to spatially coincide with the juxtaposition of head segmentation and trunk segmentation patterning systems (Vincent et al., 1997). In particular, the CF formation requires the spatially coinciding activity of two transcription factors, Even-skipped (Eve) and Buttonhead (Btd). *eve* is a primary pair-rule gene, which is expressed in 7 transverse stripes along the anteroposterior axis, and it regulates the segmentation of the embryonic trunk (Harding et al., 1986). Together with other pair-rule genes, *eve* attributes regional identity to the cells as early as blastoderm stage. *btd* is a head gap gene that is important in head patterning (Cohen and Jürgens, 1990b). Co-expression of *eve* and *btd* overlap in in *eve* stripe 1, which defines the initiator cells of the CF formation. Among the initiator cells, btd activity has been found upregulate *eve*-stripe-1 expression (Vincent et al., 1997). The control of *eve* expression by btd represents the first indication of a novel integrated regulation of two fundamental patterning systems (head and trunk) in *Drosophila* embryogenesis. However, the downstream genetic networks of this novel integration of patterning systems are yet to be clarified.

Despite being a prime model to study tissue separation mechanisms and its early formation of the CF, *D. melanogaster* has not been particularly suitable for investigating the head-trunk separation among flies, except for the invaluable genetic description. Due to the deep nature of the CF and extensive cell migration activity in the embryo, suboptimal imaging capabilities had prevented to thoroughly determine tissue dynamics generating the head-trunk separation. As the *in toto* imaging (i.e. Light-sheet microscopy) drastically progressed in recent years, we are now capable of comparing the CF formation in *D. melanogaster* and distant satellite species (i.e. *M. abdita)*. In addition, dipteran family of flies further provide the much-needed natural diversity to study the variation in head-trunk separation mechanisms, as the CF is found in only derived dipterans. To address this issue, several developmental issues must be considered: is the recruitment of homologous gene products in corresponding embryonic regions present? Can we characterize where the transition between head and trunk patterning systems lie via morphological cues? Is it possible to differentiate head cells from trunk cells? How is the boundary formation achieved at the cellular level? A comparative analysis of head-trunk separation among differently related dipteran flies will help us to evaluate the poorly understood variation of head-trunk separation mechanism in flies.

2 AIM

Tissue separation is achieved by sharp deliminations forming between different cell populations. Due to its early segmentation, *D. melanogaster* embryo can be resolved to single rows of cells (Sanson, 2001). Concomitantly, positions of tissue separation boundaries are stringently regulated by genetic patterning. One such tissue separation event is the head-trunk separation, which is recognizable as an epithelial infolding event (CF formation) in *D. melanogaster* embryo.

In the absence of such a visible separator (i.e. the CF), it remains unclear how the embryo is compartmentalized to head and trunk regions during early development. Analyses of dipteran fly embryos, which do not form a head fold during embryogenesis, but which are still receptive to molecular manipulations and imaging tools are critical to dissect the natural variation of head-trunk separation mechanisms. To address this question, I studied early development of basal non-cyclorrhaphan midge *C. riparius* and investigated divergent implications of head-trunk separation in comparison to the reference fruit fly *D. melanogaster* and its distant relative basal cyclorrhaphan scuttle fly *M. abdita*. In my thesis, I aimed quantify and analyze specific signatures of fly embryonic head and trunk cells, investigate probable genetic factors of underlying separation strategies, and examine how such a separation is achieved at the cellular, tissue and embryonic level.

3 RESULTS

In order to understand the evolution of head-trunk separation mechanisms in dipteran flies, in my thesis cell-biological and genetic aspects of early developmental stages were examined in flies with and without head fold formation.

3.1 Head and trunk development in *C. riparius*

3.1.1 Cell divisions in *C. riparius* embryonic head are primarily nonplanar

Mitotic domains that are activated after the onset of gastrulation are one of the main factors contributing to the morphogenesis early fly embryo(Foe, 1989; Momen-Roknabadi et al., 2016). Since, mitotic activity was also determined in C. riparius embryonic head before in our laboratory by antibody stainings (Laura Popp, Bsc thesis, 2014), I intended to reveal the dynamics of mitotic divisions that are likely to be involved in overall C. riparius morphogenesis.

Over the years in our laboratory, there have been generated different methods to visualize cellular components varying from injections of synthesized fluorophore tagged proteins to dye injection. In order to visualize the cell boundaries, Life-Act-GFP fluorophore tagged protein injection was the best proxy for cell shape and interface analyses for a long time. Towards the end my thesis project, I strongly benefitted from a new reporter construct, GAP43-mCherry, which allowed visualization of the cellular membrane, therefore the cell outline directly.

To quantify cell division dynamics in head region, I used GAP43-mCherry mRNA injection to reveal the cell outline in time-lapse recordings. My

initial results suggested that mitotic rounding was localized to the head region only, while the trunk cells were unaffected. Surprisingly, although nearly all mitotic cells in the head region were undergoing mitotic rounding, however, the division was completed by only a small fraction of cells. The overall cell number in the head region therefore remained almost the same from *en face* view. I hypothesized that if mitotic divisions were not taking place despite the mitotic rounding, then, the contractile actomyosin rings, that are a hallmark of mitotic division in animals, would not form. I predicted to observe contractile actomyosin rings appear as ribbons in few dividing cells, that were initially observed. In addition, I further hypothesized that if the seemingly nondividing cells were undergoing out-of-plane divisions, then, the actomyosin rings should appear as rings or ellipses from *en face* view. To visualize actomyosin ring formation, I used a *C. riparius* homolog of non-muscle myosinII (hereafter myosin) regulatory light chain-eGFP (MRLC-eGFP), together with LifeAct-mCherry (Figure 4). As expected, my analysis suggested that initially observed dividing cells were forming actomyosin rings which appeared as ribbons (Figure 4.A). Majority of cells in the head domain, however, turned out to divide nonplanarly (Figure 4.B-C). Subsequent to the mitotic rounding, an actomyosin ring started to form perpendicular the apicobasal axis compressing the cell laterally and thus forming deepening hinges in these nonplanarly dividing cells (Figure 4.B). As the division progressed, the cytokinetic actomyosin ring gradually closed, finally separating two daughter cells from each other. Daughter cells were found in a stacked-up configuration: one daughter cell laying in the plane of epithelium like the mother cell, the other daughter cell was found basally. Time-lapse recordings further suggested that the basally lying daughter cells remained underneath the plane of epithelium for a period of time until large-scale cell flow occurred.

One plausible reason for out-of-plane divisions could be tightly packed organization of the embryonic head. In this case, I hypothesized that the planar cell divisions would take place earlier, possibly crowding the head region, and therefore, nonplanar divisions would occur only after. To test this idea, cells divisions were needed to be backtracked. My results suggested that the first

divisions were of nonplanar type, while planar divisions occurred later (Figure 4.C., magenta-shaded and yellow cells, respectively). Strikingly, in all three embryos the

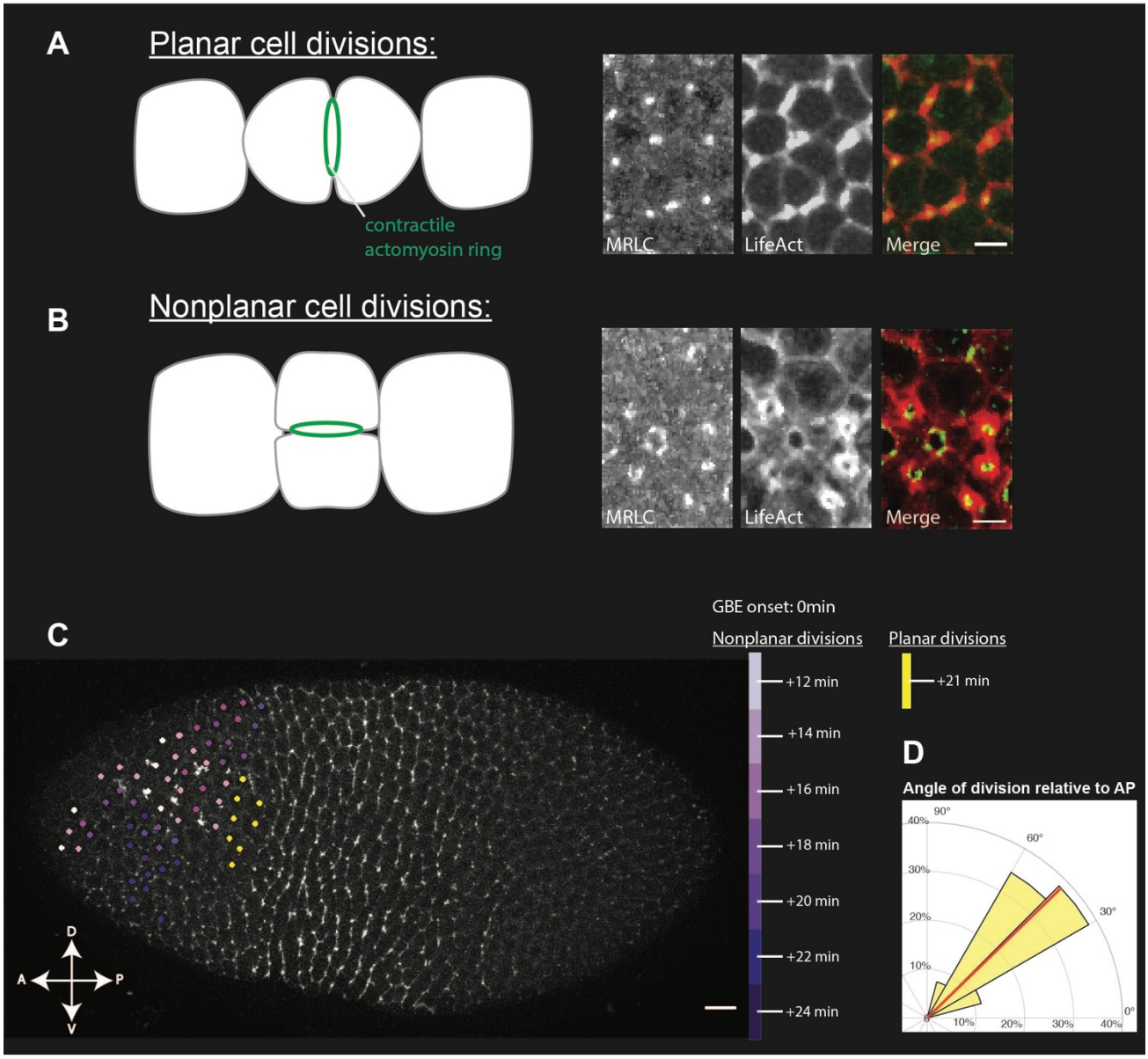

Figure 4: **Nonplanar cell division are prevalent in *C. riparius* embryonic head. A, B)** Left: Schematic illustrating planar (**A**), and nonplanar (**B**) cell divisions. Right: Still images of dividing cells labeled with non-muscle MyoII RLC (green) and LifeAct (red). During planar cell divisions actomyosin ring appear as a ribbon (**A**) and a ring (**B**) from top view (Scale bar=5µm). **C)** Nonplanar divisions (magenta) are more abundant in the embryonic head. Planar divisions (yellow) are only observed adjacent to the trunk (scale bar=10µm). **D)** Cell division angles of planarly dividing cells relative to AP axis. Red line shows the median angle (n= 3 embryos, 24 divisions).

few planar divisions were found adjacent on the interface between embryonic head and trunk (Figure 4.C, yellow cells).

To test whether spatial distribution of the planarly dividing cells were affected by the head-trunk interface organization, angles at which the actomyosin rings relative to anteroposterior axis were than quantified to measure division orientation for planarly dividing cells. My analysis of division angles showed that planar divisions mainly took place in an oblique orientation (between 60°-90° relative to the AP axis; n=24 division in 3 embryos) relative to the AP axis (Figure 4.D).

3.1.2 Apical cell area increases across head region, unlike head-trunk interface and trunk in *C. riparius*

Apical cell area has been previously shown to be related to overall tissue organization (Gutiérrez et al., 2016). In order to have a systematic overview of apical cell area change over time, time-lapse recordings of *C. riparius* embryos injected with GAP43-eGFP mRNA were analyzed. Since, the over-time examination of change in apical area of single cells required tracking of cells, I used the SEGGA software (Farrell et al., 2017) with modifications. By using this software, the cells in the anterior half of the embryo was segmented and the area change was normalized to the blastoderm-stage embryo.

Apical cell area was quantified for approximately 60 cells in the lateral embryo, spanning from embryonic head to the middle embryonic trunk over time (Figure 5). Cells were then color-coded with masks depending on their apical area at successive timepoints (Figure 5.A). Before the onset of germband extension, cells did not differ notably in their apical areas along the anteroposterior axis. My analyses showed that cells of different regions obtained distinctive apical cell areas at 15 min after the onset of germband extension (Figure 5.A-B). Identifying individual cells and plotting their normalized apical cell area over time together corroborated distinct cell populations according to apical cell area.

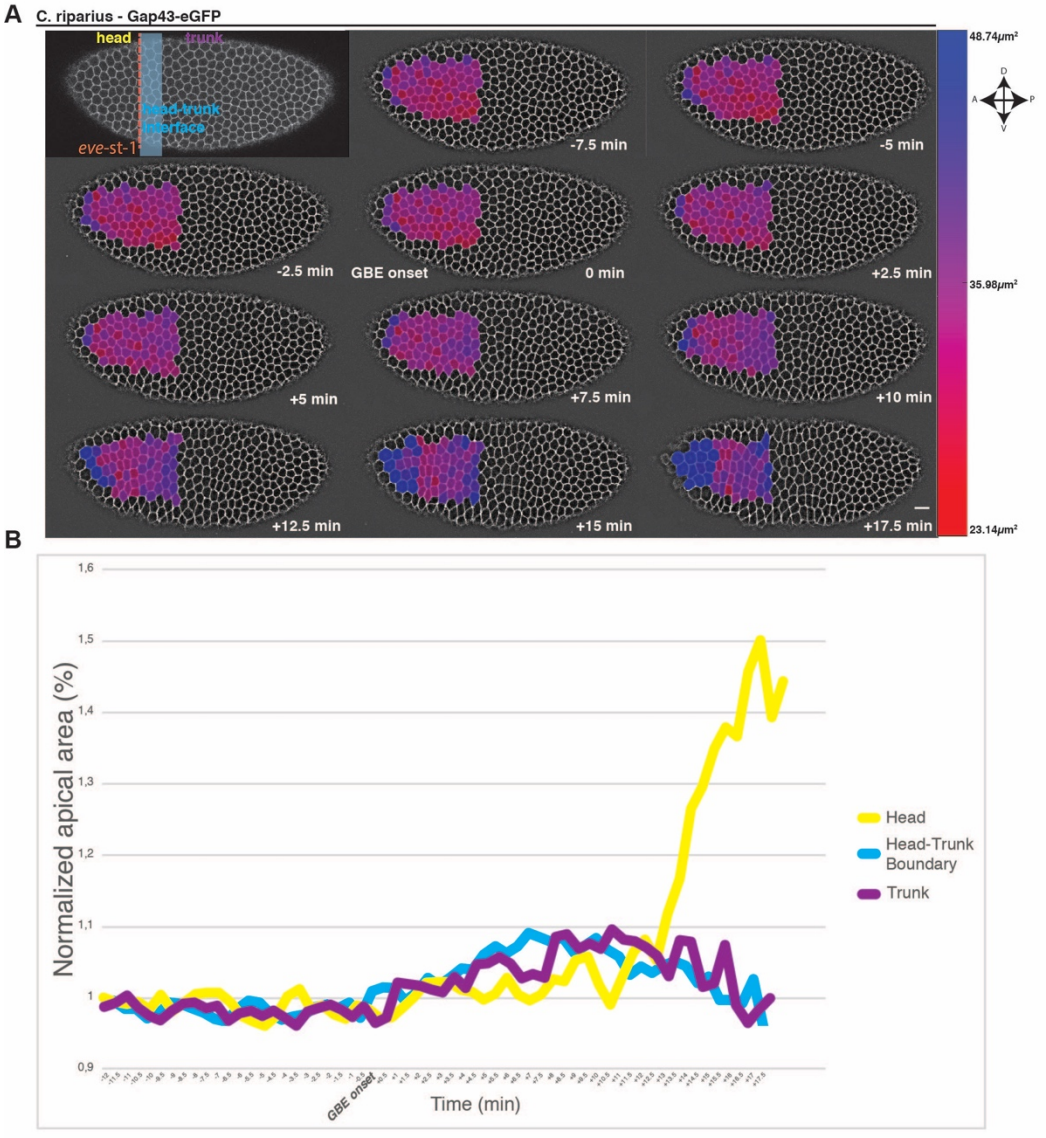

Figure 5: Apical area of embryonic head cells drastically increase in comparison to trunk cells in *C.riparius*: **A**) Snapshots of GAP43-eGFP injected embryo over time (GBE onset= 0 min). Cells are color-coded depending on their apical area size (Scale bar: 10µm). In panel 1, *eve*-stripe-1 (orange dashed line) was shown as a anterior trunk marker; blue shaded area is the presumptive head-trunk interface. **B**) Change in apical cell area normalized to blastoderm-stage measurement. Head (yellow), head-trunk boundary (cyan) and trunk cells (magenta) were identified via their anteroposterior positioning.

While embryonic head cells enlarged, head-trunk boundary cells and trunk cells largely maintained their apical areas (Figure 5.B). At 20min after the onset of germband extension, embryonic head cells reached a 1.5 fold-increase in apical area (Figure 5.B).

3.1.3 Planar cell organization show major differences between head and trunk regions in *C. riparius* embryo

In order to make a complete wild type description of tissue characteristics of head and trunk regions in *C. riparius*, I further interrogated planar cell organization patterns in the blastoderm and early gastrulation stage embryonic development. To survey planar cell organization patterns, I took advantage of the GAP43-mCherry mRNA injections again so that cell membrane interfaces across head and trunk regions could be visualized over time. Initial qualitative analysis on the surface view indicated distinct types of cell alignment patterns in head and trunk regions when germband extension started. The degree of membrane alignment was quantified by measuring straightness index (SI). The straighter the row of cell interfaces, the closer the SI to 0 (IS=0 corresponds to a straight line). Before the onset of germband extension, the membrane interfaces had comparable straightness indices (Figure 6). Trunk cells formed straighter lines adjoining membrane interfaces in the DV axis (AP interfaces), at the onset of germband extension ($p<0.005$; Figure 6.B). Four minutes into the germband extension, the difference in interface straightness indices became further significant ($p<0.0005$; Figure 6.B).

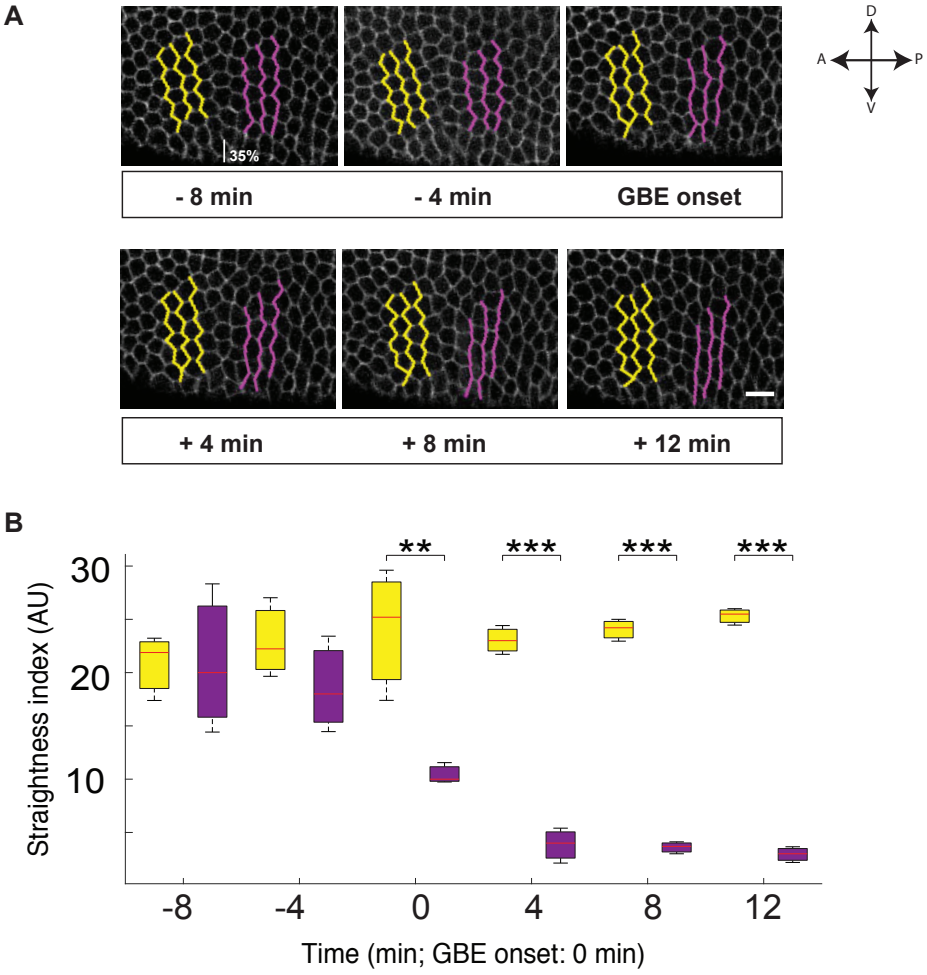

Figure 6. Membrane straightness at AP interfaces in *C. riparius* embryonic head and trunk significantly differs. **A)** Cropped snapshots of GAP43-eGFP injected embryo over time (Scale bar: 10 µm). Yellow and magenta lines represent head and trunk cell interfaces, respectively. **B)** Straightness index (SI=0 corresponds to a straight line) of head (yellow) and trunk (magenta) interfaces first significantly differed at the onset of germband extension stage and increased further over time (**, $p < 0.005$; ***, $p < 0.0005$). (n=3 embryos,18 interfaces).

3.1.4 Cell shape isotropy remains stable across embryonic head to trunk cells during *C. riparius'* early gastrulation

In addition to the aforementioned distinctive features of cell and tissue behavior in anterior half of *C.riparius* embryo, I further investigated another feature of tissue packing which is cell shape isotropy. The deformation to cell shape isotropy indicates whether cells gain or lose their neighbors over time. Hence, it can be used as a proxy for cell rearrangement events, and therefore cytoskeletal rearrangements. My analysis which covered blastoderm stage, onset of gastrulation and early gastrulation stages, allowed me to compare whether there were any alterations to cells shape between embryonic head, head-trunk boundary and trunk. In Figure 7, normalized quantifications cell shape isotropies are plotted over time. Overall, cell shape isotropy was largely preserved over time in anterior half of the embryo, especially before the onset of germband extension. During these early stages, cells maintained their relative positions and did not undergo neighbor changes keeping their hexagonal patterns. After the onset of germband extension, change events became notable in head-trunk boundary and trunk regions. Nevertheless, it is important to note that of head cells maintained their isotropic hexagonal patterns

.

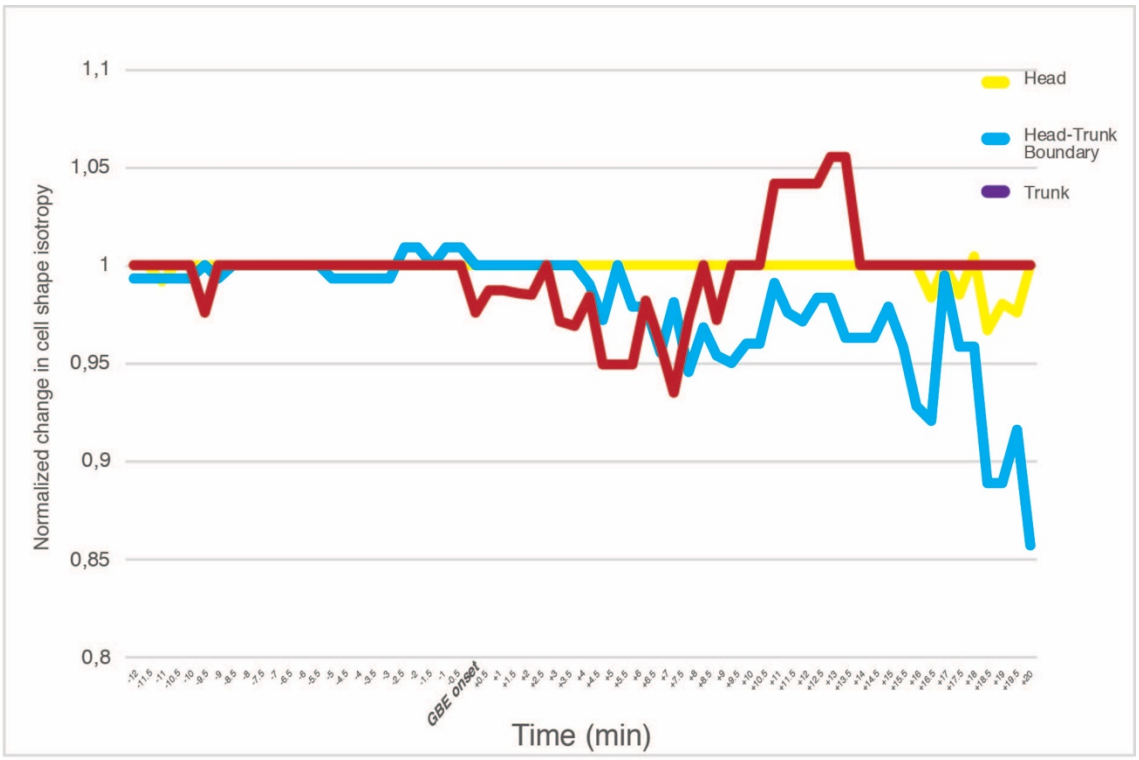

Figure 7. Changes in cell shape isotropy in head, head-trunk boundary and trunk domains during *C.riparius'* early gastrulation. Graph showing deformations in cell shape isotropy values normalized to the blastoderm stage measurements over time. Isotropy value '1' indicates no alteration; while values '>1' show neighbor gain, values '<1' suggest neighbor loss. Embryonic head cells (yellow) maintained large their shape (hexagonal pattern; fold change< 0.03), while head-trunk boundary (cyan) and trunk (magenta) cells exhibited increased neighbor exchange behavior (fold change>0.05 and >0.15 for trunk and head-trunk boundary cells, respectively.).

3.2 Actomyosin network is differentially utilized between head and trunk regions in *C. riparius*

3.2.1 Myosin distribution is heterogeneous in AP and apicobasal axes in *C. riparius*

Taking together, my results above indicated that embryonic head and trunk development involved early distinctive features at the cellular and tissue level. These findings prompted me to interrogate the differential changes in actomyosin networks, that are likely realizing a separatory behavior between these two remarkably distinct tissues. This not only could give insights in the cell-biology of a basal head-trunk separation boundary, but also could reveal more about the commencement of specific tissue properties between head and trunk regions, which are thought to be largely similar at the blastoderm stage. Therefore, I further interrogated the role of myosin which is known for its function as a molecular motor, generating contractility.

To visualize myosin localization dynamics in a high spatiotemporal manner, embryonic region spanning from 25% to 45% EL was selected so that head, head-trunk interface and trunk regions were included in kymograph analyses (Figure 8.). During cellularization, myosin was not found planarly polarized in *C. riparius* (Figure 8.A-A'). Cross section view suggested that myosin was highly enriched at basal side of the cell at the end of cellularization (Figure 8.A''). After gastrulation started, in accordance with the increasing membrane straightness shown in Figure 3, myosin cables started forming perpendicular to AP axis in the trunk region, extending in the DV axis (Figure 8.B-B'). Interestingly, cross section view revealed heterogeneity in distribution of myosin along the AP axis as well as apicobasal axis (Figure 8.B'').

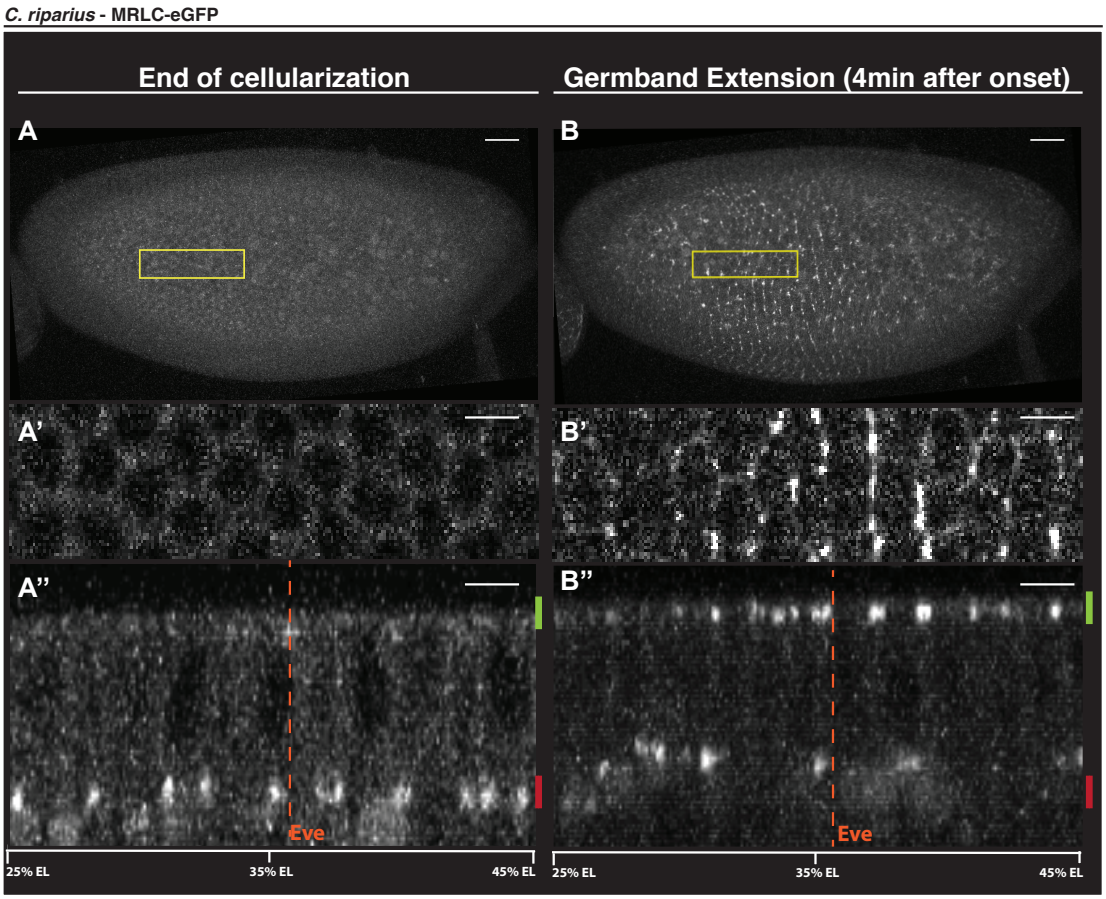

Figure 8. MyoII accumulation shows spatial differences between the head and trunk regions after the onset of germband extension in *C.riparius*. A) At the end of cellularization, apical myosin accumulation was not detected throughout the embryo surface. **A'**) Close-up view of subdomain (yellow rectangle in **A**). **A'')** Cross section view of **A'**: Myosin accumulation was found only basally. **B)** After the onset of germband extension, myosin signal was detectable in the embryo surface view. **B')** Close-up view of subdomain (yellow rectangle in **B**). **B'')** Cross section view of **B':** Basal myosin signal was visibly lower; and, apical myosin localization is visible although not homogeneous in anteroposterior axis. Subdomains denoted with yellow rectangles (**A,B)** were positioned from 25% to 45% EL, to include cells of embryonic head and trunk regions. Orange dashed lines show where the anteriormost stripe of *eve*, which is used as a trunk marker, is found. Scale bars: 10µm (**A,B)**; 5µm (**A',A''- B',B'')**. Anterior to the left, posterior to the right.

So as to precisely determine the positioning of the differential myosin localization in AP axis over time, kymographs for two separate myosin sub-pools (subapical and subbasal; shown in Figure 8.) were constructed (Figure 9). Kymograph analyses exhibited that subapical myosin accumulation was only present in embryonic trunk, with anteriormost signal detected at 34% EL. This finding was in line with my finding on localization of *eve*-stripe-1 as a trunk marker, which was approximately 35-36% EL (data not shown). Taken together, myosin activity and the front end of *eve*-stripe-1 pointed out a close spatial overlap. Furthermore, a decrease in subbasal myosin pool in trunk region was noticeable. This finding could indicate a shift in myosin localization from basal to apical in trunk cells (Figure 9.A). On the other hand, subapical myosin localization lacked in head region during cellularization as well as early germband extension stages. In Figure 9.B, a weak subbasal myosin signal intensity was detected between 60 and 30 min before the onset of GBE, which showed the actomyosin rings invaginating with the furrow canals durin cellularization. With the onset of gastrulation, subbasal myosin signal was re-detected in head region (Figure 9.B) which preceded the incoming mitotic division wave shown in Figure 4. In contrast to head region, subbasal myosin was not detected in trunk region. This result provided a clear distinction in myosin localization between head and trunk regions.

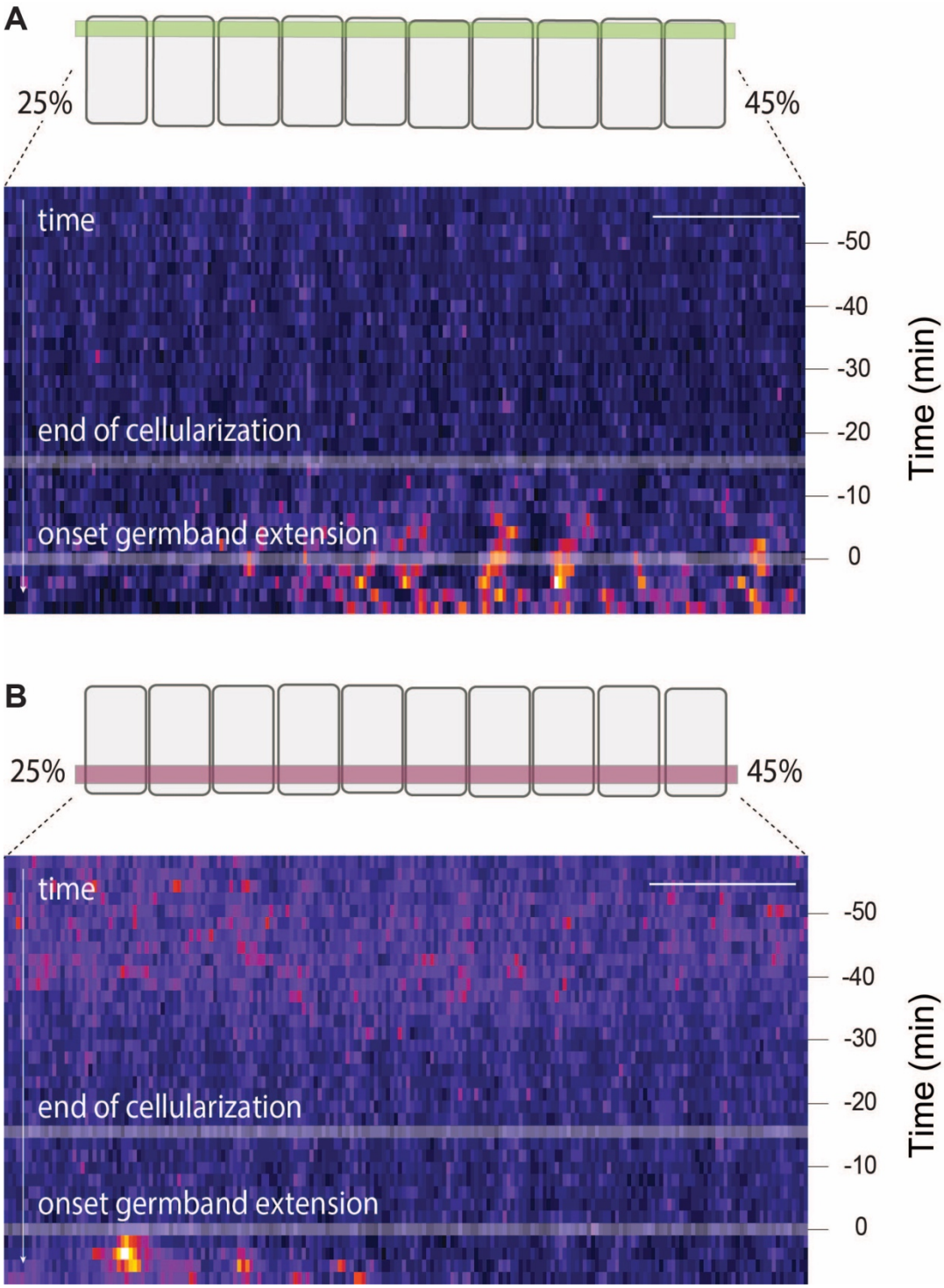

Figure 9. Kymographs showing myosin signal distribution in anteroposterior axis over time in embryonic head and trunk in *C. riparius*. MyoII accumulation in the subapical region (**A,** highlighted in green, also marked in Figure 5) showed a variation in anteroposterior axis. MyoII distribution was homogeneous in the subbasal region (**B,** highlighted in red, also marked in Figure5) until the mitotic divisions were detected in embryonic head**.** Domain of interest was positioned between 25% and 45% EL in AP, including head and trunk cells. Anterior to the left; posterior to the right.

3.2.2 Myosin activation in trunk region propagates in a stepwise manner towards the posterior end in *C. riparius*.

My analysis on myosin dynamics in anterior half of the embryo, led me notice another phenomenon which has not been documented in early fly development. Time-lapse recordings of myosin-eGPF mRNA injected *C. riparius* embryos showed a stepwise myosin activation in trunk region (Figure 10). In *C. riparius*, myosin signal first becomes detectable right after the onset of GBE, posterior to the embryonic head (Figure 10.A). At this stage (6min after the GBE onset), myosin signal is nonpolarized and rather short-formed intensifying around cell cortices. Activation of myosin cannot be further resolved into smaller domains as the commence of signal appearance takes places all at once in the domain. At 12 min-stage, first supracellular cables begin forming in the anterior part of the initiation domain (Figure 10.A). The number and length of supracellular cables increased over time along the extending germband (data not shown). As seen in the initiation domain, nonpolarized cortical myosin accumulation preceded the supracellular myosin cable formation. Since the cells largely maintained their relative positions in the anteroposterior axis, it was not necessary to specifically factor out cell position in the analysis. Instead, myosin activation wave was tracked in relation to EL. Nevertheless, there was a slight shift of the anteriormost myosin signal in stages 24-min and 30-min after the GBE onset (Figure 10.A).

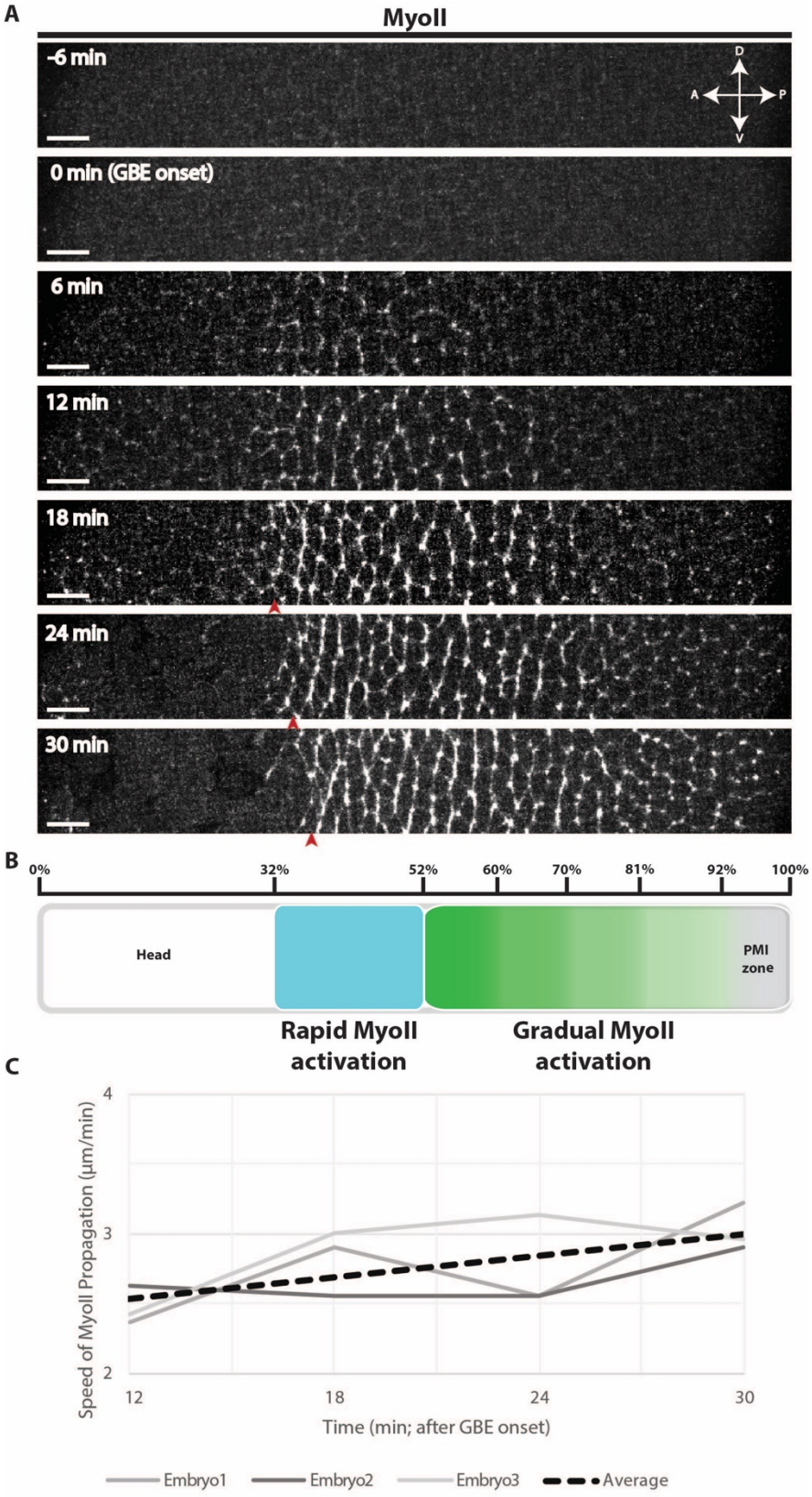

Figure 10. MyoII activation propagates in a wave-like manner during morphogenesis of the germband. **A)** MyoII activation at different timepoints, starting from 6 min before the onset of GBE, until 30 min after the GBE onset. **B)** Schematic representation of MyoII activation among the AP axis. Rapid MyoII activation zone ranged from 32% to 52% EL, exhibiting prompt MyoII accumulation. Gradual MyoII activation zone is divided into approximately four sub-zones, which were activated in 6-min-intervals. **C)** Speed of MyoII propagation in the gradual activation zone in three embryos. Dashed line shows the average speed (2.5-3µm/min); straight lines indicate separate embryos. Arrowheads show the posterior shift of the anterior most MyoII signal. (PMI: Posterior midgut invagination).

Previously in the lab, the speed of GBE was found to be approximately 2.5μm/min (Silvia Urbansky, Phd Thesis, 2016). Hence, it would be appropriate to hypothesized that the speed of myosin activation wave could be somewhat similar, as a driver for cell intercalation events. Therefore, the speed of myosin propagation was calculated in the gradual activation zone, starting from approximately 52% EL towards the posterior pole (Figure 10.B). The myosin activation wave front was identified by surpassing a threshold level. Strikingly, the speed of the myosin activation wave was found to be 2.5-3μm/min, which corresponds to ~1 cell per min (Figure 10.C), and closely coincided with the previously suggested speed of the GBE.

3.3 Head-Trunk Separation in *M. abdita* and *D. melanogaster*

After shedding light into how a basal non-cyclorrhaphan fly could render head-trunk separation in the absence of a physical folding event, I further interrogated two flies that are known to form the CF, which are a basal cyclorrhaphan scuttle fly *M. abdita* and a derived cyclorrhaphan fruit fly *D. melanogaster*. Since head-trunk separation mechanisms have changed drastically during the course of dipteran evolution, I hypothesized that I could find insightful new evidence that could improve our understanding of head-trunk mechanism in flies. Therefore, I address the following two questions: i) whether the embryonic domains that contribute to the CF formation were comparable between *M. abdita* and *D. melanogaster*; ii) whether formation dynamics of the CF was conserved or re-invented among distant dipteran flies.

3.3.1 Fate mapping on in toto-imaged embryos reveal distinct head-trunk separation domain shapes and formation dynamics between *M. abdita* and *D. melanogaster*

The cephalic furrow formation is a type of epithelial infolding event that has been observed in higher dipteran flies (Figure 1). To this date, our knowledge on how such a seemingly similar fold formation is achieved in evolutionarily distinct fly species was limited. To address this question, I investigated the CF formation dynamics in *M. abdita* and *D. melanogaster* (last common ancestor 150 mya; (Wiegmann et al., 2011)), where overall embryonic development is conserved and comparable (Wotton et al., 2014). For this purpose, I analyzed MuVI SPIM recordings that allow tracking individual cells of the embryo during gastrulation.

First of all, tissue domains that contributed to the CF formation was identified on the blastoderm stage embryo for both fly species. To achieve this, the cells delimiting anterior and posterior edges of the fully formed CF were backtracked in time. To do that, the timepoint at which the recruitment of surface cells into the CF formation stopped was determined. Then, a number of cells on each side of the mature CF were marked and tracked back to the blastoderm-stage embryo.

In *D. melanogaster* embryo*,* the CF domain appeared to be in the shape of a wide collar, maintaining its width in the vicinity of dorsal and ventral midlines (Figure 11.A, left panel). However, the CF domain in *M. abdita* embryo showed major differences: the number of cells found in the domain was lower overall and the domain was narrower along the DV axis; in addition, the shape of the domain was found to be reduced, approaching the dorsal and ventral midlines (Figure 11.B, left panel). Since overall morphology and size of the CF domain differed between two fly species, I further investigated whether these different CF domains could be utilized in a conserved manner during furrow formation.

In order to underline the possible differences or similarities of the CF formation dynamics in *D. melanogaster* and *M. abdita*, I obtained 'uninvaginated' CF domain size over successive timepoints. The early CF formation was found to

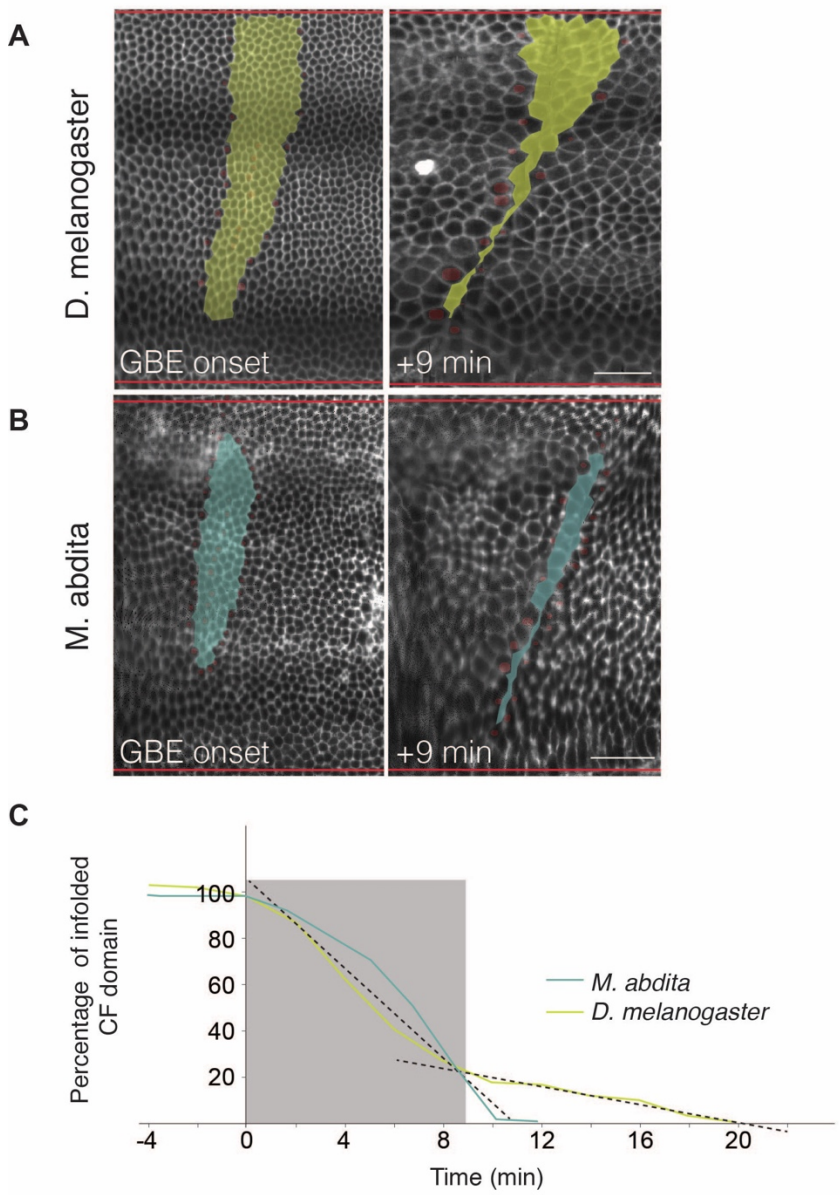

Figure 11. Cephalic furrow domains fatemapped to the blastoderm stage and their formation dynamics differ among *D. melanogaster* and *M. abdita*. A,B) Left panels: CF domains determined by backtracking SPIM movies to the blastoderm embryo. The CF domain of *D. melanogaster* **(A,** yellow**)** was found to be wider and longer than that of *M. abdita* **(B,** cyan**),** reaching dorsal midline unlike in *M. abdita.* Right panels: remaining domains to be invaginated 9 min after the onset of germband extension. Upper and lower red lines denote dorsal and ventral midlines, respectively. **C)** Percantage of infolded cephalic furrow domain in *D. melanogaster* and *M.abdiate* over time. The CF formation in *M. abdita* was completed at 9 min after the onset of germband extenstion, in contrast to *D. melanogaster* where approximately 20% of the initial domain was to be infolded. Anterior to the left; posterior to the right. Scale bars: 10μm.

have a relatively higher formation (invagination) rate than the later stages (Figure 11.C, gray-shaded zone) for both fly species. 9 min after the initiation of CF formation, 80% of the initial domains were invaginated in both fly embryos. At this timepoint, the remaining uninvaginated domains showed size and shape differences, specifically a narrow strip of cells in *M. abdita* and dorsally and overall wider domain in *D. melanogaster* , that appeared reminiscent of initial domains (Figure 11.A-B; right panels). Moreover, the CF formation rate in *M. abdita* embryo was found to be distinctively uniform in the remaining duration of formation. At timepoint 10 min, *M. abdita* CF was fully formed (Figure 11.C, blue line). Unlike *M. abdita*, *D. melanogaster* embryo showed a two-phase formation dynamics, where the remaining 20% domain was fully invaginated at timepoint 20 min (Figure 11.C, yellow line).

3.3.2 Overlapping expression of *even-skipped* and *buttonhead* coincides with the CF formation in *M. abdita*

As early fly development shows precise genetic patterning which is very well defined in the reference *D. melanogaster,* these striking differences in shape and size of initial CF domains and their formation dynamics motivated me to further investigate the underlying genetic determinants of the process and their possible differences between *M. abdita* and *D. melanogaster.*

The head-trunk separation mechanism was found to be controlled by overlapping co-expression of two genes encoding transcription factors: a pair rule gene *even-skipped (eve)* and a head gap gene *buttonhead (btd)* in *D. melanogaster* (Vincent et al., 1997). In *D. melanogaster*, *eve* and *btd* are the only two genes which have been identified to be crucial for the CF formation. Likewise, *eve* or *btd* knockdown by RNAi had been shown to prevent the CF formation in *M.abdita* (Ozge Akbulut, Master thesis, 2015). To determine what could account for different

domain determination and formation dynamics of CF in *M. abdita* and *D. melanogaster* embryos*,* I first investigated the expression patterns of *eve* and *btd* in *M. abdita*. Previously, *eve* expression in early *M.abdita* embryo was found to display a conventional pair-rule pattern, composed of seven stripes, similar to that of *D. melanogaster* (Rohr et al., 1999).

To reveal whether an overlapping expression of these two aforementioned genes were also a phenomenon in *M.abdita,* I first established the double fluorescent *in situ* hybridization method in our laboratory after numerous attempts by mainly benefitting from a previously published protocol (Rafiqi et al., 2012). My double fluorescent *in situ* hybridization analysis in *M. abdita* embryos suggested an overlapping co-expression of *btd* and *eve* (Figure 9.A-A'') on the lateral embryo, similar to *D. melanogaster* (Vincent et al., 1997) but with differences elsewhere.

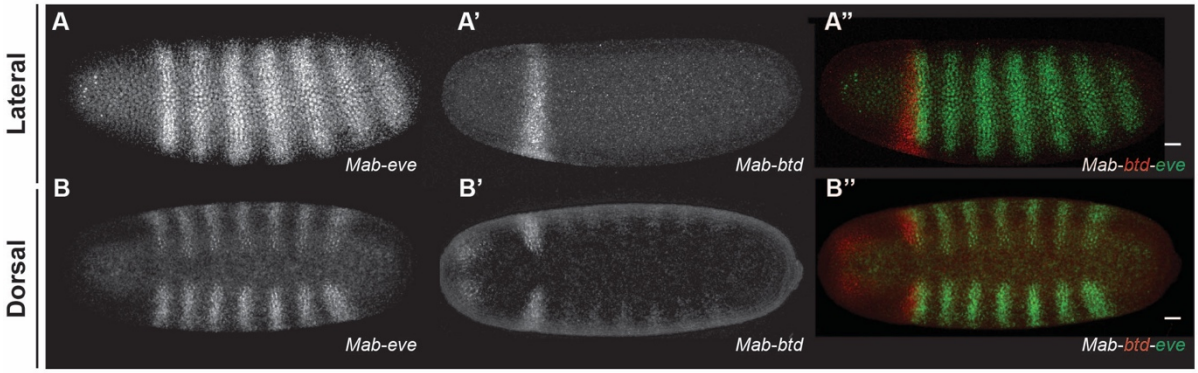

Figure 12. Double fluorescent *in situ* hybridizations showing expressions of *eve* and *btd* overlap and are dorsally repressed in *M. abdita.* A-A'') *btd* and *eve* expressions in *M. abdita* overlap at the anterior end of *eve-stripe 1*, as shown3 in *D. melanogaster* **.B-B'')** Both *btd* and *eve* expressions are interrupted along the dorsal midline with a gap of 6-7 cells (See Appendix). Anterior to the left; posterior to the right. Scale bars: 10µm.

3.3.3 Overlapping co-expression of *eve* and *btd* is dorsally repressed in *M. abdita*

In order to address what could account for different formation dynamics of CF in *M. abdita* and *D. melanogaster,* I further investigated the expression patterns of *eve* and *btd*. In *D. melanogaster*, overlapping expression of these two genes are also found on the dorsal and ventral sides of the embryo, denoting a fully circumferential overlap (collaborating Wang Laboratory's unpublished data).

My analysis on *M. abdita* further suggested that, the overlapping co-expression of *btd* and *eve* genes is repressed along the dorsal midline, creating a gap in the overlapping expression (Figure 12.B-B''). The gap of expression of *eve* stripes were previously described in *M. abdita* (Rafiqi et al., 2012); however, it was not known for *btd* expression to this date. DAPI staining further allowed me to obtain that this gap of expression is only seen in a seven-cell wide domain along the dorsal midline (data not shown), as described for *eve* (Rafiqi et al., 2012). This finding suggested that both genes are possibly repressed by a common genetic determinant. In *M. abdita,* knocking down a dorsoventral patterning gene *zerknüllt* (*zen*) by RNAi has been shown to prevent the dorsal repression of *eve* (Rafiqi et al., 2012).

3.3.4 Non-overlapping expression of *buttonhead* and *even-skipped* coincides with the lack of cephalic furrow formation in *C. riparius*

Taken together, the coinciding overlapping co-expression of *btd* and *eve* appeared to be conserved among evolutionarily distant fly species. To test this idea, whether the shift in head patterning and trunk systems could be the key genetic switch for the evolution of the cephalic furrow, I investigated the early genetic patterning of midge *C. riparius,* where head-trunk separation is achieved without a head fold.

To investigate co-expression patterns in early *C. riparius* embryo, I first established a double fluorescent *in situ* hybridization protocol after exhaustive attempts. Fluorescent double *in situ* hybridizations suggested that *btd* expression domain in the head was distributed into three main subdomains (on each lateral sides): a laterodorsally positioned expression domain close to anterior terminal, a laterally positioned relatively smaller domain and a longitudinal band-like expression domain spanning ventrally closer to the trunk region (Figure 13, left panel). Similar to *M. abdita, eve* stripes were found to be dorsally repressed. Furthermore, the 7th *eve*-stripe appeared after the onset of gastrulation, as only 6 *eve*-stripes were detectable at blastoderm stage embryos. All three subdomains of *btd* expression found anterior to the *eve*-stripe-1, indicating a lack of overlap between *btd* and *eve* expression domains. Thus, the lack of CF formation coincided with the non-overlapping expressions of *eve* and *btd* in *C.riparius*.

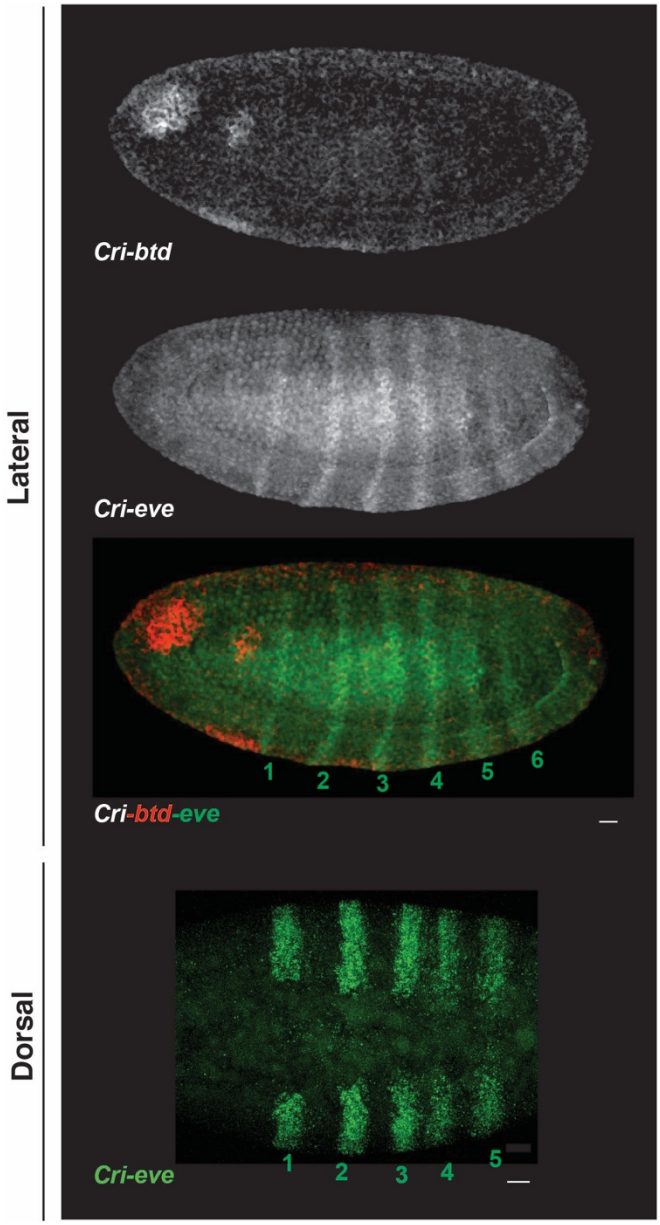

Figure 13. Expressions of *eve* and *btd* do not overlap in *C. riparius* embryo. Top panels: *btd* expression domain consists of two separate head domains positioned dorsolaterally and laterally ;and, a ventral domain. *eve*-stripe-1 does not coincide with any of the aforementioned *btd* expression domains. Bottom panel: *eve* stripes are not circumferential as they are interrupted along the dorsal midline. Scale bars: 10µm.

3.3.5 Ubiquitous overexpression of *buttonhead* did not induce putative, ectopic cephalic furrow formation in *C. riparius*

My findings on the expression patterns of *btd* and *eve* on wildtype *M. abdita*, and *C. riparius* embryos, together with the previous reports on *D. melanogaster* (Vincent et al., 1997), allowed me to hypothesize that the overlapping co-expression of these two genes could be key for the origin of CF formation. Testing this idea would not only an attempt to recapitulate the evolution of a novel morphogenetic structure, but also reveal insight on the formation and function of CF in a distant fly species.

I hypothesized that *btd* overexpression would artificially overlap btd expression with eve stripes, and therefore mimic the patterning observed in basal cyclorrhaphan *M. abdita* and derived dipteran *D. melanogaster*, possibly inducing ectopic cephalic furrow formation.

In order to test this hypothesis, I overexpressed *btd* by mRNA injections in *C. riparius* embryos. My several attempts at inducing furrow formation by artificially overlapping *btd* and *eve,* did not lead to ectopic fold formation. Strategies to alleviate potentially unstable and therefore readily degraded mRNA material by prolonged poly-A-tailing and or capping steps, did not induce fold formation either. On rare occasions, ectopic infolding events in the trunk region were observed in fixed data (2 out of 107 embryos; <2%). Because the frequency of ectopic fold formation was rare, it was not possible to determine the mechanism of formation of these infolding events via live-imaging (i.e. myosin activity and localization). Recent data from our collaborators, however, suggested an alternative read-out. Since they identified that accumulation of lateral myosin as the driving mechanism for the CF formation, I investigated myosin localization behavior in *btd* mRNA-injected embryos. Similar to the rare ectopic infolding phenotype, only a few interfaces revealed have lateral myosin accumulation per embryo. Due to the rare incidences, these findings could not substantiate further explanation. Considering gene overexpression by mRNA injection is a long-established method in our laboratory, I then concluded that *btd* and *eve* co-expression was a crucial

prerequisite for CF formation and origin, but this solely was not sufficient. Therefore, I hypothesized that overlapping *btd* and *eve* activity was not sufficient for inducing ectopic CF formation. This finding encouraged me to systematically search for downstream targets of *eve* and *btd* transcription factors that were responsible for cell-biological changes during the CF formation.

3.4 Searching for downstream targets of *even-skipped* and *buttonhead* overlap using single cell transcriptomics data

In order to unravel unknown factors that are possibly active in the genetic regulation of the CF formation I constructed a comprehensive screening scheme. Stemming from this idea, I used a publicly available dataset that dissects the stage 6 *D. melanogaster* embryo into single cells; and remaps single cell-transcriptomes into a 3-dimensional embryo (Karaiskos et al., 2017). The dataset in total included 1293 cells, and expressions of 8924 genes in total which provided a spatially resolved comprehensive picture of the early *D. melanogaster* embryo at the advent of morphogenetic movements.

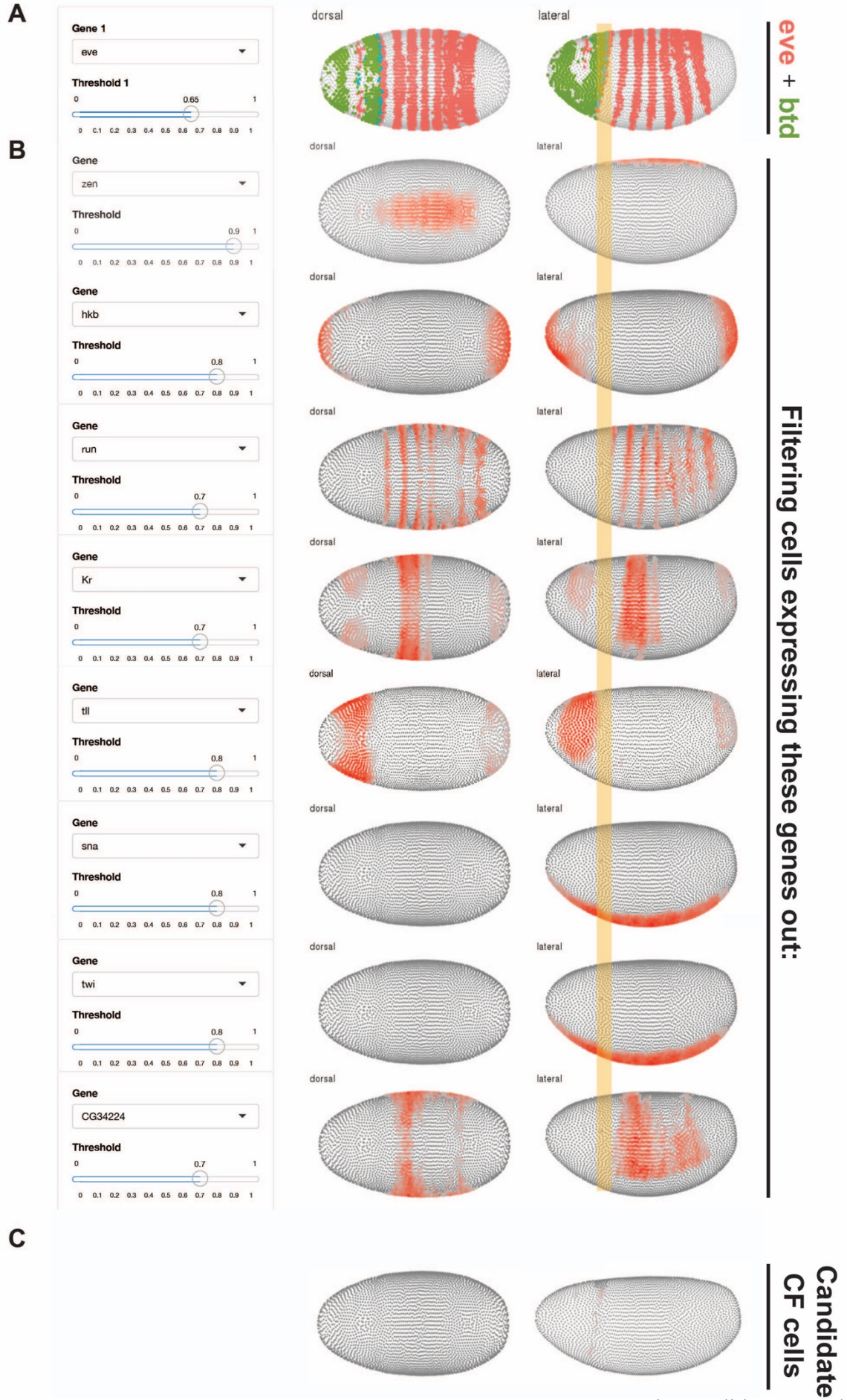

Figure 14: Cell filtering scheme to select candidate CF cells. A) The candidate CF cells were selected depending on their candidate gene expression levels (*btd-eve* co-expression). **B)** Cells that express genes that are known to be expressed elsewhere in embryo were eliminated: dorsal embryo (*zen),* ventral embryo *(twi, sna),* embryo terminals (*tll, hkb)* and trunk posterior to the CF (*run, CG34224).* **C)** The remaining candidate CF cells found on lateral embryo. Yellow highlighted region exhibits the CF region. Snapshots were generated on and taken from (https://shiny.mdc-berlin.de/DVEX/).

3.4.1 Cell filtering using known gene expression patterns.

To begin with, primary cell filtering criterion to select for candidate CF cells was the dual expression of *eve* and *btd.* Since the initiator cell activity of the CF formation first appears on lateral embryo, and dorsoventral and terminal patterning systems profoundly diversify gene expression profiles, I reasoned that confining my analysis to lateral embryo would allow me to better run the differential expression analysis. Therefore, I further filtered out candidate CF cells that had expressions of genes that are known to be expressed elsewhere (rather than lateral) in the embryo. For this purpose, I employed the genes that have specific expression domains in ventral, dorsal, terminal, and middle embryo regions. That is to say, all *eve-btd* expressing cells were first identified, then cells that can be mapped to ventral (*twist (twi), snail (sna))*, terminal (*huckekbein (hkb)), (tailles (tll))*, or middle regions (*knirps(kni), runt (run), CG34224)* of the embryo were eliminated (Figure 14). Followingly, I selected non-CF cells to compare the transcriptional profiles of candidate CF cells by applying the same filtering approach for non-CF cells positioned in the lateral embryo. This time, I selected for *eve* and *Krüppel* (*Kr*) positive cells. *Krüppel* is expressed in the middle region of embryonic body, overlapping with *eve*-stripes 3 and 4 (Kosman et al., 1998a; 1998b). Not only this cell filtering approach allowed me to neutralize the effect of dorsoventral patterning, but also allowed me to pinpoint cells with high spatial precision in the anteroposterior axis. Ultimately, 7 cells were selected as candidate CF cells, and 118 cells as non-CF cells. Subsequently, I ran PCA and hierarchical clustering analyses on selected cells to explore overall similarity in expression profiles.

3.4.2 PCA and hierarchical clustering analyses did not reveal separation among selected cells

PCA analysis on the gene expression profiles of candidate CF (7 cells) and non-CF cells (118 cells) did not suggest an apparent separation between two groups of cells (Figure 15; PC1:14%, PC2:8%). This finding could possibly indicate that

only a very low number of genes were differentially expressed between two groups, and as a result no separation was achieved. Furthermore, a heatmap was constructed showing hierarchical clustering of candidate cells (125 cells in total), and the expression of all 8924 genes in the dataset. Parallel to the PCA analysis, the candidate CF cells did not cluster according to their gene expression profiles (Figure 16, highlighted in red). In addition to the PCA analysis, hierarchical clustering further suggested that differences in expression patterns of the candidate CF effector were most likely insufficient to identify sub-populations of cells. This prompted me to filter out genes that were included in the analysis, which would decrease the volume and complexity of the dataset, thereby increasing the robustness of differential expression analysis.

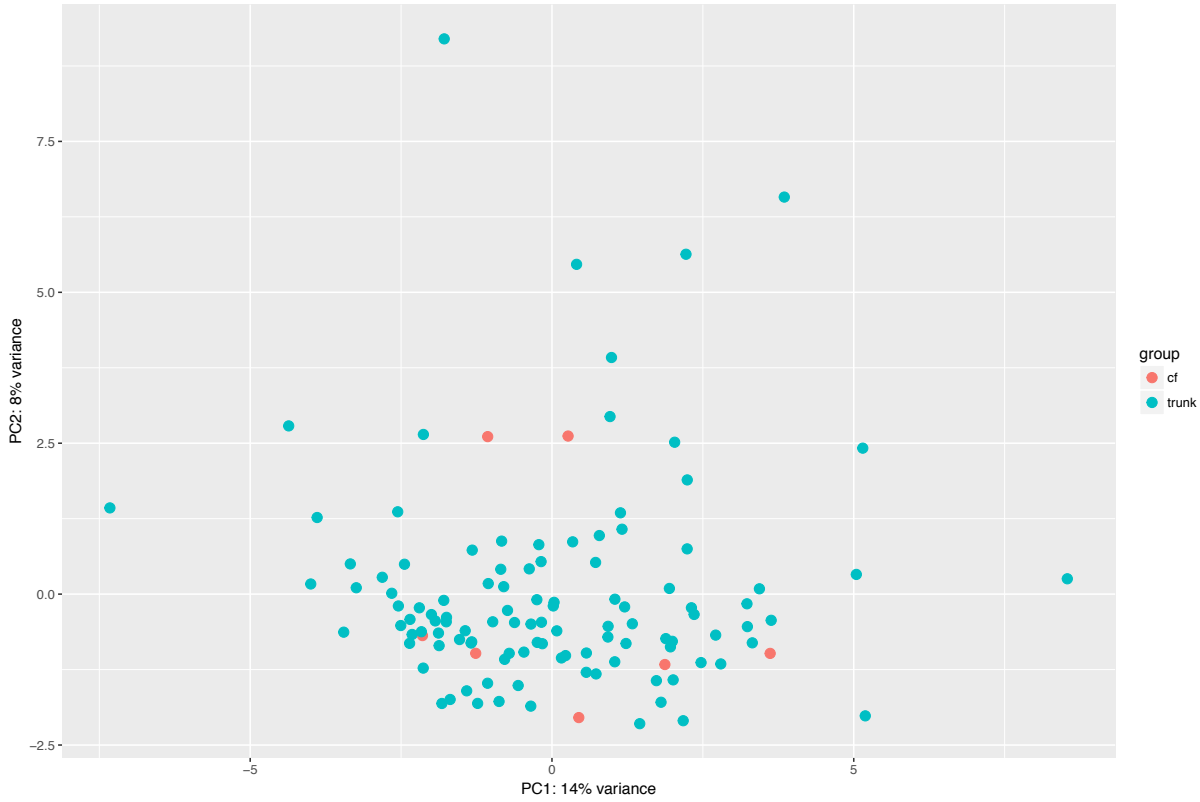

Figure 15: PCA analysis of gene expression levels on candidate CF and trunk cells. Selected candidate CF and trunk cells were analyzed via PCA analysis to evaluate whether differential grouping would be attained. Only 14% of variation could be explained by PC1, and 8% variance by PC2. Candidate cephalic furrow and trunk (non- CF cells) exhibited no significant inter or intravariation.

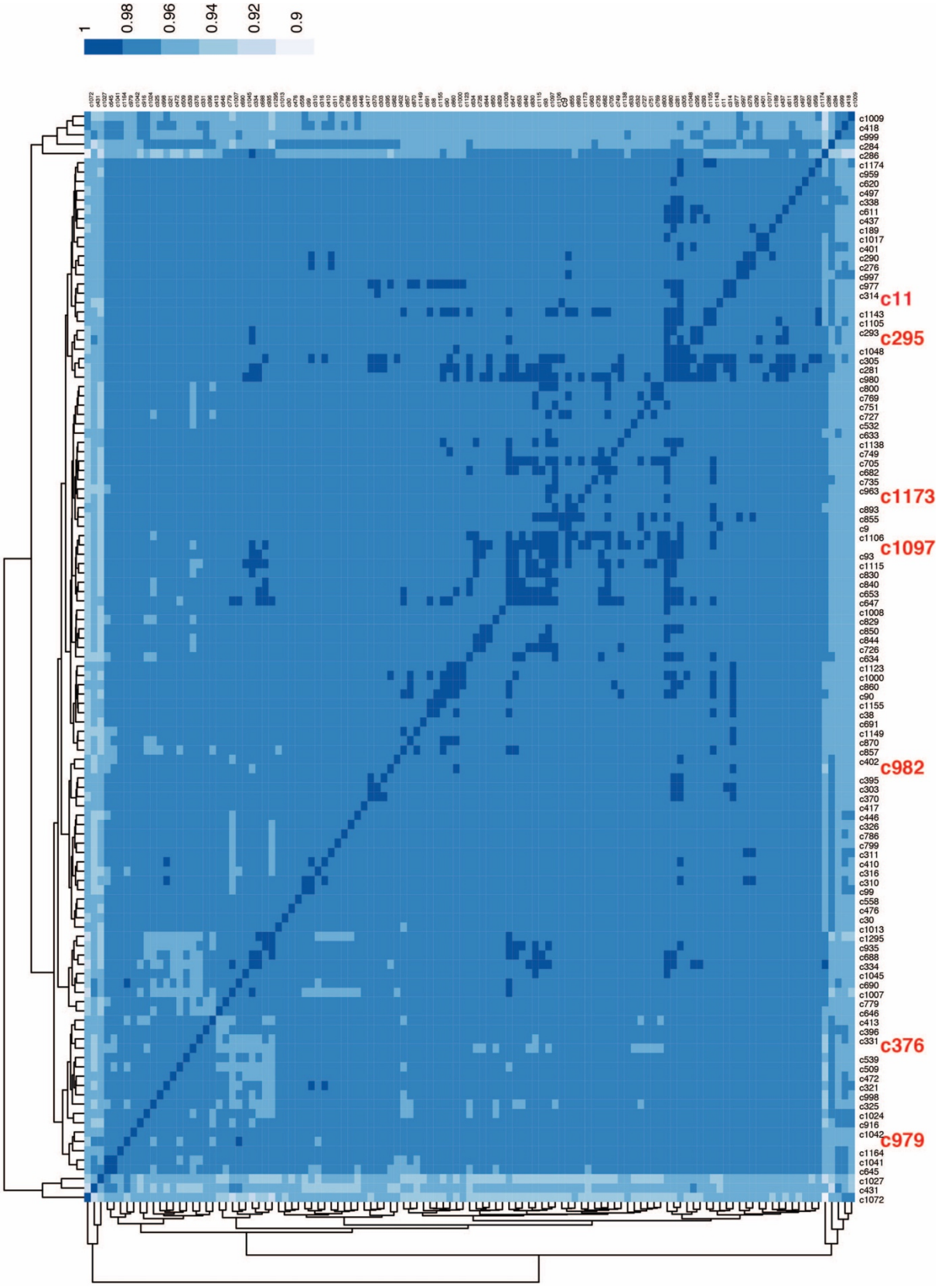

Figure 16: Hierarchical clustering analysis to evaluate transcriptional profile similarity between and within selected candidate cells. Candidate CF cells are highlighted in red. Clustering analysis provided no separation between the candidate CF and non-CF cells depending on expression profiles.

3.4.3 Gene filtering according to variance among candidate non-CF cells.

Before genes were filtered according to their differential expression levels, I reasoned the candidate gene should have one of the following three different expression patterns for pre-selection: a) Anterior expression domain covering the head region, as well as the CF region; b) Expression domain in the embryonic trunk, overlapping with the CF region, with a lack of expression in the head; c) Stripe-like expression domain only specific to the CF region. One feature that was common to all three suggested expression patterns, was that the candidate gene should be expressed at similar levels (low variance) among the non-CF trunk cells. Variance analysis of all 8924 genes in non-CF cells suggested that 1856 genes had less than 70% variance; and, 1325 genes displayed less than 80% variance in their expression levels among 118 non-CF (trunk) cells. 843 genes showed less than 90% variance, that was determined as cut-off value in this study, which were incorporated in differential gene expression analysis (Figure 17).

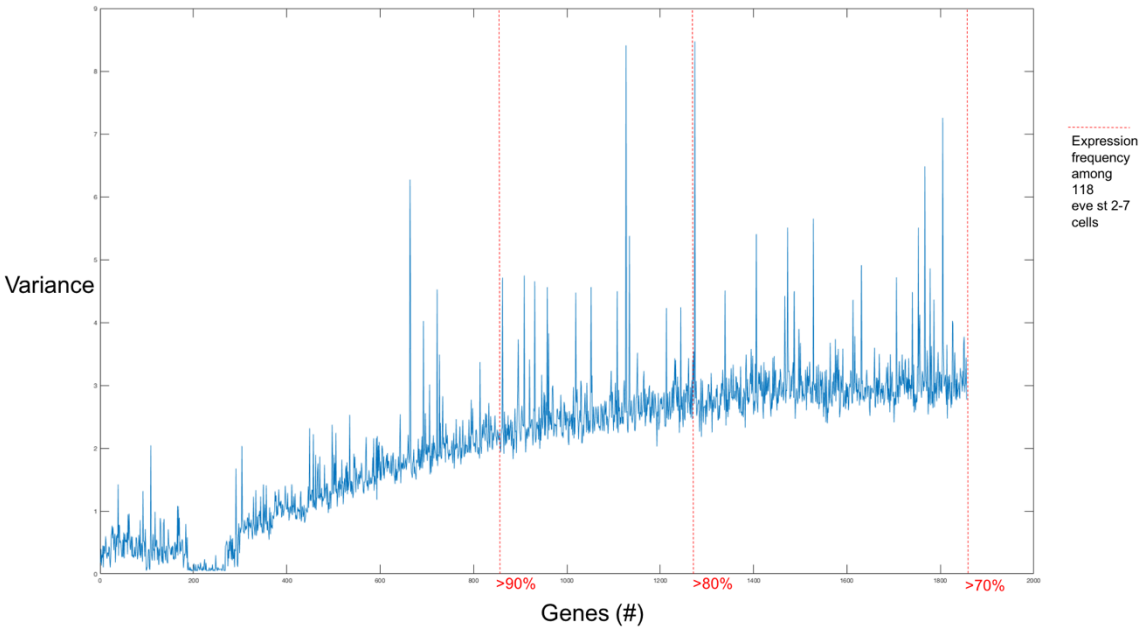

Figure 17: Variance analysis was performed to filter out genes that exhibit inconsistent expression levels in selected candidate trunk cells. 1856 genes had less than 70% variance; and, 1325 genes displayed less than 80% variance out of 8924 genes in the dataset. 843 genes showed less than 90% variance (determined cut-off value in this study) in their expression levels among 118 candidate trunk cells, which were incorporated in differential gene expression search.

3.4.4 Comparative gene expression analysis between CF and non-CF cells

Candidate CF effector genes were determined according to their differential expression levels (student's t-test) between selected CF cells and a non-CF cells. Candidate genes were then further filtered for relevant gene ontology (GO) terms such as cytoskeleton remodeling, actomyosin network regulation etc. Genes that were un- or under-studied and therefore had no GO terms identified for were also included in the analysis, depending on their expression patterns. The most significantly differentially expressed 22 genes were analyzed by their ability to disrupt the CF formation or to induce ectopic fold formation by RNAi experiments in *D. melanogaster*. RNAi experiments revealed no function for any of the candidate genes on cephalic furrow formation (Figure 18; Table 1).

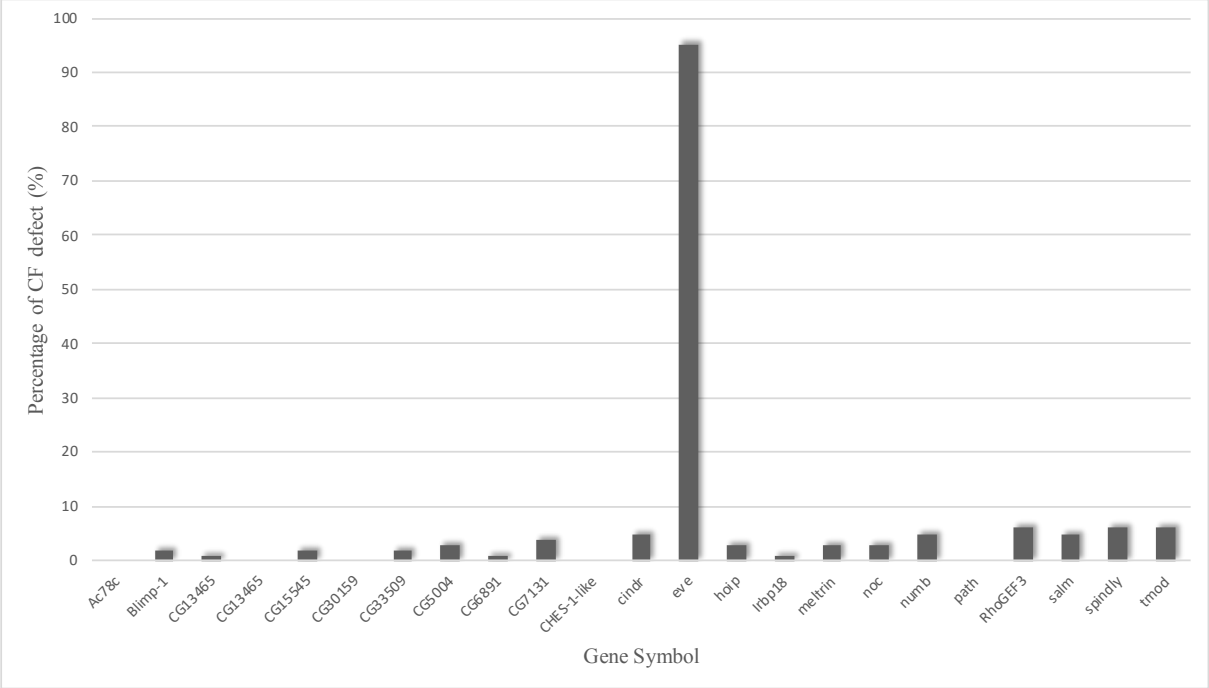

Figure 18: Screening candidate CF genes by RNAi knockdown experiments. 22 genes were tested for their role in CF formation by RNAi knockdown experiments. The gene *eve* was included as a positive control in the analysis. The lack of CF formation was not differentiated from the overall aberrant development. The number of embryos that were injected with dsRNAs and evaluated afterwards are given in Table 1.

Table 1: Overview of candidate CF gene screening RNAi injections.

Gene symbol	Annotation symbol	Flybase ID	No. embryos injected	No. embryos with wt develop.	No. embryos with hindered develop.	Percentage affected embryos
Ac78c	CG10564	FBgn0024150	61	61	0	0
Blimp-1	CG5249	FBgn0035625	43	42	1	2
CG13465	CG13465	FBgn0040809	78	77	1	1
CG13894	CG13894	FBgn0035157	54	54	0	0
CG15545	CG15545	FBgn0039806	49	48	1	2
CG30159	CG30159	FBgn0050159	31	31	0	0
CG33509	CG33509	FBgn0053509	48	47	1	2
CG5004	CG5004	FBgn0260748	59	57	2	3
CG6891	CG6891	FBgn0030955	53	52	1	1
CG7131	CG7131	FBgn0038598	61	58	3	4
CHES-1-like	CG12690	FBgn0029504	47	47	0	0
cindr	CG31012	FBgn0027598	52	49	3	5
eve	CG2328	FBgn0000606	46	2	44	95
hoip	CG3949	FBgn0015393	82	79	3	3
Irbp18	CG6272	FBgn0036126	65	64	1	1
meltrin	CG7649	FBgn0265140	54	52	2	3
noc	CG4491	FBgn0005771	62	60	2	3
numb	CG3779	FBgn0002973	59	56	3	5
path	CG3424	FBgn0036007	71	71	0	0
RhoGEF3	CG43976	FBgn0264707	43	40	3	6
salm	CG6464	FBgn0261648	56	53	3	5
spindly	CG15415	FBgn0031549	64	60	4	6
tmod	CG1539	FBgn0082582	63	59	4	6

4 DISCUSSION

In my thesis, I aimed to unravel the different mechanisms of head-trunk separation in early development by using dipteran flies as models. I was particularly intrigued by the fact that most insect can manage to separate head and trunk without forming a visible separator. Hence, I first searched for different characteristics of tissue organization and cell behavior between the developing head and trunk domains in *C. riparius,* that could be used to set one apart from the other. My findings on heterogeneous localization of myosin activity between head and trunk domains further indicated distinct tissue properties for embryonic head and trunk *C. riparius,* and suggested a tissue separation mechanism as well. In addition, abundant out-of-plane divisions in the embryonic head region, and the wave-like propagation of myosin activity also further reveal that *C.riparius'* head and trunk development are quite atypical in comparison to its derived relatives. These findings provide significant insight into how head-trunk separation which is commonly found in most animals can fit into the overall morphogenesis of an embryo.

4.1 Converging shift of head and trunk patterning systems might be key for the CF formation as a head-trunk separation mechanism in dipteran flies

Head-trunk separation in *D. melanogaster* embryo is defined by a specific overlapping co-expression of two transcription factors, *eve* and *btd* (Vincent et al., 1997). As a result of this unique overlap of head and trunk patterning genes, the CF is established as a head-trunk separation mechanism in the early embryo. My results

suggested that, analogous to *D. melanogaster,* overlapping co-expression of *eve* and *btd* genes coincided with the CF formation in *M. abdita*. The extent of the overlap of these two genes were however different, since the dorsal repression of both genes in *M. abdita* created a gap in the overlap. Consistent with this finding, the initial CF domain and its formation dynamics differed in both species. My results indicated that in *D. melanogaster* the dorsal contribution to the CF formation was overall more substantial. Collectively, these findings suggested that the genetic basis of the CF formation was essentially conserved and the naturally non-overlapping conditions were related to diminished or reduced folding. The conserved genetic control of the CF formation, prompted the question that what downstream targets could be playing a role for head-trunk separation in these derived dipteran flies. My functional attempts to pinpoint the genes that directly alters cytoskeleton network, and thereby, could be building the CF did not give any positive results. Nonetheless, as a preliminary attempt to tackle this long-waiting question, the candidate genes that have not been analyzed in this thesis still remain to be valuable targets.

In the basal fly *C. riparius* embryo*,* which lack the CF formation, my results concomitantly suggested that *eve* and *btd* expression patterns do not overlap. My attempts to artificially overlap these two genes by *btd* overexpression assays did not reliably yield ectopic CF formations. There can a number explanations to it. First, although *eve* and *btd* overlap is crucial for the CF formation, it might not be sufficient. That is to say, the overlap of complete head and trunk genetic patterning systems might be essential for the CF formation. Secondly, one has to bear in mind that this molecular approach to induce ectopic CF-like infolding depends on the assumption that *btd* gene function was conserved among diptera. Unfortunate for the evo-devo research, gene function frequently changes during evolution. When the outgroup insect *Tribolium castaneum* examined, for example, the *btd* gene was found to be expensable during early development, also did not hold a head-gap gene function (Schinko et al., 2008). A recent report, in contrast, has exhibited the improper head development in *btd*-knockdown embryos (Jeon et al., 2019). However, these contradictory findings should be carefully approached, as the penetrance and severity of phenotypes in knockdown experiments in *T. castaneum*

has been shown to be drastically affected by the genotype of the strain (Kitzmann et al., 2013). According to our current understanding, I hypothesize that evolution of head-trunk separation involves a step of genetic convergence, i.e. overlap of head and trunk patterning systems, which naturally includes additional factors beside *eve* and *btd*. This new intermediate zone could have conceptually allowed the emergence of novel morphogenetic events, that were not possible by either patterning systems solely.

4.2 Myosin localization heterogeneity provide boundary conditions for head-trunk separation in *C. riparius*

My analysis on the dynamics of the myosin activity suggested that head-trunk adjoining region in *C. riparius* embryo harbored a sharp distinction across head and trunk regions. Along the apicobasal axis, myosin localization was mostly reserved to subbasal region in the embryonic head. In contrast, myosin was subapically localized in the trunk region. This finding was indeed in line with my prediction. Since distinct developmental programs of head and trunk development did not overlap in *C.riparius* embryo, it was conceivable to expect an abrupt transition, representative of nonoverlapping patterning systems, between head and trunk regions.

Such deliminating boundary formation via regulation of myosin accumulation has also been reported in *D. melanogaster*. During the development of wing imaginal disc, for example, myosin accumulation was found to be specifically upregulated at the dorsoventral boundary, that separate the growing disc into two domains (Major and Irvine, 2006). In addition, subapical myosin contractility was found to provide barrier function at parasegment boundaries (PSBs) that separate individual compartments in the early *D. melanogaster* embryo (Monier et al., 2010). Authors further suggested that cell divisions challenged the boundary conditions, however, myosin contractility prevented cell mixing by pushing back dividing cells. Similar to the PSBs, I did not observe any cell-

intermingling between head and trunk domains. Functional analyses such as reducing myosin contractility, for example, by injecting constitutively active myosin phosphatase will help us further understand how the development is compromised, if any (Munjal et al., 2015). One advantage of targeting the myosin activity rather than genetic determinants of development is that overall head and trunk development will be mostly preserved. Therefore, we could better evaluate the significance of the myosin contractility during head-trunk separation.

4.3 Wave-like propagation of myosin activation in the trunk region is indicative of distinct trunk development in *C. riparius.*

My results suggested a peculiar phenomenon in trunk development in *C. riparius.* The myosin activation first appeared in the anterior trunk in *en face* view, and propagated posteriorly. In line with this, not all seven *eve*-stripes are established at the blastoderm stage, as the 7th stripe appears after the onset of gastrulation. These findings were indicative of retention of some characteristics of a more ancestral trunk development, similar to that of *T. castaneum*, where the germband is sequentially patterned. Hence, the presence of a marginal growth zone can be speculated in *C. riparius'* trunk. Propagating myosin activity, therefore, suggested that the force generation appears to be implemented in a step-wise manner. I hypothesize that the sequential propagation of myosin can channel the building stress towards to the posterior end, dissipating it along the anteroposterior axis in *C. riparius*. The unidirectional nature of myosin activation, together with the suggestive growth zone at the posterior end, can therefore indicate a less compressed tissue organization in *C. riparius* trunk.

A seemingly similar myosin activation wave was recently reported for posterior midgut invagination *D. melanogaster,* where authors suggested that the wave initiation was transcriptionally controlled, however the subsequent propagation was mechanically induced (Bailles et al., 2019). Along the trunk,

however, myosin activity is detected simultaneously (Zallen and Wieschaus, 2004), and all seven *eve*-stripes are established in the blastoderm-stage embryo. Hence, intrinsic elevated levels of stress due to simultaneous myosin activation might lead to an overall compressed environment in the trunk of *D. melanogaster,* which is most likely not the case in *C. riparius.* This finding is further strengthened by the previous findings in our laboratory that indicated the extending germband in *D. melanogaster* embryo proceeded bidirectionally, pushing into the head region ventrally (Lucas Schütz, PhD Thesis, 2018). Taken together, distinct trunk development programs in *C. riparius* and *D. melanogaster,* are very likely to modulate the need for establishment of distinct head-trunk separation strategies differently, which will be discussed in 4.6.

4.4 Prominent increase of apical cell area might provide embryonic head integrity in *C. riparius*.

In *C. riparius* embryo, one determining feature to distinguish head cells from trunk domain cells was the increasing apical cell area. Cells found anterior to 36% EL (position of *eve*-stripe-1), underwent apical cell enlargement after the onset of germband extension. The timing of apical cell area enlargement preceded the cell divisions in embryonic head, therefore could be related. In *D. melanogaster*, a slight apical cell area enlargement was also found in cells that are about the undergo mitosis (Foe, 1989). Since *D. melanogaster* head cells undergo planar cell divisions, shape changes enlarging apical area helps bring the center of mass closer to the plane of epithelium where the division occurs. Considering columnar shape of epithelial cells in *D. melanogaster*, apical to lateral aspect ratio drops after mitotic rounding.

Due to volume conservation, apical cell enlargement can therefore prepare the mother cells to polarize and divide cellular material. In *C. riparius* embryonic head, interestingly, a remarkably high degree of enlargement (1.5 fold) was quantified among the head cells in this project. This was indeed contradicting to my

expectations, since divisions were mainly happening nonplanarly, and apical cell enlargement would serve against the polarization of mother cells by bringing the poles of daughter cells closer to each other. This feature of head cells could therefore serve a different function. I hypothesize that apical area enlargement could provide structural strength to the head, and as a result could also explain the slight shift of head-trunk interface posteriorly despite the bidirectional extension of the germband. In line with this, a recent *in vitro* study has proved that stiffness of adherent epithelial cells increase exponentially as the apical cell area rises (Nehls et al., 2019). The authors further suggested that this impact could be only observed in confluent monolayer, which can be roughly accepted as analogous to single layer epithelium of blastoderm stage fly embryo. Therefore, I further hypothesize that this enlargement phenomenon can also serve an important function. While planar cell divisions are crowding the epithelium, nonplanar divisions would cause shrinkage in the plane of epithelium as the half of cellular mass is positioned below the plane of epithelium. Preceding enlargement could be therefore preparing the tissue for the loss of the cell height to a second layer of cells, preserving the head integrity.

4.5 Out-of-plane divisions are a hallmark of the *C. riparius'* head development

My analysis on wildtype *C. riparius* embryos unraveled a scarcely observed phenomenon in fly early embryonic development, which was the nonplanar division taking place in the embryonic head region. The first divisions after the blastoderm formation were of nonplanar type, when cell-fate determination is not yet initiated as we know of, thereby stacking daughter cells up one on top of another. This finding indicated strikingly unique developmental programming of the *C. riparius'* embryonic head, in comparison to trunk development, where cell division happen in the plane of epithelium. During *D. melanogaster* early development, cell divisions have been reported to occur only in the plane of epithelium so that both

daughter cells are found at the embryo surface. Out-of-plane cell divisions were reported to take place at a significantly later stage (stage 10; 85 min after the onset of germband extension) in mitotic domain 8 and 9, where the cells contribute to larval brain formation (Foe, 1989). A gene named *inscuteable* was identified to have a role orienting asymmetric cell division in the mitotic domains (Kraut et al., 1996). To start with, the expression pattern of *C. riparius* homolog of this gene must be determined. It is possible that early and strong expression of *inscuteable* might be responsible for abundant nonplanar divisions. Following knockdown experiments will functionally address whether the same gene is recruited for nonplanar divisions. This would in turn allow us to argue that a spatiotemporal shift in the expression pattern of a single gene could be modulating head morphogenesis to a great extent.

Furthermore, another interesting finding was the small fraction of planar divisions and their spatial distribution in the head region. In all embryos that I investigated these planar divisions were confined adjacent to the head-trunk interface. In context with the data on differential membrane straightness, myosin localization and activity in the embryonic trunk, that these few planar divisions might be owing to the anisotropic tension that adjacent tissues encounter. Such phenomenon has been reported in *D. melanogaster,* where authors showed that the division axis is largely determined by the adjacent myosin activity in compartmental boundaries (Scarpa et al., 2018). In line with this, tension exerted by the myosin activity at the head-trunk interface could be most affecting in the adjacent head cells, due to the viscosity of epithelial tissue(Wessel et al., 2015). If disruption of myosin activity at the head-trunk interface leads to solely nonplanar divisions in the head domain, this would indicate that all head cells are programmed to undergo nonplanar divisions, with the exception that head cells found in close proximity to the head-trunk interface are under the effect of tension, overriding their genetic programming. The oblique (30°-60°) angle of planar divisions that these cells are undergoing most likely limits tension anisotropy on both sides, head and trunk regions.

After the onset of gastrulation, programmed cell proliferation in distinct mitotic domains contributes to embryonic development (Foe, 1989). To maintain tissue architecture and integrity of the epithelium, individual epithelial cells undergo mitotic divisions in a constrained manner. Cell division have been found to play a major role during epithelial tissue morphogenesis (Guillot and Lecuit, 2013). Therefore, it would be plausible to approach this early nonplanar divisions in the context of epithelial organization. Hence, the research on how single cells sustain their own proliferative programming and still reconcile with the gross morphology of the development is of utmost importance.

4.6 Putative analogous functions of out-of-plane divisions and the CF

In order to drive large-scale morphogenetic events of gastrulation, cells undergo shape change events, migrate via neighbor exchange and under the effect of pull-and-push forces exerted by key gastrulation events such as extra embryonic tissue expansion, mesoderm invagination and posterior midgut invagination. Morphogenetic events of gastrulation on one hand create stress and on the other hand decrease stress. To accommodate the increasing stress, epithelial infoldings have been identified as mechanical sinks (Munjal et al., 2015), storing cells in, and thereby accommodating tension which would otherwise overcrowd embryo surface and likely to cause random buckling events.

In the context of head-trunk separation, nonplanar division therefore could act as a mechanism to withhold tension build-up, inhibiting a need for a 'cell sink', which is analogous to cephalic furrow in higher flies in this regard. Hence, I hypothesize that, basal non-cyclorrhaphan *C. riparius* might utilize nonplanar cell divisions in such a way that a cephalic furrow is rendered unnecessary to separate head and trunk development. Unfortunately, I did not have the time to test this hypothesis further in my thesis project. Previously, stiffness in the epithelium has been speculated to play a role in keeping mitotic division axes of dividing cells in

the epithelial plane (Campinho et al., 2013; Kane and Adams, 2002; Kimmel et al., 1990) . To test this idea, it is most conceivable to ask whether the nonplanar divisions in *C. riparius* could be converted to in-plane. Two methods can be extremely applicable to address this question: i) ectopic expression of pins that are known to randomize division axis in *D.melanogaster* (Chanet et al., 2017); or, ii) inhibiting myosin phosphatase activity via drug injection (e.g. Calyculin-A, (Ishihara et al., 1989)) to increase active state of myosin contractility (at apical or basal sides of the epithelium) and thereby stiffen the epithelium (Fernandez-Gonzalez et al., 2009). It is plausible to reason that in a stiffened epithelium, cell divisions are expected to be biased to be planar, due to the counteracting apical and basal constraints. Therefore, my expectation would be those division will be instead forced to stay in-plane, which would then drastically increase the cell number on the embryo surface. This induced overcrowded tissue plane would than mimic an intrinsically higher stress environment. Under this condition, the embryo could possibly undergo random tissue buckling events to alleviate some of the stress. This scenario could therefore indicate the role of out-of-plane divisions as a tension buffering mechanism. Complementary experiment in *D. melanogaster* could be, conversely, liberating cells from the constraints of a stiff epithelium by expression of a constitutively active myosin phosphatase (Munjal et al., 2015). It is conceivable to predict that a subset of cells, would change their division axis from planar to nonplanar orientation. Linking the proportion of nonplanarly dividing cells and correlating it to the possible reduction in depth of the CF would then allow indicate the role of nonplanar divisions in soaking up compression. All in all, these hypothesized experiments would therefore help us address the function of the CF better. Parallel to this, although not mentioned in the literature, *btd* mutant *D. melanogaster* embryos form ectopic folds in the absence of the CF formation. This observation implies that the CF may have evolved as a mechanical solution to possibly relieve tension due to gastrulation movements.

4.7 Perspective: Early head-trunk separation could have enabled later head involution

The CF functions as a head-trunk separator during early development in derived flies. However, our knowledge of what happens to the CF cells after it retracts back to the surface is limited. The question why embryo only transiently forms such a deep fold remains to be answered. In other words, could the derived flies have found an alternative way to make use of the CF tissue after it resurfaces.

By collating the phylogenetic data found in the literature, we have now strong evidence that the CF formation and a later morphogenetic event called 'head involution' are found concurrently. In other words, all identified CF-forming dipteran fly families also undergo 'head involution' during development. Head involution is a recent morphogenetic innovation that is only seen in higher dipteran flies called cyclorrhaphan flies. It is a complex event about which our knowledge is limited. As a result of head involution, the head region is internalized and the subsequent larva appears to be acephalic, due to hidden head structures. During head involution dorsal, lateral and ventral cells of embryonic head are involved. Recently, patterned contractile forces have been found to be responsible for the spreading of epithelium and ordering of correct segmental positioning during head involution (Czerniak et al., 2016). In non-cyclorraphan clade of dipteran flies, head involution does not occur which is analogous to ancient insect head development. A fully everted head with a putative biting mechanism is a hallmark of the larvae of non-cyclorrhaphan flies as well as of the out group insect *T. castaneum.*

I assume that the CF formation evolved as a head-trunk separation strategy, while regulating tissue tension during early development. I further hypothesize that the CF formation and the later occurring head involution might be causally related morphogenetic events. As a transiently forming epithelial fold the invaginated CF cells after retracting back to the surface, might help provide essential 'skin material' to cover the head structures that are sliding in during head involution. The genetic evidence coming from *buttonhead* mutant flies are also invaluable to reconsider. As

well as the lack of the CF, these flies cannot successfully complete head involution process, hence the name '*buttonhead'* during larval stages. This phenotype, in fact, is very similar to the non-cyclorrhaphan larvae' head appearance, which might suggest a causal relevance. To investigate this better, *D. melanogaster* flies expressing only *eve*-stripes-2-7 (generated by collaborating Yu-Chiun Wang) needs to be investigated carefully. In this fly line, overall trunk development and head development are accomplished similar to the wild-type conditions, only the CF formation is missing. However, later developmental stages of these flies have not been interrogated yet. Coinciding with the absence of the CF, in these flies, I predict that the head-involution could be impaired as well. Evidence from wild-type *D. melanogaster* also suggest that the developmental timing of these two processes are relatively close (2h apart; (Campos-Ortega and Hartenstein, 1997)). Therefore, it is necessary to look at the relationship between head involution and the CF formation. Moreover, surveying of dipteran fly development must be continued. Until contradictory evidence is found, such as identification of fly species that forms the CF but not undergo head involution, or vice versa, my hypothesis will be a viable option to reconsider the novel head-trunk separation mechanisms can act as an enabler for later morphogenetic events.

5 MATERIALS and METHODS

5.1 Materials

5.1.1 Fly cultures

In my thesis, I worked on three fly species: *Drosophila melanogaster, Megaselia abdita and Chironomus riparius.* The Drosophila line used as reference was *w1118* (BDSC Stock # 5905, donated by Micheal Ashburner, University of Cambridge) acquired from the Ingrid Lohmann's Lab (COS, Heidelberg).

Chironomus riparius and *Megaselia abdita* cultures were acquired from Urs Schmidt-Ott (The University of Chicago, Chicago, USA), which had previously received the cultures from Gerald K. Bergtrom (University of Wisconsin, USA) and Johannes Jäger (Centre for Genomic Regulation, Spain), respectively. All fly cultures were kept at 25°C. While D melanogaster and C riparius cultures were maintained in 17/7h day/night cycle; M abdita culture was kept in 18/8h day/night culture.

5.1.2 Chemicals

Chemical	Company	Catalogue #
Agar	Roth	5210.2
Agarose universal	peq GOLD	35-1020
Ampicillin	Sigma	A9518
BCIP	Roche	11383221001
$C_2H_3KO_2$	Grüssing	12001
Chloral hydrate	Sigma	15307

Chloroform/Isoamyl alcohol	Fluka/Sigma	25666
DAPI	Molecular Probes Life Technologies	D1306
DNA ladder mix ready to use	Thermo Scientific	SM1173
dNTP	Sigma	D7295
DIG RNA Labeling Mix	Roche	11277073910
EDTA	Applichem	A3553
EtBr	Roth	2218.2
Ethanol	Sigma	52603
Formaldehyde 37%	Sigma-Aldrich	252549
Formamide	Sigma-Aldrich	47670
Glacial Acetic acid	Merk	607002006
Glycerol	Sigma	54997
Glycogen	Thermo Scientific	R0561
Goat serum	Sigma	G6768
Heparin	Sigma	H5515
Image iT FX Signal Enhancer	Invitrogen	136933
Isopropanol	Sigma	69694
Kanamycin sulphate	Sigma	60615
KCl	Applichem	A3582
$KH_2\ PO_4$	Applichem	3620
LiCl	Merck	B481279512
Methanol	Sigma	32213-2.5L
NaCl	Sigma	31434
$Na_2\,EDTA \cdot 2\ H_2\ O$	Fluka/Sigma	34549
$Na_2\ HPO_4$	Grüssing	12133
NaOAc	Grüssing	1131

NaOH	Fluka/Sigma-Aldrich	35256-1L
NBT	Roche	11383213001
n-Heptane	Roth	8654.3
NTPs	Thermo Scientific	R0481
Phenol/Chloroform/ Isoamylalcohol	Roth	A156.1
SDS pellet	Roth	CN30.2
tRNA	Sigma	R8508
Triton X100	Merck	1086031000
Trizol	Life technologies	15596062
Tween-20	Sigma	P1379
Tris Base	Roth	4855.2
Tris HCl	Roth	9090.3
X-Gal	Roth	2315.2
Xylene	VWR Prolabo Chemicals	28975.325

5.1.3 General solutions and media

Luria-Bertani medium (LB)

NaCI	10g
Yeast extract	5g
Trypton	10g
H_2O	add up to 1L
pH= 7.5	

LB plates

Bacto-Agar (15g) was added to LB medium (1L) and autoclaved. After the plates were cooled down to about 50°C, antibiotic (either Ampicillin; final concentration: 100µg/ml; or kanamycin; final concentration: 50µg/ml) was spread on top. The plates were then stored at -4°C.

TAE 50X

Tris/Acetate (pH 7.9 / 40mM)	242 g
EDTA (2mM)	14.7g
Acetic acid	57.1ml
H_2O	add up to 1L

PBS 10X

NaCI	80g
KCl	2g
$Na_2 HPO_4$	14.4g
KH_2PO_4	2.4g
H_2O	add up to 1L
pH=7.4	

PBT

PBS 1X
Tween-20 0.1%

5.1.4 Kits and Enzymes

5.1.4.1 Kits

Kit	Company	Catalogue#
MAXIscript T7 kit	Ambion	AM1314
mMessage mMachine T7 Ultra Kit	Ambion Life Technologies	AM1345
Plasmid midi kit	QIAGEN	12143
QIAquick gel extraction kit	QIAGEN	28706
QIAprep Spin Miniprep kit	QIAGEN	27106
Oligotex mRNA Midi kit	QIAGEN	70042
RNA easy MiniKit	QIAGEN	74104
SMART RACE cDNA Amplification Kit	Clonetech	634923
RedTaq Jumpstart Ready Mix	Sigma	P0982

5.1.4.2 Enzymes

Enzyme	Company	Catalogue number
BamH I	Thermo Scientific	ER0051
*Bsa*I FD	New England BioLabs	R3535S
*Dra*I FD	Thermo Scientific	FD0224
*EcoR*I FD	Thermo Scientific	FD0274
Hind III HF	New England BioLabs	R3104
iProof DNA Polymerase	BioRad	172-5331
Not I	Thermo Scientific	ER0591
Protector RNase inhibitor	Roche	11801800
Proteinase K	Invitrogen	25530-015
Pst I	Thermo Scientific	ER0611
RNA SP6 polymerase	Roche	10810274001

RNA T7 polymerase	Roche	10886520
RNaseA	Thermo Scientific	EN0531
T4 Ligase 5U/µl	Thermo Scientific	EL0011

5.1.5 Antibodies

5.1.5.1 Primary Antibodies

Antibody	**Company**	**Catalogue number**
Anti-DIG-AP Fab fragment	Roche	11093274910
Mouse anti-DIG Fab Fragment	Roche	11333062910
Anti-Fluorescein/Oregon Green rabbit IgG Fraction	Life Technologies	A889
Anti-Fluorescein-AP Fab fragment	Roche	11 426 338 910

5.1.5.2 Secondary Antibodies

Antibody	**Company**	**Catalogue Number**
Anti- Rabbit IgG Alkaline Phosphatase	Sigma	A3687
Goat anti-mouse IgG Alkaline Phosphatase	Sigma	A7434
Goat anti-mouse Alexa488	Jackson ImmunoResearch	115-546-062
Anti-rabbit Alexa 647	Jackson ImmunoResearch	711-606-152

5.1.6 Primers and Plasmids

5.1.6.1 Primers

Primer	Gene	Sequence
SL0795	meltrin	AGCACAGTCCTAACCCGGCAATGG
SL0796	meltrin	CTCCAGATCCTGCCTTCGAGCACG
SL0797	numb	TCACGAACGCGGCTTCAGCTACAT
SL0798	numb	AGTGCTCGGGATTGGCAAGTCTGG
SL0799	Blimp-1	AATCATCGGCCAGGATCGATCGCC
SL0800	Blimp-1	TGGGGATATCCTCAGCGGGGACAA
SL0910	RhoGEF3	GTCGCGAATCCCAAAACCTG
SL0911	RhoGEF3	GAGCTGTCCGTTGGCACTAG
SL0918	Ac78c	GTTTACCCCGCTGCCTGAA
SL0919	Ac78c	AGCAGACCATCACCAGGAAG
SL0922	CG15545	GGAAGAGGACGAACAACGCT
SL0923	CG15545	TTGATGACCAGTGCTGTGGA
SL0924	CG13894	CAGCAACAGCAGCACTTTGC
SL0925	CG13894	TTAACCCTCGACCAGTGTGG
SL0996	CG33509	GGATCTCAGTGCGATCGGTT
SL0997	CG33509	GCCAAGGCCATTTCCATGAC
SL1000	CG30159	ATTTTGCGGTGGCCAAGTAC
SL1001	CG30159	CGGCAGCAGCTTCTCCTT
SL1006	CG5004	GAGTGCCCCAAGGTCTTCTC
SL1007	CG5004	CCAATTGCTGCTGCTTTCGT
SL1008	lrbp18 (CG6272)	GGCCAAAAAGAGAACTGCCG
SL1009	lrbp18 (CG6272)	TGTCCTTGGGATCGGGATCT
SL1010	CG6891	TGGAGAAGGACTCGATTCGC
SL1011	CG6891	GGATGCCCGTTCCGTAGTT
SL1012	CG7131	CAAAATGCCTGCGATCCCTG

SL1013	CG7131	ACCGGCATGTACGACAACTT
SL1014	CHES-1-like	GCATCAGCATCAGCATCAGC
SL1015	CHES-1-like	AAGCTACTGGTCTTGGGCAC
SL1016	eve	GTTGTGGACCTCTTGGCCA
SL1017	eve	GCTCCGCAATCACAGTTGTC
SL1042	tmod	GCCAAAGAAGTGGATCCCGA
SL1043	tmod	GTTCTTCTCCACCAGGTCGG
SL1058	hoip	TAATCCCAAGGCATTCCCGC
SL1059	hoip	CGCTCGATCTCCTGCTGAAT
SL1060	noc	CCCAAGTCGAGCACTCCAAT
SL1061	noc	GACATGGGACTCAGTGGTGG
SL1062	path	TCCTGACGTACTTTGGCACC
SL1063	path	GCGTTCTTCCACAGGATCCA
SL1064	spindly	CTGTGTGCTCATTGATCGCG
SL1065	spindly	GAACAATGGGATCGTTCGCG
SL1066	cindr	CAAGCAATTCCAGCACCACC
SL1067	cindr	AAGGCGCCTTCTTCTTCTCC
SL1070	CG13465	GCCGAAACCGCTCTTGTTTC
SL1071	CG13465	ATTGCCATGGCCTCCAGTTT

5.1.6.2 Plasmids

Plasmid	Gene	Vector
LP157	Mab-eve	pCRII TOPO-TA
LP459	Mab-btd	pCRII TOPO-TA
LP462	Cri-btd	pSP
LP494	CG13894	pCRII TOPO-TA
LP521	CG15545	pCRII TOPO-TA
LP522	Blimp-1	pCRII TOPO-TA
LP523	meltrin	pCRII TOPO-TA

LP537	3'-eGFP	pSP
LP550	numb	pCRII TOPO-TA
LP595	GAP43-eGFP	pSP
LP620	CG33509	pCRII TOPO-TA
LP621	CG30159	pCRII TOPO-TA
LP622	CG5004	pCRII TOPO-TA
LP623	CG6272	pCRII TOPO-TA
LP624	CG6891	pCRII TOPO-TA
LP625	CG7131	pCRII TOPO-TA
LP626	CHES-1-like	pCRII TOPO-TA
LP627	eve	pCRII TOPO-TA
LP632	CG13465	pCRII TOPO-TA
LP633	cindr	pCRII TOPO-TA
LP634	hoip	pCRII TOPO-TA
LP635	noc	pCRII TOPO-TA
LP636	path	pCRII TOPO-TA
LP637	spindly	pCRII TOPO-TA
LP638	tmod	pCRII TOPO-TA
LP645	Mab-sqh-eGFP	pSP
LP649	GAP43-mCherry	pSP

5.1.7 Instruments

MicroPulser (BioRad) electroporator

Incubation Shaker Model G25, New Brunswick Scientific Co. Inc., Edison, USA

Megafuge 1.0R (Heraeus Sepatech GmbH, Osterode)

Microscopy: Leica SPE and SP8 confocal microscopes were used during my thesis to image both fixed and live imaging. In the fly culture room, Zeiss Stemi 2000-C with Zeiss CL 1500 light source were generally used.

5.2 Methods:

5.2.1 Genomic DNA extraction

The genomic DNA was extracted from 10 adult flies that were homogenized in 500µl lysis buffer with a micropestle. Following, 15µl ProteinaseK (10µg/µl) were added and incubated 1h at 56°C. The DNA was cleaned by phenol/chloroform extraction and the RNA was degraded with 5µl RNaseA (10µg/µl) and an incubation of 10 min at 37°C. In order to purify the genomic DNA, phenol/chloroform extraction was performed and the DNA was precipitated with 50µl NaOAc (3M pH6) and 1ml EtOH. The pellet was dissolved in 30µl Tris/HCl 10mM pH 8.5 and stored at -20°C.

5.2.2 Polymerase Chain Reaction

The polymerase chain reaction (PCR) was applied to amplify DNA fragments *in vitro*. For PCR reactions, either the RedTaq Ready Mix (Sigma), or the iProof High-Fidelity DNA polymerase (BioRad) was used. The final reaction volume was 25µl. The producers' recommended protocols were altered according to different fragments to be amplified. Below, reaction mixes and protocols which were generally used to amplify approximately 1kb fragments.

RedTaq Jumpstar Ready Mix

Volume	Reagent	Final concentration
12.5 µL	JumpStart REDTaq ReadyMix	1×
1µL	Forward Primer (20µM)	0.4 µM
1 µL	Reverse primer (20 µM)	0.4 µM
--- µL	Template DNA	1-200 ng

q.s.	Water	
25µL		Total volume

PCR program:

Initial denaturation	94 °C	2 min
30-35 cycles:		
Denaturation	94 °C	30 sec
Annealing	55 °C to 68 °C	30 sec
Extension	72 °C	2 min
Final extension	72 °C	5 min
Hold	4 °C	

iProof Reaction Mix

Volume	**Reagent**	**Final concentration**
12.5 µL	5X iProof GC Buffer	1×
0.5µL	dNTPmix	
0.5µL	Forward Primer (20µM)	0.4 µM
0.5µL	Reverse primer (20 µM)	0.4 µM
--- µL	Template DNA	1-200 ng
add up to 25µL	Water	
25µL	Total volume	

PCR program

Initial denaturation	98 °C	2 min
30-35 cycles:		
Denaturation	98 °C	30 sec
Annealing	Tm +3°C	30 sec
Extension	72 °C	2 min
Final extension	72 °C	8 min
Hold	4 °C	

5.2.3 Agarose Gel Electrophoresis

Agarose gel electrophoresis was used to quantify DNA and RNA fragments and also to evaluate their quality and length. In most cases, 1% agarose gel in TAE buffer was used for this purpose. Heat-dissolved agarose gel solution was let cool down before the addition of intercalating agent EtBr (2µg/ml). Samples before loading was mixed with 6X loading dye. Under constant voltage separation of DNA/RNA fragments were achieved. DNA ladder was used as a reference to determine size and quality of the material under a UV illuminator.

Extraction of DNA from Agarose gel

After the desired bands were cut from the agarose gel, isolation of DNA was performed using 'QIAquick Gel Extraction Kit (Qiagen, Germany) according to manufacturer's directions.

5.2.4 Cloning:

Purified DNA fragments were ligated into two different vectors in this thesis.

5.2.4.1 TOPO TA Cloning

Gene fragments to be used as templates for dsRNA synthesis or RNA probe synthesis were cloned into pCR21.-TOPO TA vector (ThermoFischer Scientific). Since the fragments amplified by the taq polymerase in RedTaq Jumpstart Ready Mix already contained adenine overhangs, ligation to the vectors' respective thymine overhangs was efficiently performed. To secure higher yield, however, the reaction mix was held at room temperature for 1h, in contrast to manufacturer's suggested 5min.

Reaction mix

10x buffer	1µL
PCR product	3µL
pCR2.1-TOPO TA vector	1µL
H_2O	5µL

5.2.4.2 DNA restriction

In order to determine whether the cloning worked as intended, isolated plasmids were checked via DNA restriction. In each DNA restriction reaction, about 2-10U of restriction enzyme was used for each µg of plasmid according to manufacturer's directions. To ensure proper digestion, the reaction was held for between 1-4h at the suggested working temperature. If suggested by the manufacturer, inactivation of enzyme was accomplished by incubation at 70°C for about 20min. Digested plasmids for test purposes were then checked by agarose gel electrophoresis. Correctly cloned plasmids were then sent for sequencing before addition to the database.

5.2.5 Bacterial Transformation

5.2.5.1 Electrocompetent bacterial cell preparation

To prepare electrocompetent bacterial cell stock, a pre-culture of 100mL was made by inoculating a single colony. The pre-culture was then incubated at 37°C in a shaking incubator over night. The next day, 8mL of the pre-culture was used to inoculate each of four preheated 800mL LB-filled flasks. Culture were then incubated at 37°C, until a concentration reading of 0.6-0.8 at OD600nm was achieved. Afterwards, the cultures were kept on ice for 15min, which was followed by a centrifugation step at 4000rpm for 20min. After the supernatant was discarded, the remaining pellets were dissolved in 20mL ice-cold water. The tubes were then filled with 400mL water, and the centrifugation step was re-applied. Pellets were again dissolved in 20mL water, which were then topped up to 100mL. Tubes were pooled together as doublets, and a third centrifugation step was performed. Lastly, the pellets were dissolved in 15mL ice-cold 10% glycerol and the culture was distributed into 50mL falcon tubes filled with 50mL ice-cold 10% glycerol. A final centrifugation round at 4000 rpm for 40min. After the supernatant was disposed, the pellet was resuspended in 4mL 10% glycerol. Aliquots of 50µL in 1.5mL tubes were prepared. The aliquots were snap frozen in liquid nitrogen prior to the storage at -80°C.

5.2.5.2 Bacterial transformation via electroporation and blue/white selection

Electrocompetent cell aliquots were thawed on ice after fetched from -80°C freezer. Electroporation cuvettes, which were pre-cooled on ice, were filled with 40µL competent cells. In general, 1ng of plasmid (corresponded to 1µL on average) were added to the cuvette. The electroporation was performed at 1800V in a MicroPulser (BioRad). The cuvettes were then filled with 250 µL LB (or SOC medium). Afterwards, the culture were transferred into 1.5mL tubes and placed in

a shaking incubator at 37°C for 1h to promote recovery of the bacterial cells. The cell culture was then spread on 20mg/mL X-Gal containing LB plates with ampilicin (100µg/mL) or kanamycin (50µg/mL), depending on the vector. Plates were then incubated at 37°C overnight. Lastly, white colonies indicative of correct ligation were then picked and grown overnight in 4mL LB medium containing ampicillin or kanamycin according to the used vector.

5.2.5.3 Plasmid isolation

4mL of each overnight-grown culture was spun down for 2min at 4000 rpm. The bacterial pellets were resuspended in 200µL ice-cold P1 buffer and then lysed in 200µL P2 buffer. The lysis reaction was stopped by adding 200µL P3 buffer, and the tubes were centrifuged at 14000rpm for 15min. The supernatants were transferred into fresh tubes. Afterwards, DNA was precipitated for 10min with 500µL isopropanol, which was followed by a centrifugation step of 15min at 14000rpm. Subsequently, the pellets were washed in 70% EtOH. After air drying for about 30min at RT, the pelleted plasmid DNA was dissolved in 30µL EB. The plasmid isolates were tested for accuracy of the prior cloning step via DNA restriction reactions, which were then visualized with agarose gel electrophoresis. The plasmids which seemed to have accurate integration were sent for sequencing before adding them to the plasmid stock. The clones that were used frequently were amplified in larger cultures, and isolated by using the QIAGEN Midi Plasmid Kit, according to the manufacturer's directions.

P1 Buffer (stored at 4°C)

Tris base (pH 8.0)	50mM
EDTA	10mM
RNase A	100mg/mL

P2 Buffer

NaOH	200mM
SDS	1% (w/v)

P3 Buffer (stored at 4°C)

$C_2H_3KO_2$ (pH 5.5)	3mM

EB buffer

EDTA	1mM
Tris (pH 8.0)	10mM

RNase working solution

NaCl	150mM
RNase	10mg/mL

5.2.6 RNA synthesis

5.2.6.1 mRNA synthesis

For mRNA synthesis, full-length coding sequence of the gene-of-interest had previously subcloned into expression vectors (pSP). 5-10µg of the pSP plasmids were linearized by the restriction enzyme (PstI, SacI or EcoRI) at 37°C for 1h, and subsequently inactivated at 65°C for 20min.

The linearized template was purified from protein traces by treating the reaction mix with 2µL ProteinaseK (10mg/mL) and 5 µL 10% SDS at 50°C for 30min. Afterwards, the reaction mix was filled with nuclease-free H_2O to a final volume of 200µL, and phenol-chloroform extraction was performed. The template DNA was then precipitated by adding 1/10 volume of NaOAc and 3 volumes of EtOH and keeping the tubes at -20°C for 2h. After the supernatant was discarded,

the remaining was rehydrated in 10µL H_2O. The quality and concentration of the purified linear plasmid DNA was evaluated by agarose gel electrophoresis.

For the mRNA synthesis reaction, the reaction below using the mMessage mMachine T7 Ultra Kit (Ambion) was set up.

Linearized template pSP clone	1µg
10x reaction buffer	4µL
2x NTP/CAP	20µL
Enzyme mix	4 µL
H_2O	Add up to 40µL

The reaction mix was held at 37°C for 15min.

5.2.6.2 dsRNA synthesis

To synthesize dsRNA, linearized pCRII-TOPO plasmids were PCR amplified with primers containing T7 promoter sequences.

10X buffer	10µL
Linearized pCRII-TOPO plasmid	1µL
dNTPs (10mM)	2µL
SL0049 (10µM)	3µL
SL0050 (10µM)	3µL
Taq Polymerase	2µL
H_2O	Add up to 100µL

The reaction mastermix was then aliquoted to three PCR tubes, and the following protocol was run:

1. 94°C	2min
2. 94°C	20s
3. 60°C	30s
4. 72°C	1min
Repeat 45 times from step 2 to 4	
72°C	5min

The PCR product was purified via phenol/chloroform extraction and the pelleted template was dehydrated in 10µL H_2O.

The dsRNA synthesis reaction was then run for 4-6h at 37°C.

10X Transcription Buffer	10µL
NTPs (2.5mM each)	40µL
DNA template	1-2µg
RNase inhibitor	2µL
T7 RNA polymerase	2.5µL
RNase free H_2O	Add up to 100µL

The DNA template in the reaction was then degraded by addition of 1.5µL DNase and incubating at 37°C for 15min. Subsequently, phenol/chloroform extraction was performed to purify RNA. The RNA was then precipitated in EtOH at -20°C for 2h or overnight. The pellet was first air-dried and resuspended in 20µL H_2O.

Serial dilutions of RNA concentration was checked on agarose gel. Depending on the gel results, an addition annealing step was performed in some cases, by decreasing the temperature from 94°C to RT in small decrements in a thermal cycler.

Before use, the dsRNA was spun down and the supernatant (15 out of 20µL) was transferred into a fresh tube. The dsRNA was stored at -20°C.

Run protocol:

94°C	5min
94°C	40s / -0.1°C per cycle (in total 749cycles)

5.2.7 Embryo fixation

5.2.7.1 Heat Fixation

The fixative solution in a flask was heated in a microwave (800W) for 20 s, which brought the solution to boiling point. The solution was then quickly poured upon the dechlorinated embryos in 50mL-falcon tube. For 20s the embryos were fixated in the solution, then 30mL water was added. After the elevated embryos sank down to the tube bottom, they were transferred into 1.5mL tubes via micropipettes with cut tips.

To devitellinize the embryos, first 500µL Heptane and then 500µL MeOH was added, the tubes were rigorously shaken by hand for 30s. With gentle tapping on the tube walls, the embryos were helped sunk down to the bottom. After discarding the supernatant, the embryos were washed three times in MeOH.

Fixative solution I

TritonX 100 (5%)	200µL
NaCl (28% w/v)	500µL
H_2O	19.3mL

For *D. melanogaster* and *M. abdita* embryos (not *C. riparius),* a secondary fixation protocol was applied. The fixation solution II was added onto the tubes and

the secondary fixation was held on a rocker for 25 min at RT. Lastly, the embryos were washed three times in MeOH, and stored at -20°C.

Formaldehyde (37%)	135µL
PBS	648.75µL
MeOH-	216.25µL

The embryos that were injected beforehand were first cleaned off the overlaying oil with heptane. Then, the embryos were pushed into a falcon tube by squirting water from spray bottle. After the water was discarded, the embryos were fixed according to the aforementioned protocol.

5.2.7.2 Formaldehyde Fixation

Formaldehyde fixation method was also applied during the optimization of the double fluorescent *in situ* hybridization protocol in *M. abdita* and in *C. riparius.*

After the embryos were dechorionated, they were fixed for 30min on a rocker in the following solution:

PBS	450 µL
Heptane	500 µL
37% Formaldehyde	54 µL (final 4%)

The fixation solution was then removed and devitellinization of the embryos was performed as mentioned above.

5.2.8 Whole mount *in situ* Hybridizations

5.2.8.1 *In situ* Probe Synthesis

The pCRII-TOPO plasmids containing fragments of gene-of-interest was linearized according to the insert orientation. For the linearization reaction, 10µg of plasmid was used in a total of 50µL reaction volume. The reaction was performed for 4h to ensure complete linearization. The linear plasmid was purified via phenol/chloroform extraction. Subsequently, the linearized plasmid was precipitated with the addition of 1µl glycogen (10mg/ml), 1/10 volume of NaOAc (3M, pH 6.0) and 3 volumes of EtOH. After the removal of the supernatant and air-drying, pellet was dissolved in 10µL H_2O. The concentration of the linearized template plasmids was then checked on an agarose gel. Lastly, the RNA probe synthesis reaction was performed in the following reaction mix:

Linearized template plasmid	1µg
10x Transcription Buffer	1µg
DIG-NTP (or FITC-NTP)	1µL
RNase Inhibitor	1µL
RNA polymerase	1µL
RNase-free H_2O	Add up to 10µL

The concentration of synthesized RNA probe was checked in a series of dilutions, via agarose gel electrophoresis.

After the addition of 90µL RNase-free H_2O, the RNA probe was precipitated with 10µL LiCl (4M), 10µL tRNA (10mg/mL) and 300µL EtOH at -20°C overnight. According to the approximated concentration, the RNA probe pellet was dissolved in a respective volume of HYB solution so that the final concentration was about 10µg/µL.

HYB Buffer

50% Formamide
5X SSC
Torula yeast RNA (5mg/ml)
Heparin (50µg/ml)
Tween-20 (0.1%)
RNase-free H_2O

5.2.8.2 Wholemount in situ hybridization

The heat- or formaldehyde-fixed embryos were washed in EtOH first to wash off MeOH that they were stored in. Then a series of Xylene/EtOH washes were applied to clear the embryos. First in 1:1 Xylene:EtOH, then 3:1 Xylene:EtOH on a rocker for 1h and a final was in 1:1 Xylene:EtOH. Afterwards, the embryos were washed in EtOH three times, and then three times in MeOH. To rehydrate the embryos, they were first washed in 1:1 PBT:MeOH, and three times in PBT (0.1% Tween 20 in PBS). *M. abdita* embryos were treated with ProteinaseK (0.08U/ml) for 2 min at RT and then placed on ice for 1h. The *C. riparius* embryos, however, were directly placed and kept on ice for 1h after addition of ProteinaseK. The embryos were then washed in ice-cold PBT three times and post-fixed in 5% formaldehyde in PBT for 25 min on a rocker. The embryos were then washed five times in PBT and transferred to 0.5ml tubes, which were then washed in 1:1 PBT:HYB for 10min on a rocker. The embryos were then washed in only HYB for 2min and prehybridized in HYB at 56°C for 1h. RNA probes were heated up to 80°C for 5min to prevent secondary RNA structures and snap-frozen in ice water. The amount of RNA probes that were used was calculated according to the amount of embryos. While conventional colorimetric *in situ* hybridization reactions final concentration of 1-2ng/µl of RNA probes were used, for double fluorescent *in situ* hybridizations a final concentration of 3-5ng/µl for each probe was used. After

removing the prehybridization HYB solution, the snap-frozen probes were added onto embryos, which were hybridized for 12-16h at 56°C. The next day, embryos were first post-hybridized for 15min by addition of pre-heated HYB solution and further post-hybridized twice for 30min in HYB at 56°C. The embryos were then washed in PBT five times. For fluorescent *in situ* hybridizations, embryos were washed in 4-5 drops of Image iT FX Signal Enhancer for 30min, which help reduce the high background signal. For blocking, 5% goat serum or 1% w/v blocking reagent (Roche) in PBT was added onto the embryos and kept for 1h. For double fluorescent *in situs,* primary mouse anti-digoxigenin (Roche, 11 333 062 910) antibody (1:250, 2h), and Alexa Fluor 488 labeled goat anti-mouse secondary antibody (1:400, 1h, Jackson ImmunoResearch, 115 545 062) was used to detect one of the transcripts. For the other transcript, primary rabbit anti-fluorescein antibody (1:250; 2h; Life Technologies, A889), and Alexa Fluor 647 labeled donkey anti-rabbit secondary antibody (1:400; 1h; Jackson ImmunoResearch, 711 605 152) were used. After antibody incubations, the embryos were washed three times in PBT, and then four times on a rocker for 15min. Lastly, the embryos were soaked in a series of glycerol and mounted on glass slides for imaging.

5.2.9 Confocal imaging

For double fluorescent *in situ* hybridization embryos, confocal scans with 0.56 μm step size were done with a single-photon confocal imaging on a Leica System (SP8) using 20x immersion objective (HC PL APO CS2 20x/0.75 IMM).

5.2.10 Image Processing

5.2.10.1 Activation of myosin along the AP axis.

sqh::GFP mRNA injection was used to label myosin network in the embryo. A limited number of z-planes around the apical plane of cells were projected by maximum-intensity projection. This provided visualization of junctional and supracellular myosin activation and better S/N ratio compared with projections over complete cell height.

To examine the spatiotemporal distribution of myosin activity in the anteroposterior axis, a strip of 2-3 cells wide were selected along the lateral axis, spanning from the anterior tip to the posterior end of the embryo. On the resulting image, integrated intensity values of myosin fluorescence on successive timepoints were calculated. For all images background substraction was done by substracting background intensities from pre-GBE stages. Brightness-weighted average of all pixels (center of mass) over the AP axis were than calculated to inspect spatial distribution of myosin activation.

5.2.10.2 Quantification of speed of the myosin wave

Measurement of the activation wave speed was manually done. Activation was defined by mean MyoII intensity crossing a threshold. The position of myosin activation was read directly in microscopy images, which included the complete frame of the embryo. Time 0 is defined as the time of activation of the first cell.

5.2.10.3 Quantification of membrane straightness

The straightness index (SI) was calculated by substracting the theoretical minimal length from the actual measured distance and normalizing it to the actual distance. The SI unit is given in arbitrary units (AU). Therefore, for a straight line the SI is calculated to be zero. For example, a value of 5 AU means that the actual

length was 5% longer than the theoretical minimal distance between two points. Measurements were manually done by using the line tool in the Fiji software (Schindelin et al., 2012).

5.2.11 Contributions

I thank to Francesca Caroti and Everardo Gonzales, for providing me the Muvi SPIM recording that was analyzed in this project. I also thank Maike Wosch who helped me with the benchwork towards the end of my project.

6 Acknowledgements

First of all, I cannot thank Steffen enough for introducing me the realm of flies with endless insights and extreme patience. His enthusiasm for science has always been extraordinary and he generously radiated it over the years, which has been a driving force for me in dire times, which were not very uncommon. Besides being a great supervisor, he has always shown a sincere understanding of life outside the lab, and made sure to be welcoming to talk, which I very much appreciated. I see myself lucky and I feel very happy that I worked on my PhD thesis in his lab.

I also would like to thank my TAC members Jochen and Ingrid, who were always willing to help me find my direction in my project. They have always made sure to provide me with their genuinely challenging, but therefore rewarding, feedbacks.

I further like to thank Sebastian and Guido, who accepted to be by my side in the last stretch of my journey. I am already feeling excited to hear their ideas on how to further increase the impact of my project during my defense.

I am also grateful to all the past and current members of the Lemke Lab. They have always been very helpful and made the lab a fun place. I must also specifically mention Viola, who has been a good friend and colleague with whom I shared most over the years, residing in the same bay.

Lastly, I would like to thank my family who always made me feel loved, no matter what. Hicbir zaman desteklerini esirgemeyen, her zaman yanimda olan ve varliklariyla bana guc veren canim anne ve babama, her ihtiyacim oldugunda comertce yardimima kosan sevgili agabeyime sonsuz tesekkurlerimi sunarim. Iyi ki hayatimdalar. Hayatimin en zorlu ve en guzel anlarinda yanimda olan, en yakin dostum ve sirdasim; varligiyla icimi isitan, birlikte yollara dusmeye can attigim canim Sunam'a cok tesekkur ederim.

7 APPENDIX

7.1 Matlab and Fiji Scripts

7.1.1 Kymograph Analysis for myosin localization in Fiji

```
i=0
for(i=0;i<201;i=i+1){

selectWindow("MAX_MAX_apical_selection(3.5um)_singlePixel.tif");
makeLine(i, 0, i, 0);


run("Multi Kymograph", "linewidth=1");
run("Rotate 90 Degrees Right");
run("Flip Horizontally");
saveAs("Tiff", "/folder_path");

close();

}
```

7.1.2 Analysis of the Single Cell Transcriptomics Data in Matlab

```
%CF_trunk_variance
[data,varnames,casenames] = tblread('dge_cherries_mel_cell_names.txt','tab');
%%
genes=casenames;
cells=varnames;
genes_cell_array=cellstr(genes);
cells_cell_array=cellstr(cells);
%%
eve=data(strmatch('eve',genes_cell_array,'exact'),:);
eve_sub= eve(eve>0);
i_eve=find(eve);
compl_exp_all_eve_434cells=data(:,i_eve);
```

```
mean_eve_sub=mean(eve_sub);
[desc_eve,i_desc_eve]=sort(eve,'descend');
desc_eve_sub=desc_eve(1:ceil(length(eve_sub)));
i_desc_eve_sub=i_desc_eve(1:ceil(length(eve_sub)));
i_desc_eve_sub_highest30=i_desc_eve(1:ceil(length(eve_sub)*0.3));
t_i_desc_eve_sub_highest30=transpose(i_desc_eve_sub_highest30);

%%

Dfd=data(strmatch('Dfd',genes_cell_array,'exact'),:);
Dfd_sub=Dfd(Dfd>0);
all_indices=[1:1297];
i_Dfd_sub=find(Dfd>0);
i_wo_Dfd=setdiff(all_indices,i_Dfd_sub);

eve_Dfd=eve&Dfd;
i_eve_Dfd=find(eve_Dfd);
t_i_Dfd_sub=transpose(i_Dfd_sub);
mean_Dfd_sub=mean(Dfd_sub);
[desc_Dfd,i_desc_Dfd]=sort(Dfd,'descend');
desc_Dfd_sub=desc_Dfd(1:ceil(length(Dfd_sub)));
i_desc_Dfd_sub=i_desc_Dfd(1:ceil(length(Dfd_sub)));
eve_Dfd=eve&Dfd;
eve_Dfd_cellno=sum(eve_Dfd(:)==(1));
i_eve_Dfd=find(eve_Dfd);
i_eve_Dfd_highest30=intersect(i_desc_eve_sub_highest30,i_Dfd_sub);
i_eve_highest30_wo_Dfd=intersect(i_desc_eve_sub_highest30,i_wo_Dfd);
compl_exp_eve_highest30_wo_Dfd=data(:,i_eve_highest30_wo_Dfd);

%%
gsb=data(strmatch('gsb',genes_cell_array,'exact'),:);

i_gsb=find(gsb);
gsb_sub=gsb(gsb>0);
i_gsb_sub=find(gsb>0);

%%
prd=data(strmatch('prd',genes_cell_array,'exact'),:);

i_prd=find(prd);
prd_sub=prd(prd>0);
i_prd_sub=find(prd>0);


%%

btd=data(strmatch('btd',genes_cell_array,'exact'),:);
[desc_btd,i_desc_btd]=sort(btd,'descend');
btd_sub=btd(btd>0);
i_btd_sub=find(btd);
i_btd_sub=find(btd>0);
desc_btd_sub=desc_btd(1:ceil(length(btd_sub)));
%%

eve_btd=eve&btd;
eve_btd_cellno=sum(eve_btd(:)==(1));
i_eve_btd=find(eve_btd);
```

```
eve_btd_Dfd=eve_btd&Dfd;
eve_btd_Dfd_cellno=sum(eve_btd_Dfd(:)==(1));
i_eve_btd_Dfd=find(eve_btd_Dfd);
btd_Dfd=btd&Dfd;
btd_Dfd_cellno=sum(btd_Dfd(:)==(1));
i_eve_Dfd_wo_btd=setdiff(i_eve_Dfd,i_eve_btd_Dfd);

%%
eve_btd_prd=eve_btd&prd;
eve_btd_prd_cellno=sum(eve_btd_prd(:)==(1));
i_eve_btd_prd=find(eve_btd_prd);

btd_prd=btd&prd;
btd_prd_cellno=sum(btd_prd(:)==(1));
i_btd_prd=find(btd_prd);

eve_prd=eve&prd;
eve_prd_cellno=sum(eve_prd(:)==(1));
i_eve_prd=find(eve_prd);

%%
compl_exp_eve_btd=data(:,i_eve_btd);
t_compl_exp_eve_btd=transpose(compl_exp_eve_btd);

mean_t_compl_exp_eve_btd=mean(t_compl_exp_eve_btd);
[desc_mean_t_compl_exp_eve_btd,i_desc_mean_t_compl_exp_eve_btd]=sort(mean_t_compl_exp_eve_btd,'desc
end');
genes_mean_t_compl_exp_eve_btd=genes_cell_array(i_desc_mean_t_compl_exp_eve_btd);
%%
i_eve_btd_wo_prd=setdiff(i_eve_btd,i_eve_btd_prd);
compl_exp_eve_btd_wo_prd=data(:,i_eve_btd_wo_prd);
t_compl_exp_eve_btd_wo_prd=transpose(compl_exp_eve_btd_wo_prd);

mean_t_compl_exp_eve_btd_wo_prd=mean(t_compl_exp_eve_btd_wo_prd);
[desc_mean_t_compl_exp_eve_btd_wo_prd,i_desc_mean_t_compl_exp_eve_btd_wo_prd]=sort(mean_t_compl_exp
_eve_btd_wo_prd,'descend');
genes_mean_t_compl_exp_eve_btd_wo_prd=genes_cell_array(i_desc_mean_t_compl_exp_eve_btd_wo_prd);
%%

compl_exp_eve_btd_prd=data(:,i_eve_btd_prd);
t_compl_exp_eve_btd_prd=transpose(compl_exp_eve_btd_prd);

i_btd_prd_wo_eve=setdiff(i_btd_prd,i_eve_btd_prd);
compl_exp_btd_prd_wo_eve=data(:,i_btd_prd_wo_eve);
t_compl_exp_btd_prd_wo_eve=transpose(compl_exp_btd_prd_wo_eve);

mean_t_compl_exp_btd_prd_wo_eve=mean(t_compl_exp_btd_prd_wo_eve);
[desc_mean_t_compl_exp_btd_prd_wo_eve,i_desc_mean_t_compl_exp_btd_prd_wo_eve]=sort(mean_t_compl_exp
_btd_prd_wo_eve,'descend');
genes_mean_t_compl_exp_btd_prd_wo_eve=genes_cell_array(i_desc_mean_t_compl_exp_btd_prd_wo_eve);
%%
[Httest_eve_btd_prd_wo_prd,Pttest_eve_btd_prd_wo_prd,stats_eve_btd_prd_wo_prd]=ttest2(t_compl_exp_e
ve_btd_prd,t_compl_exp_eve_btd_wo_prd,'Alpha',0.05,'Tail','right','Vartype','unequal');
[sort_Pttest_eve_btd_prd_wo_prd,i_Pttest_eve_btd_prd_wo_prd]=sort(Pttest_eve_btd_prd_wo_prd);
t_i_Pttest_eve_btd_prd_wo_prd=transpose(i_Pttest_eve_btd_prd_wo_prd);
sig_genes_eve_btd_prd_wo_prd=genes_cell_array(t_i_Pttest_eve_btd_prd_wo_prd,:);
%%
```

```
        [Httest_eve_btd_prd_wo_btd,Pttest_eve_btd_prd_wo_btd,stats_eve_btd_prd_wo_btd]=ttest2(t_compl_exp_e
ve_btd_prd,t_compl_exp_eve_prd_wo_btd,'Alpha',0.05,'Tail','right','Vartype','unequal');
        [sort_Pttest_eve_btd_prd_wo_btd,i_Pttest_eve_btd_prd_wo_btd]=sort(Pttest_eve_btd_prd_wo_btd);
        t_i_Pttest_eve_btd_prd_wo_btd=transpose(i_Pttest_eve_btd_prd_wo_btd);
        sig_genes_eve_btd_prd_wo_btd=genes_cell_array(t_i_Pttest_eve_btd_prd_wo_btd,:);

        %% Comparison of gene expression in eve/btd/prd+ cells and only btd/prd+cells but no eve cells
        [Httest_eve_btd_prd_wo_eve,Pttest_eve_btd_prd_wo_eve,stats_eve_btd_prd_wo_eve]=ttest2(t_compl_exp_e
ve_btd_prd,t_compl_exp_btd_prd_wo_eve,'Alpha',0.05,'Tail','right','Vartype','unequal');
        [sort_Pttest_eve_btd_prd_wo_eve,i_Pttest_eve_btd_prd_wo_eve]=sort(Pttest_eve_btd_prd_wo_eve);
        t_i_Pttest_eve_btd_prd_wo_eve=transpose(i_Pttest_eve_btd_prd_wo_eve);
        sig_genes_eve_btd_prd_wo_eve=genes_cell_array(t_i_Pttest_eve_btd_prd_wo_eve,:);

        %% Comparison of gene expression in eve/btd/prd+ cells and all the other cells

        i_wo_eve_btd_prd=setdiff(all_indices,i_eve_btd_prd);
        compl_exp_wo_eve_btd_prd=data(:,i_wo_eve_btd_prd);
        t_compl_exp_wo_eve_btd_prd=transpose(compl_exp_wo_eve_btd_prd);

        [Httest_eve_btd_prd,Pttest_eve_btd_prd,stats_eve_btd_prd]=ttest2(t_compl_exp_eve_btd_prd,t_compl_ex
p_wo_eve_btd_prd,'Alpha',0.05,'Tail','right','Vartype','unequal');
        [sort_Pttest_eve_btd_prd,i_Pttest_eve_btd_prd]=sort(Pttest_eve_btd_prd);
        t_i_Pttest_eve_btd_prd=transpose(i_Pttest_eve_btd_prd);
        sig_genes_eve_btd_prd=genes_cell_array(t_i_Pttest_eve_btd_prd,:);

        %%
        i_eve_prd_wo_btd=setdiff(i_eve_prd,i_eve_btd_prd);
        compl_exp_eve_prd_wo_btd=data(:,i_eve_prd_wo_btd);
        t_compl_exp_eve_prd_wo_btd=transpose(compl_exp_eve_prd_wo_btd);

        mean_t_compl_exp_eve_prd_wo_btd=mean(t_compl_exp_eve_prd_wo_btd);
        [desc_mean_t_compl_exp_eve_prd_wo_btd,i_desc_mean_t_compl_exp_eve_prd_wo_btd]=sort(mean_t_compl_exp
_eve_prd_wo_btd,'descend');
        genes_mean_t_compl_exp_eve_prd_wo_btd=genes_cell_array(i_desc_mean_t_compl_exp_eve_prd_wo_btd);

        %%
        compl_exp_eve_btd_prd=data(:,i_eve_btd_prd);
        t_compl_exp_eve_btd_prd=transpose(compl_exp_eve_btd_prd);

        %i_no_eve_btd_prd=setdiff(
        %compl_exp_eve_btd_prd=data(:,


        mean_t_compl_exp_eve_btd_prd=mean(t_compl_exp_eve_btd_prd);
        [desc_mean_t_compl_exp_eve_btd_prd,i_desc_mean_t_compl_exp_eve_btd_prd]=sort(mean_t_compl_exp_eve_b
td_prd,'descend');
        genes_mean_t_compl_exp_eve_btd_prd=genes_cell_array(i_desc_mean_t_compl_exp_eve_btd_prd);
        %%

        gsb_prd=gsb&prd;
        i_gsb_prd=find(gsb_prd);
        i_eve_btd_gsb_prd=intersect(i_eve_btd,i_gsb_prd);

        eve_btd_gsb_prd=eve_btd&gsb_prd;

        eve_btd_gsb_prd_cellno=sum(eve_btd_gsb_prd(:)==(1));

        cells_eve_btd_gsb_prd_all=cells_cell_array(i_eve_btd_gsb_prd);
```

```
i_eve_btd_wo_gsb_prd=setdiff(i_eve_btd,i_eve_btd_gsb_prd);

%%

%%
compl_exp_eve_btd_gsb_prd=data(:,i_eve_btd_gsb_prd);
t_compl_exp_eve_btd_gsb_prd=transpose(compl_exp_eve_btd_gsb_prd);

mean_t_compl_exp_eve_btd_gsb_prd=mean(t_compl_exp_eve_btd_gsb_prd);
[desc_mean_t_compl_exp_eve_btd_gsb_prd,i_desc_mean_t_compl_exp_eve_btd_gsb_prd]=sort(mean_t_compl_e
xp_eve_btd_gsb_prd,'descend');
genes_mean_t_compl_exp_eve_btd_gsb_prd=genes_cell_array(i_desc_mean_t_compl_exp_eve_btd_gsb_prd);

%%


%%Enrichment eve-btd cell over all data

t_data=transpose(data);
mean_t_data=mean(t_data);
enrichment_mean_eve_btd_over_alldata= mean_t_compl_exp_eve_btd ./ mean_t_data;
[desc_enrichment_mean_eve_btd_over_alldata,i_desc_enrichment_mean_eve_btd_over_alldata]=sort(enrich
ment_mean_eve_btd_over_alldata,'descend');
genes_enrichment_mean_eve_btd_over_alldata=genes_cell_array(i_desc_enrichment_mean_eve_btd_over_all
data);


%%


%%


gt=data(strmatch('gt',genes_cell_array,'exact'),:);
gt_sub=gt(gt>0);
i_gt_sub=find(gt>0);
mean_gt_sub=mean(gt_sub);
[desc_gt,i_desc_gt]=sort(gt,'descend');
desc_gt_sub=desc_gt(1:ceil(length(gt_sub)));
i_desc_gt_sub=i_desc_gt(1:ceil(length(gt_sub)));
i_desc_gt_sub_highest25=i_desc_gt(1:ceil(length(gt_sub)*0.25));
combined_indices_btd_Dfd=union(i_btd_sub,i_Dfd_sub);
combined_indices_btd_Dfd_gt_highest25=union(combined_indices_btd_Dfd,i_desc_gt_sub_highest25);
i_eve_highest30_wo_btd_Dfd_gt_highest25=setdiff(i_desc_eve_sub_highest30,combined_indices_btd_Dfd_g
t_highest25);
cells_eve_highest30_wo_btd_Dfd_gt_highest25=cells_cell_array(i_eve_highest30_wo_btd_Dfd_gt_highest2
5);
cells_eve_btd_all=cells_cell_array(i_eve_btd);
i_eve_btd_highest30=intersect(i_desc_eve_sub_highest30,i_btd_sub);

cell_ID_CFcells=cells_cell_array(i_eve_btd_highest30);

%%

compl_exp_eve_btd_all_32_cells=data(:,i_eve_btd);
compl_exp_eve_highest30_btd=data(:,i_eve_btd_highest30);
compl_exp_eve_highest30_wo_btd_Dfd_gt_highest25=data(:,i_eve_highest30_wo_btd_Dfd_gt_highest25);
```

```
        compl_exp_combined_eve_highest30_btd_wo_btd_Dfd_gt_highest25=horzcat(compl_exp_eve_highest30_btd,co
mpl_exp_eve_highest30_wo_btd_Dfd_gt_highest25);
        i_eve_btd_highest30=intersect(i_desc_eve_sub_highest30,i_btd_sub);
        compl_exp_eve_highest30_btd=data(:,i_eve_btd_highest30);
        compl_exp_eve_highest30_wo_btd_Dfd_gt_highest25=data(:,i_eve_highest30_wo_btd_Dfd_gt_highest25);
        compl_exp_combined_eve_highest30_btd_wo_btd_Dfd_gt_highest25=horzcat(compl_exp_eve_highest30_btd,co
mpl_exp_eve_highest30_wo_btd_Dfd_gt_highest25);
        %%
        compl_exp_eve_btd_gsb_prd=data(:,i_eve_btd_gsb_prd);
        compl_exp_eve_btd_wo_gsb_prd=data(:,i_eve_btd_wo_gsb_prd);
        t_compl_exp_eve_btd_gsb_prd=transpose(compl_exp_eve_btd_gsb_prd);
        t_compl_exp_eve_btd_wo_gsb_prd=transpose(compl_exp_eve_btd_wo_gsb_prd);

        [Httest_gsb_prd,Pttest_gsb_prd,stats_gsb_prd]=ttest2(t_compl_exp_eve_btd_gsb_prd,t_compl_exp_eve_bt
d_wo_gsb_prd,'Alpha',0.05,'Tail','right','Vartype','unequal');
        [sort_Pttest_gsb_prd,i_Pttest_gsb_prd]=sort(Pttest_gsb_prd);
        t_i_Pttest_gsb_prd=transpose(i_Pttest_gsb_prd);
        sig_genes_gsb_prd=genes_cell_array(t_i_Pttest_gsb_prd,:);



        %%



        btd_gt=btd&gt;
        btd_gt_cellno=sum(btd_gt(:)==(1));
        eve_btd_gt=btd_gt&eve;
        eve_btd_gt_cellno=sum(eve_btd_gt(:)==(1));
        eve_gt=eve&gt;
        eve_gt_cellno=sum(eve_gt(:)==(1));
        cell_ID_trunkcells=cells_cell_array(i_eve_highest30_wo_btd_Dfd_gt_highest25);

        zeros_compl_exp_combined_eve_highest30_btd_wo_btd_Dfd_gt_highest25=sum(compl_exp_eve_highest30_wo_b
td_Dfd_gt_highest25==0);
        t_compl_exp_trunkcells=transpose(compl_exp_eve_highest30_wo_btd_Dfd_gt_highest25);


        zeros_t_compl_exp_trunkcells = sum(t_compl_exp_trunkcells==0);


        exp_positive_t_compl_exp_trunkcells=(size(t_compl_exp_trunkcells, 1))-zeros_t_compl_exp_trunkcells;


        %%
        ratio_exp_positive_t_compl_exp_trunkcells=exp_positive_t_compl_exp_trunkcells/(size(t_compl_exp_tru
nkcells, 1));
        ratio_greater_90=ratio_exp_positive_t_compl_exp_trunkcells(ratio_exp_positive_t_compl_exp_trunkcell
s>0.9);
        ratio_greater_80=ratio_exp_positive_t_compl_exp_trunkcells(ratio_exp_positive_t_compl_exp_trunkcell
s>0.8);
        ratio_greater_70=ratio_exp_positive_t_compl_exp_trunkcells(ratio_exp_positive_t_compl_exp_trunkcell
s>0.7);

        [desc_ratio_exp_pos_trunkcells,i_desc_ratio_exp_pos_trunkcells]=sort(ratio_exp_positive_t_compl_exp
_trunkcells,'descend');

        desc_exp_pos_greater90=desc_ratio_exp_pos_trunkcells(1:ceil(length(ratio_greater_90)));
        desc_exp_pos_greater80=desc_ratio_exp_pos_trunkcells(1:ceil(length(ratio_greater_80)));
```

```
desc_exp_pos_greater70=desc_ratio_exp_pos_trunkcells(1:ceil(length(ratio_greater_70)));

i_desc_exp_pos_greater90=i_desc_ratio_exp_pos_trunkcells(1:ceil(length(ratio_greater_90)));
i_desc_exp_pos_greater80=i_desc_ratio_exp_pos_trunkcells(1:ceil(length(ratio_greater_80)));
i_desc_exp_pos_greater70=i_desc_ratio_exp_pos_trunkcells(1:ceil(length(ratio_greater_70)));

genes_greater90=genes_cell_array(i_desc_exp_pos_greater90);
genes_greater80=genes_cell_array(i_desc_exp_pos_greater80);
genes_greater70=genes_cell_array(i_desc_exp_pos_greater70);

%%
ratio_zero_t_compl_exp_trunkcells= zeros_t_compl_exp_trunkcells/(size(t_compl_exp_trunkcells, 1));

ratio_zero_all=ratio_zero_t_compl_exp_trunkcells(ratio_zero_t_compl_exp_trunkcells== 1);
ratio_zero_greater_90=ratio_zero_t_compl_exp_trunkcells(ratio_zero_t_compl_exp_trunkcells>0.9);
ratio_zero_greater_80=ratio_zero_t_compl_exp_trunkcells(ratio_zero_t_compl_exp_trunkcells>0.8);
ratio_zero_greater_70=ratio_zero_t_compl_exp_trunkcells(ratio_zero_t_compl_exp_trunkcells>0.7);


[desc_ratio_zero_trunkcells,i_desc_ratio_zero_trunkcells]=sort(ratio_zero_t_compl_exp_trunkcells,'d
escend');

desc_exp_zero_greater90=desc_ratio_zero_trunkcells(1:ceil(length(ratio_zero_greater_90)));
desc_exp_zero_greater80=desc_ratio_zero_trunkcells(1:ceil(length(ratio_zero_greater_80)));
desc_exp_zero_greater70=desc_ratio_zero_trunkcells(1:ceil(length(ratio_zero_greater_70)));

i_desc_zero_greater90=i_desc_ratio_zero_trunkcells(1:ceil(length(ratio_zero_greater_90)));
i_desc_zero_greater80=i_desc_ratio_zero_trunkcells(1:ceil(length(ratio_zero_greater_80)));
i_desc_zero_greater70=i_desc_ratio_zero_trunkcells(1:ceil(length(ratio_zero_greater_70)));

genes_zero_greater90=genes_cell_array(i_desc_zero_greater90);
genes_zero_greater80=genes_cell_array(i_desc_zero_greater80);
genes_zero_greater70=genes_cell_array(i_desc_zero_greater70);
%%

compl_zero_greater90_trunkcells=compl_exp_eve_highest30_wo_btd_Dfd_gt_highest25(i_desc_zero_greater
90,:);
t_compl_zero_greater90_trunkcells=transpose(compl_zero_greater90_trunkcells);


%It's not necessary to find the indeces in the overall gene list, as they
%are already from that list:
%[~,loc_zero_greater90]=ismember(genes_zero_greater90,genes_cell_array);


compl_zero_greater90_CFcells=compl_exp_eve_highest30_btd(i_desc_zero_greater90,:);
t_compl_zero_greater90_CFcells=transpose(compl_zero_greater90_CFcells);

%% T-TEST FOR THE NORMALIZED DATA (ZERO EXPRESSION).

[Httestzero,Pttestzero,stats_zero]=ttest2(t_compl_zero_greater90_CFcells,t_compl_zero_greater90_tru
nkcells,'Alpha',0.05,'Tail','right','Vartype','unequal');
[sort_Pttestzero,i_Pttestzero]=sort(Pttestzero);
t_i_Pttestzero=transpose(i_Pttestzero);
sig_genes_zero=genes_zero_greater90(t_i_Pttestzero,:);
```

```
%%


compl_exp_greater90=compl_exp_eve_highest30_wo_btd_Dfd_gt_highest25(i_desc_exp_pos_greater90,:);
compl_exp_greater80=compl_exp_eve_highest30_wo_btd_Dfd_gt_highest25(i_desc_exp_pos_greater80,:);
compl_exp_greater70=compl_exp_eve_highest30_wo_btd_Dfd_gt_highest25(i_desc_exp_pos_greater70,:);

t_compl_exp_greater90=transpose(compl_exp_greater90);
t_compl_exp_greater80=transpose(compl_exp_greater80);
t_compl_exp_greater70=transpose(compl_exp_greater70);


omitnan_t_compl_exp_greater90=t_compl_exp_greater90;
omitnan_t_compl_exp_greater80=t_compl_exp_greater80;
omitnan_t_compl_exp_greater70=t_compl_exp_greater70;

omitnan_t_compl_exp_greater90(omitnan_t_compl_exp_greater90== 0) = NaN;
omitnan_t_compl_exp_greater80(omitnan_t_compl_exp_greater80== 0) = NaN;
omitnan_t_compl_exp_greater70(omitnan_t_compl_exp_greater70== 0) = NaN;


var_compl_exp_greater90=var(t_compl_exp_greater90,'omitnan');
var_compl_exp_greater80=var(t_compl_exp_greater80,'omitnan');
var_compl_exp_greater70=var(t_compl_exp_greater70,'omitnan');

[asce_var_greater90,i_asce_var_greater90]=sort(var_compl_exp_greater90,'ascend');
[asce_var_greater80,i_asce_var_greater80]=sort(var_compl_exp_greater80,'ascend');
[asce_var_greater70,i_asce_var_greater70]=sort(var_compl_exp_greater70,'ascend');



genes_asce_var_greater90=genes_greater90(i_asce_var_greater90);
genes_asce_var_greater80=genes_greater80(i_asce_var_greater80);
genes_asce_var_greater70=genes_greater70(i_asce_var_greater70);

%genes_asce_var_greater90_top1000=genes_asce_var_greater90(1:1000);
genes_asce_var_greater80_top1000=genes_asce_var_greater80(1:1000);
%genes_asce_var_greater70_top1000=genes_asce_var_greater70(1:1000);

% ismember doesn't keep the indices in order.
%find(ismember(genes_cell_array,genes_asce_var_greater90_top1000) == 1)

%to do that use the one script below that keeps the indices in order:
%[~,loc_asce_greater90_top1000]=ismember(genes_asce_var_greater90_top1000,genes_cell_array);
[~,loc_asce_greater80_top1000]=ismember(genes_asce_var_greater80_top1000,genes_cell_array);
%[~,loc_asce_greater70_top1000]=ismember(genes_asce_var_greater70_top1000,genes_cell_array);

%%
%compl_asce_greater90_trunkcells=compl_exp_eve_highest30_wo_btd_Dfd_gt_highest25(loc_asce_greater90
_top1000,:);
compl_asce_greater80_trunkcells=compl_exp_eve_highest30_wo_btd_Dfd_gt_highest25(loc_asce_greater80_
top1000,:);
%compl_asce_greater70_trunkcells=compl_exp_eve_highest30_wo_btd_Dfd_gt_highest25(loc_asce_greater70
_top1000,:);

%compl_asce_greater90_CFcells=compl_exp_eve_highest30_btd(loc_asce_greater90_top1000,:);
compl_asce_greater80_CFcells=compl_exp_eve_highest30_btd(loc_asce_greater80_top1000,:);
```

```
%compl_asce_greater70_CFcells=compl_exp_eve_highest30_btd(loc_asce_greater70_top1000,:);


t_compl_asce_greater80_CFcells=transpose(compl_asce_greater80_CFcells);
t_compl_asce_greater80_trunkcells=transpose(compl_asce_greater80_trunkcells);

%% T-TEST FOR THE NORMALIZED DATA.

[Httest,Pttest,stats]=ttest2(t_compl_asce_greater80_CFcells,t_compl_asce_greater80_trunkcells,'Alph
a',0.05,'Tail','both','Vartype','unequal');
[sort_Pttest,i_Pttest]=sort(Pttest);
t_i_Pttest=transpose(i_Pttest);
sig_genes=genes_asce_var_greater80(t_i_Pttest,:);

%%

combi_compl_exp=horzcat(compl_asce_greater80_CFcells,compl_asce_greater80_trunkcells);
mapcaplot(combi_compl_exp);
combi_cell_ID=vertcat(cell_ID_CFcells,cell_ID_trunkcells);
mapcaplot(combi_compl_exp,combi_cell_ID);
```

8 REFERENCES

Acampora, D., Gulisano, M., Broccoli, V., Simeone, A., 2001. Otx genes in brain morphogenesis. Progress in Neurobiology 64, 69–95. doi:10.1016/S0301-0082(00)00042-3

Acampora, D., Postiglione, M.P., Avantaggiato, V., Di Bonito, M., Simeone, A., 2000. The role of Otx and Otp genes in brain development. Int. J. Dev. Biol. 44, 669–677. doi:10.1387/ijdb.11061431

Anderson, D.T., 1966. The Comparative Embryology of the Diptera. http://dx.doi.org/10.1146/annurev.en.11.010166.000323 11, 23–46. doi:10.1146/annurev.en.11.010166.000323

Bailles, A., Collinet, C., Philippe, J.-M., Lenne, P.-F., Munro, E., Lecuit, T., 2019. Transcriptional induction and mechanical propagation of a morphogenetic wave. bioRxiv 430512.

Brown, S., Fellers, J., Shippy, T., Denell, R., Stauber, M., Schmidt-Ott, U., 2001. A strategy for mapping bicoid on the phylogenetic tree. Current Biology 11, R43–4. doi:10.1016/s0960-9822(01)00007-0

Campinho, P., Behrndt, M., Ranft, J., Risler, T., Minc, N., Heisenberg, C.-P., 2013. Tension-oriented cell divisions limit anisotropic tissue tension in epithelial spreading during zebrafish epiboly. Nat. Cell Biol. 15, 1405–1414. doi:10.1038/ncb2869

Campos-Ortega, J.A., Hartenstein, V., 1997. The Embryonic Development of Drosophila melanogaster. Springer Berlin Heidelberg, Berlin, Heidelberg. doi:10.1007/978-3-662-22489-2

Chanet, S., Sharan, R., Khan, Z., Martin, A.C., 2017. Myosin 2-Induced Mitotic Rounding Enables Columnar Epithelial Cells to Interpret Cortical Spindle Positioning Cues. Curr. Biol. 27, 3350–3358.e3. doi:10.1016/j.cub.2017.09.039

Cohen, S.M., Jürgens, G., 1990a. Mediation of Drosophila head development by gap-like segmentation genes. Nature 346, 482–485. doi:10.1038/346482a0

Cohen, S.M., Jürgens, G., 1990b. Mediation of Drosophila head development by gap-like segmentation genes. Nature 346, 482–485. doi:10.1038/346482a0

Costa, M., Sweeton, D., Wieschaus, E., 1993. Gastrulation in Drosophila: Cellular mechanisms of morphogenetic movements, in:. Cold Spring Harbor: Laboratory Press, pp. 425–465.

Cuvier, G., 1817. Le règne animal distribué d'après son organisation, Nouvelle édition rev. et aug. ed. Paris. doi:https://doi.org/10.5962/bhl.title.49223

Czerniak, N.D., Dierkes, K., D'Angelo, A., Colombelli, J., Solon, J., 2016. Patterned Contractile Forces Promote Epidermal Spreading and Regulate Segment

Positioning during Drosophila Head Involution. Current Biology 26, 1895–1901. doi:10.1016/j.cub.2016.05.027

Dahmann, C., Oates, A.C., Brand, M., 2011. Boundary formation and maintenance in tissue development. Nat. Rev. Genet. 12, 43–55. doi:10.1038/nrg2902

Davy, A., Bush, J.O., Soriano, P., 2006. Inhibition of Gap Junction Communication at Ectopic Eph/ephrin Boundaries Underlies Craniofrontonasal Syndrome. PLoS Biol. 4, e315. doi:10.1371/journal.pbio.0040315

De Robertis, E.M., Sasai, Y., 1996. A common plan for dorsoventral patterning in Bilateria. Nature 380, 37–40. doi:10.1038/380037a0

Farrell, D.L., Weitz, O., Magnasco, M.O., Zallen, J.A., 2017. SEGGA: a toolset for rapid automated analysis of epithelial cell polarity and dynamics. Development 144, 1725–1734. doi:10.1242/dev.146837

Fernandez-Gonzalez, R., Simões, S. de M., Röper, J.-C., Eaton, S., Zallen, J.A., 2009. Myosin II Dynamics Are Regulated by Tension in Intercalating Cells. Dev. Cell 17, 736–743. doi:10.1016/j.devcel.2009.09.003

Finklstein, R., Perrimon, N., 1990. The orthodenticle gene is regulated by bicoid and torso and specifies Drosophila head development. Nature 346, 485–488. doi:10.1038/346485a0

Foe, V.E., 1989. Mitotic domains reveal early commitment of cells in Drosophila embryos. Development 107, 1–22.

Foe, V.E., Alberts, B.M., 1983. Studies of nuclear and cytoplasmic behaviour during the five mitotic cycles that precede gastrulation in Drosophila embryogenesis. J. Cell. Sci. 61, 31–70.

García-Bellido, A., Ripoll, P., MORATA, G., 1973. Developmental Compartmentalisation of the Wing Disk of Drosophila. Nature New Biology 1973 245:147 245, 251–253. doi:10.1038/newbio245251a0

Guillot, C., Lecuit, T., 2013. Mechanics of Epithelial Tissue Homeostasis and Morphogenesis. Science 340, 1185–1189. doi:10.1126/science.1235249

Guthrie, S., Lumsden, A., 1991. Formation and regeneration of rhombomere boundaries in the developing chick hindbrain. Development 112, 221–229.

Gutiérrez, D.S., Tozluoglu, M., Barry, J.D., Pascual, A., Mao, Y., Escudero, L.M., 2016. Fundamental physical cellular constraints drive self-organization of tissues. EMBO J. 35, 77–88. doi:10.15252/embj.201592374

Harding, K., Rushlow, C., Doyle, H.J., Hoey, T., Levine, M., 1986. Cross-regulatory interactions among pair-rule genes in Drosophila. Science 233, 953–959.

Harris, A.K., 1976. Is cell sorting caused by differences in the work of intercellular adhesion? A critique of the steinberg hypothesis. Journal of Theoretical Biology 61, 267–285. doi:10.1016/0022-5193(76)90019-9

Hartmann, B., Reichert, H., 1998. The Genetics of Embryonic Brain Development inDrosophila. Molecular and Cellular Neuroscience 12, 194–205. doi:10.1006/mcne.1998.0716

Hirth, F., Hartmann, B., Reichert, H., 1998. Homeotic gene action in embryonic brain development of Drosophila. Development 125, 1579–1589.

Holland, L.Z., Holland, N.D., 1999. Chordate origins of the vertebrate central nervous system. Current Opinion in Neurobiology 9, 596–602. doi:10.1016/S0959-4388(99)00003-3

Holtfreter, J., 1939. Gewebeaffinitat, ein Mittel der embryonalen Formbildung. Arch. Exp. Zellforsch. 23, 169–209.

Irvine, K.D., Wieschaus, E., 1994. Cell intercalation during Drosophila germband extension and its regulation by pair-rule segmentation genes. Development 120, 827–841.

Ishihara, H., Martin, B.L., Brautigan, D.L., Karaki, H., Ozaki, H., Kato, Y., Fusetani, N., Watabe, S., Hashimoto, K., Uemura, D., Hartshorne, D.J., 1989. Calyculin A and okadaic acid: Inhibitors of protein phosphatase activity. Biochemical and Biophysical Research Communications 159, 871–877. doi:10.1016/0006-291X(89)92189-X

Jeon, H., O, J., Jin, S., Lim, J., Choe, C.P., 2019. A Role for buttonhead in the Early Head and Trunk Development in the Beetle Tribolium castaneum. Development & Reproduction 23, 63–72. doi:10.12717/DR.2019.23.1.063

Kane, D., Adams, R., 2002. Life at the Edge: Epiboly and Involution in the Zebrafish, in: Pattern Formation in Zebrafish, Results and Problems in Cell Differentiation. Springer, Berlin, Heidelberg, Berlin, Heidelberg, pp. 117–135. doi:10.1007/978-3-540-46041-1_7

Karaiskos, N., Wahle, P., Alles, J., Boltengagen, A., Ayoub, S., Kipar, C., Kocks, C., Rajewsky, N., Zinzen, R.P., 2017. The Drosophila embryo at single-cell transcriptome resolution. Science 358, 194–199. doi:10.1126/science.aan3235

Kimmel, C.B., Ballard, W.W., Kimmel, S.R., Ullmann, B., Schilling, T.F., 1995. Stages of embryonic development of the zebrafish. Developmental Dynamics 203, 253–310. doi:10.1002/aja.1002030302

Kimmel, C.B., Warga, R.M., Schilling, T.F., 1990. Origin and organization of the zebrafish fate map. Development 108, 581–594.

Kitzmann, P., Schwirz, J., Schmitt-Engel, C., Bucher, G., 2013. RNAi phenotypes are influenced by the genetic background of the injected strain. BMC Genomics 14, 1–14. doi:10.1186/1471-2164-14-5

Klomp, J., Athy, D., Kwan, C.W., Bloch, N.I., Sandmann, T., Lemke, S., Schmidt-Ott, U., 2015. Embryo development. A cysteine-clamp gene drives embryo polarity in the midge Chironomus. Science 348, 1040–1042. doi:10.1126/science.aaa7105

Kmita, M., 2003. Organizing Axes in Time and Space; 25 Years of Colinear Tinkering. Science 301, 331–333. doi:10.1126/science.1085753

Knoll, A.H., Carroll, S.B., 1999. Early animal evolution: emerging views from comparative biology and geology. Science 284, 2129–2137. doi:10.1126/science.284.5423.2129

Kosman, D., Reinitz, J., on, D.S.O.T.1.P.S., 1998a. Automated assay of gene expression at cellular resolution. Citeseer

.

Kosman, D., Small, S., Reinitz, J., 1998b. Rapid preparation of a panel of polyclonal antibodies to Drosophila segmentation proteins. Dev. Genes Evol. 208, 290–294. doi:10.1007/s004270050184

Kraut, R., Chia, W., Jan, L.Y., Jan, Y.N., Knoblich, J.A., 1996. Role of inscuteable in orienting asymmetric cell divisions in Drosophila. Nature 383, 50. doi:10.1038/383050a0

Landsberg, K.P., Farhadifar, R., Ranft, J., Umetsu, D., Widmann, T.J., Bittig, T., Said, A., Jülicher, F., Dahmann, C., 2009. Increased Cell Bond Tension Governs Cell Sorting at the Drosophila Anteroposterior Compartment Boundary. Current Biology 19, 1950–1955. doi:10.1016/j.cub.2009.10.021

Lawrence, P.A., Johnston, P., Macdonald, P., Struhl, G., 1987. Borders of parasegments in Drosophila embryos are delimited by the fushi tarazu and even-skipped genes. Nature 328, 440–442. doi:10.1038/328440a0

Leptin, M., Casal, J., Grunewald, B., Reuter, R., 1992. Mechanisms of early Drosophila mesoderm formation. Development 116, 23–31.

Leuzinger, S., Hirth, F., Gerlich, D., Acampora, D., Simeone, A., Gehring, W.J., FINKELSTEIN, R., Furukubo-Tokunaga, K., Reichert, H., 1998. Equivalence of the fly orthodenticle gene and the human OTX genes in embryonic brain development of Drosophila. Development 125, 1703–1710.

Lynch, J., Desplan, C., 2003. Evolution of Development: Beyond Bicoid. Current Biology 13, R557–R559. doi:10.1016/S0960-9822(03)00472-X

Major, R.J., Irvine, K.D., 2006. Localization and requirement for Myosin II at the dorsal-ventral compartment boundary of the Drosophila wing. Developmental Dynamics 235, 3051–3058. doi:10.1002/dvdy.20966

Major, R.J., Irvine, K.D., 2005. Influence of Notch on dorsoventral compartmentalization and actin organization in the Drosophila wing. Development 132, 3823–3833. doi:10.1242/dev.01957

Martinez-Arias, A., Lawrence, P.A., 1985. Parasegments and compartments in the Drosophila embryo. Nature 313, 639–642. doi:10.1038/313639a0

McGregor, A.P., 2005. How to get ahead: the origin, evolution and function of bicoid. BioEssays 27, 904–913. doi:10.1002/bies.20285

Momen-Roknabadi, A., Di Talia, S., Wieschaus, E., 2016. Transcriptional Timers Regulating Mitosis in Early Drosophila Embryos. Cell Rep 16, 2793–2801. doi:10.1016/j.celrep.2016.08.034

Monier, B., Pelissier-Monier, A., Brand, A.H., Sanson, B., 2010. An actomyosin-based barrier inhibits cell mixing at compartmental boundaries in Drosophila embryos. Nat. Cell Biol. 12, 60–U147. doi:10.1038/ncb2005

Moscona, A., Moscona, H., 1952. The dissociation and aggregation of cells from organ rudiments of the early chick embryo. Journal of Anatomy 86, 287–301. doi:10.1111/(ISSN)1469-7580

Munjal, A., Philippe, J.-M., Munro, E., Lecuit, T., 2015. A self-organized biomechanical network drives shape changes during tissue morphogenesis. Nature 524, 351–355. doi:10.1038/nature14603

Nehls, S., Nöding, H., Karsch, S., Ries, F., Janshoff, A., 2019. Stiffness of MDCK II Cells Depends on Confluency and Cell Size. Biophys. J. 116, 2204–2211. doi:10.1016/j.bpj.2019.04.028

Oliveri, P., Tu, Q., Davidson, E.H., 2008. Global regulatory logic for specification of an embryonic cell lineage. Proc. Natl. Acad. Sci. U.S.A. 105, 5955–5962. doi:10.1073/pnas.0711220105

Pomares, J.M.P., Foty, R.A., 2006. Tissue fusion and cell sorting in embryonic development and disease: biomedical implications. BioEssays 28, 809–821. doi:10.1002/bies.20442

Rafiqi, A.M., Park, C.-H., Kwan, C.W., Lemke, S., Schmidt-Ott, U., 2012. BMP-dependent serosa and amnion specification in the scuttle fly Megaselia abdita. Development 139, 3373–3382. doi:10.1242/dev.083873

Reichert, H., Simeone, A., 1999. Conserved usage of gap and homeotic genes in patterning the CNS. Current Opinion in Neurobiology 9, 589–595. doi:10.1016/S0959-4388(99)00002-1

Rohani, N., Canty, L., Luu, O., Fagotto, F., Winklbauer, R., 2011. EphrinB/EphB Signaling Controls Embryonic Germ Layer Separation by Contact-Induced Cell Detachment. PLoS Biol. 9, e1000597. doi:10.1371/journal.pbio.1000597

Rohr, K.B., Tautz, D., Sander, K., 1999. Segmentation gene expression in the mothmidge Clogmia albipunctata (Diptera, Psychodidae) and other primitive dipterans. Dev. Genes Evol. 209, 145–154. doi:10.1007/s004270050238

Sanson, B., 2001. Generating patterns from fields of cells. EMBO reports 2, 1083–1088. doi:10.1093/embo-reports/kve255

Scarpa, E., Finet, C., Blanchard, G.B., Sanson, B., 2018. Actomyosin-Driven Tension at Compartmental Boundaries Orients Cell Division Independently of Cell Geometry In Vivo. Dev. Cell 47, 727–740.e6. doi:10.1016/j.devcel.2018.10.029

Schindelin, J., Arganda-Carreras, I., Frise, E., Kaynig, V., Longair, M., Pietzsch, T., Preibisch, S., Rueden, C., Saalfeld, S., Schmid, B., Tinevez, J.-Y., White, D.J.,

Hartenstein, V., Eliceiri, K., Tomancak, P., Cardona, A., 2012. Fiji: an open-source platform for biological-image analysis. nmeth 9, 676–682. doi:10.1038/nmeth.2019

Schinko, J.B., Kreuzer, N., Offen, N., Posnien, N., Wimmer, E.A., Bucher, G., 2008. Divergent functions of orthodenticle, empty spiracles and buttonhead in early head patterning of the beetle Tribolium castaneum (Coleoptera). Developmental Biology 317, 600–613. doi:10.1016/j.ydbio.2008.03.005

Schmidt-Ott, U., González-Gaitán, M., Jäckle, H., Technau, G.M., 1994. Number, identity, and sequence of the Drosophila head segments as revealed by neural elements and their deletion patterns in mutants. Proc. Natl. Acad. Sci. U.S.A. 91, 8363–8367.

Schneider-Maunoury, S., Topilko, P., Seitanidou, T., Levi, G., Cohen-Tannoudji, M., Pournin, S., Babinet, C., Charnay, P., 1993. Disruption of Krox-20 results in alteration of rhombomeres 3 and 5 in the developing hindbrain. Cell 75, 1199–1214. doi:10.1016/0092-8674(93)90329-O

Snodgrass, R.E., 1935. Principles of Insect Morphology. McGRaw Hill, New York.

Sommer, R., Tautz, D., 1991. Segmentation gene expression in the housefly Musca domestica. Development 113, 419–430.

Spencer, A.K., Siddiqui, B.A., Thomas, J.H., 2015. Cell shape change and invagination of the cephalic furrow involves reorganization of F-actin. Developmental Biology 402, 192–207. doi:10.1016/j.ydbio.2015.03.022

St Johnston, D., Nüsslein-Volhard, C., 1992. The origin of pattern and polarity in the Drosophila embryo. Cell 68, 201–219.

Stauber, M., Jäckle, H., Schmidt-Ott, U., 1999. The anterior determinant bicoid of Drosophila is a derived Hox class 3 gene. PNAS 96, 3786–3789. doi:10.1073/pnas.96.7.3786

Steinberg, M.S., 1970. Does differential adhesion govern self-assembly processes in histogenesis? Equilibrium configurations and the emergence of a hierarchy among populations of embryonic cells. Journal of Experimental Zoology 173, 395–433. doi:10.1002/jez.1401730406

Swiatek, P.J., Gridley, T., 1993. Perinatal lethality and defects in hindbrain development in mice homozygous for a targeted mutation of the zinc finger gene Krox20. Genes Dev. 7, 2071–2084. doi:10.1101/gad.7.11.2071

Tallafuss, A., Wilm, T.P., Crozatier, M., Pfeffer, P., Wassef, M., Bally-Cuif, L., 2001. The zebrafish buttonhead-like factor Bts1 is an early regulator of pax2.1 expression during mid-hindbrain development. Development 128, 4021–4034.

Tepass, U., 2002. Cell sorting in animal development: signalling and adhesive mechanisms in the formation of tissue boundaries. Curr. Opin. Genet. Dev. 12, 572–582. doi:10.1016/S0959-437X(02)00342-8

Thisse, B., Stoetzel, C., Thisse, C.G., Schmitt, F.P., 1988. Sequence of the twist gene and nuclear localization of its protein in endomesodermal cells of early Drosophila embryos. EMBO J. 7, 2175–2183. doi:10.1002/j.1460-2075.1988.tb03056.x

Townes, P.L., Holtfreter, J., 1955. Directed movements and selective adhesion of embryonic amphibian cells. Journal of Experimental Zoology 128, 53–120. doi:10.1002/jez.1401280105

Treichel, D., Schöck, F., Jäckle, H., Gruss, P., Mansouri, A., 2003. mBtd is required to maintain signaling during murine limb development. Genes Dev. 17, 2630–2635. doi:10.1101/gad.274103

Turner, F.R., Mahowald, A.P., 1977. Scanning electron microscopy of Drosophila melanogaster embryogenesis. II. Gastrulation and segmentation. Developmental Biology 57, 403–416.

Twigg, S.R.F., Kan, R., Babbs, C., Bochukova, E.G., Robertson, S.P., Wall, S.A., Morriss-Kay, G.M., Wilkie, A.O.M., 2004. Mutations of ephrin-B1 (EFNB1), a marker of tissue boundary formation, cause craniofrontonasal syndrome. PNAS 101, 8652–8657. doi:10.1073/pnas.0402819101

Vincent, A., Blankenship, J.T., Wieschaus, E., 1997. Integration of the head and trunk segmentation systems controls cephalic furrow formation in Drosophila. Development 124, 3747–3754.

Weber, H., 1966. Grundriss der Insektenkunde, fourth ed. ed. Gustav Fischer Verlag, Stuttgart.

Wessel, A.D., Gumalla, M., Großhans, J., Schmidt, C.F., 2015. The mechanical properties of early Drosophila embryos measured by high-speed video microrheology. Biophys. J. 108, 1899–1907. doi:10.1016/j.bpj.2015.02.032

Wiegmann, B.M., Trautwein, M.D., Winkler, I.S., Barr, N.B., Kim, J.-W., Lambkin, C., Bertone, M.A., Cassel, B.K., Bayless, K.M., Heimberg, A.M., Wheeler, B.M., Peterson, K.J., Pape, T., Sinclair, B.J., Skevington, J.H., Blagoderov, V., Caravas, J., Kutty, S.N., Schmidt-Ott, U., Kampmeier, G.E., Thompson, F.C., Grimaldi, D.A., Beckenbach, A.T., Courtney, G.W., Friedrich, M., Meier, R., Yeates, D.K., 2011. Episodic radiations in the fly tree of life. Proc. Natl. Acad. Sci. U.S.A. 108, 5690–5695. doi:10.1073/pnas.1012675108

Wilson, H.V., 1907. On some phenomena of coalescence and regeneration in sponges. Journal of Experimental Zoology 5, 245–258.

Wimmer, E.A., Simpson-Brose, M., Cohen, S.M., Desplan, C., Jäckle, H., 1995. Trans- and cis-acting requirements for blastodermal expression of the head gap gene buttonhead. Mech. Dev. 53, 235–245. doi:10.1016/0925-4773(95)00439-8

Wotton, K.R., Jiménez-Guri, E., Garcia Matheu, B., Jaeger, J., 2014. A Staging Scheme for the Development of the Scuttle Fly Megaselia abdita. PLoS ONE 9. doi:10.1371/journal.pone.0084421

Zallen, J.A., Wieschaus, E., 2004. Patterned gene expression directs bipolar planar polarity in Drosophila. Dev. Cell 6, 343–355. doi:10.1016/S1534-5807(04)00060-7